This is to certify that the
dissertation entitled

Phenomenology of the Littlest Higgs Model with T-parity

presented by

Chuan-Ren Chen

has been accepted towards fulfillment
of the requirements for the

Ph. D. degree in Physics and Astronomy

Major Professor's Signature

2/26/2008

Date

PHENOMENOLOGY OF THE LITTLEST HIGGS MODEL WITH T-PARITY

By

Chuan-Ren Chen

A DISSERTATION

Submitted to
Michigan State University
in partial fulfillment of the requirements
for the degree of

DOCTOR OF PHILOSOPHY

Department of Physics and Astronomy

2008

ABSTRACT

PHENOMENOLOGY OF THE LITTLEST HIGGS MODEL WITH T-PARITY

by

Chuan-Ren Chen

Even though the Standard Model has been very successful in describing almost all of the experimental data in high energy physics, it is widely believed that a new physics theory will occur at TeV scale. Motivated by the "Little Hierarchy problem", Little Higgs models were proposed. In Little Higgs models, the Higgs boson is a pseudo-Nambu-Goldstone boson, and its mass is protected by enough symmetries so that no tree level mass term exists. Two or more couplings in the effective Lagrangian are needed to break these symmetries and generate the Higgs boson mass at the one-loop level, which is called the "collective symmetry breaking" mechanism. The quadratically divergent corrections to the Higgs boson mass are neatly canceled at one-loop level: the corrections from the top quark loop is canceled by a new heavy quark and the corrections from the Standard Model gauge bosons are canceled by a set of new gauge bosons. With T-parity, the mass scale of the Little Higgs models is allowed to be less than one TeV by the precision electroweak tests due to the absence of mixings between the new gauge bosons and the Standard Model gauge bosons. Furthermore, Little Higgs model with T-parity also predicts a dark matter candidate and leads to the very interesting collider phenomenology that is different from the Standard Model prediction.

In this work, I investigate top quark physics and Higgs boson physics in the Littlest Higgs model with T-parity at the Large Hadron Collider (LHC) at CERN. The effects through the virtual appearance of the new particles have a large impact on the Higgs boson production total cross section via the gluon-gluon fusion process and decay

branching ratios. For the top quark physics, since the wtb coupling is modified at the tree level due to the mixings between the top quark and a T-even heavy quark, the single-top quark production cross sections will be reduced, as compared to Standard Model predictions. I also present the one-loop electroweak corrections to the $gt\bar{t}$ coupling, which leads to an anomalous coupling written in terms of several form factors. And I further examine the effects in the top quark pair production via the quark annihilation process at the LHC. The negative corrections from the Standard Model particle loops are partially canceled by the positive contributions from the loops of the new heavy particles, and the latter dominates in the large invariant mass of the top quark pair.

I also investigate the collider signatures of the new particles in the Littlest Higgs model with T-parity at the LHC and a Linear Collider (LC). I show the total cross sections, the typical decay branching ratios of the new particles and estimate the event rates for some interesting signatures at the LHC. Since the mass of the heavy gauge boson only depends on the symmetry breaking scale of the model, I study in detail the heavy gauge boson pair production at both the LHC and the LC, including the backgrounds from the Standard Model. By using a charged lepton pair with large missing energy signature at the LHC, the discovery potential of the heavy gauge boson pair production could reach a 5σ statistical significance. However, it is difficult to reconstruct the mass of the heavy gauge boson at the LHC. By using the four jets with missing energy signature at the LC, both mass and spin of the heavy gauge boson could be determined. It is also possible to distinguish different models at the LC by using the spin correlations.

To my parents, my wife and my daughters,

my true love and inspiration.

ACKNOWLEDGMENTS

I would like to express my deepest gratitude to my adviser, Professor C.-P. Yuan, who always gives me many helpful suggestions on both physics and life through these years. I have benefited from his teaching and many discussions with him. His constant encouragement and his indulgence over my failure to meet his requirement keep my research skills growing. Having an ambition to reach his achievement in physics is an inspiration for me in my future research career.

I am very grateful to Professor R. Sekhar Chivuluka for his help and teaching me many physics during his wonderful lectures. I am also grateful to Professor Wayne Repko for his help and answering my physics questions. I also thank Professor Wu-Ki Tung for his encouragement. I would like to thank all the faculty members in the High Energy Theory Group: Jon Pumplin, Carl Schmidt, Elizabeth H. Simmons and Daniel Stump. I also want to thank my committee members: Professors Joey Huston, Vladimir Zelevinsky and S. D. Mahanti for useful guidance.

I am further grateful to Francisco Larios, who was my first colleague and taught me a lot in my first research project; to our former and current postdocs: Alexander S. Belyaev for teaching me CalcHEP, LanHEP and many collider physics, Daisuke Nomura, Ken Hsieh, Neil Christensen and Pavel Nadolsky for many useful discussions. I would like to express my appreciation particularly to Kazuhiro Tobe and Qing-Hong Cao, who give me a lot of essential help and suggestions; to all the students in the office: Baradhwaj Collepa, Stefano Di Chiara, Mohammad Hussein, Jianghao Yu and Kurtis Geerlings for the cheerful and humorous working atmosphere.

I also want to thank our lovely and kind secretaries: Debbie Simmons and Brenda Wenzlick for their help. I am very grateful to John for reviewing my manuscript and giving me many useful suggestions in English writing.

Contents

List of Figures

List of Tables

Chapter 1

Introduction

Up to now, the Standard Model, a $SU(3)_c \times SU(2)_L \times U(1)_Y$ gauge theory [1–3], has been very successful in describing almost all of the experimental data in high energy physics. The predictions of the Standard Model (SM) have been tested precisely with electroweak measurements in the LEP and SLD experiments at the e^+e^- linear collider. The comparisons between experimental data and the Standard Model predictions are shown in Fig. 1.1 [4]. As we see there, except for the forward-backward asymmetry measurement of $Z \to b\bar{b}$ ($A_{fb}^{0,b}$), the best fit in the Standard Model agrees very well with the data.

However, it is hard to believe that the SM is the most fundamental theory realized in Nature based on the following. The combination of a variety of data from solar [5–14], atmospheric [15–18], reactor [19,20] and accelerator [21] neutrino experiments now firmly establishes the discovery of neutrino masses. Even though we still don't know the values of neutrino masses themselves, the fact that the neutrino has a mass already indicates the incompleteness of the SM in which neutrinos are massless. Moreover, cosmological studies of galaxies [22,23] show that the galaxies have huge "halos" of "dark matter," which is invisible and with mass 3-10 times that of luminous matter. The recent Wilkinson Microwave Anisotropy Probe (WMAP) data

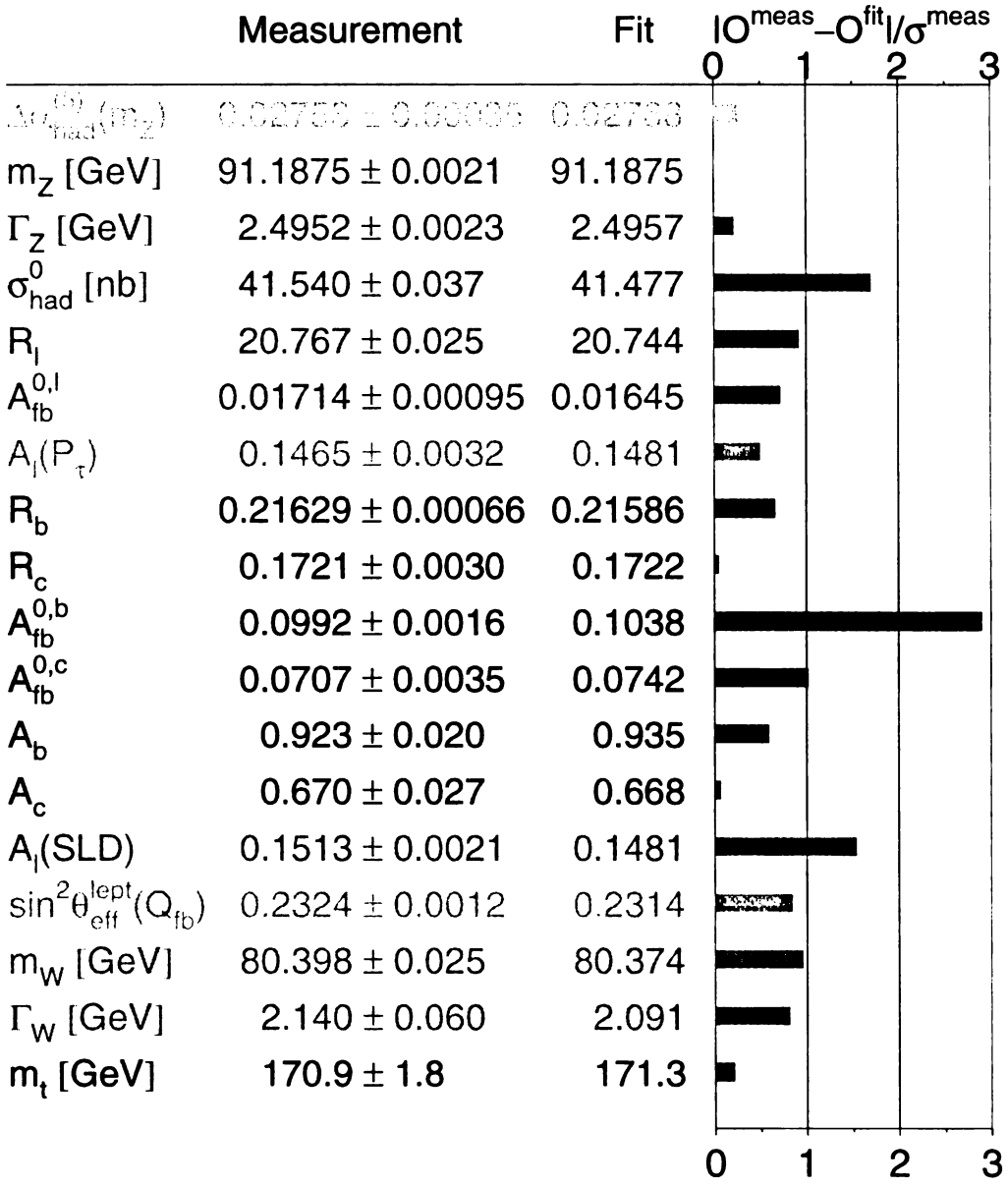

Figure 1.1: The comparison between the predictions in the SM and the experimental data.

show that the dark matter contributes about 20% to the total energy density of the Universe while the contribution from baryons is just about 4% [24]. The microscopic composition of dark matter remains a mystery, but it is clear that it cannot consist of any elementary particles that have been discovered in the laboratory so far. It is therefore widely believed that the SM is only an effective theory at the weak scale, which is valid only up to a cutoff scale Λ. In other words, a new physics model is expected to occur at the energy scale Λ.

In order to explain the phenomena in the real world, the $SU(2)_L \times U(1)_Y$ electroweak symmetry has to break down to $U(1)_{EM}$ symmetry. The mechanism for breaking the electroweak symmetry is described by the Higgs mechanism. The SM also predicts the existence of a fundamental scalar particle, Higgs boson, which has not been found yet in any high energy experiments. Therefore, the standard Higgs theory has not been tested and confirmed, and the true mechanism of electroweak symmetry breaking (EWSB) remains unanswered. Moreover, there exists a so-called "fine-tuning problem" or "hierarchy problem" arising from the SM Higgs boson, which is one of the motivations to look for new models beyond the SM. In this Chapter, I will review the hierarchy problem and possible solutions from two different models, Supersymmetry and Little Higgs models, focusing on the latter.

1.1 Hierarchy problem

From the χ^2 fit of electroweak data, as shown in Fig. 1.2, a light Higgs boson ($\sim$ 100 GeV) boson is preferred [4]. If we calculate the quantum corrections to the mass of the Higgs boson from the top quark, the gauge boson and the Higgs boson self interaction loops, as seen in Fig. 1.3, it turns out to be proportional to the cutoff square, which is quadratically sensitive to the scale of new physics. The largest

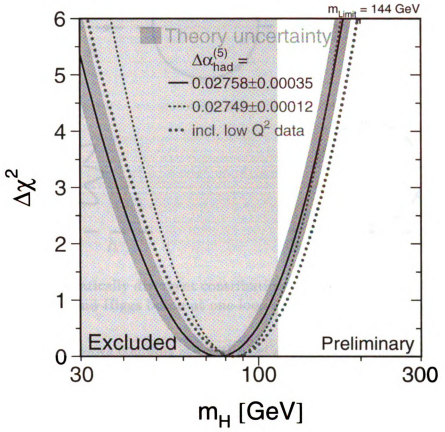

Figure 1.2: The χ^2 fit derived from high-Q^2 pecision electroweak measurements, performed at LEP and by SLD, CDF and D0, as a function the Higgs boson mass, assuming the SM.

contribution is from the top quark loop because of its large Yukawa coupling to the Higgs boson, which is

$$\delta m_h^2 = -\frac{3\lambda_t^2}{8\pi^2}\Lambda^2,$$

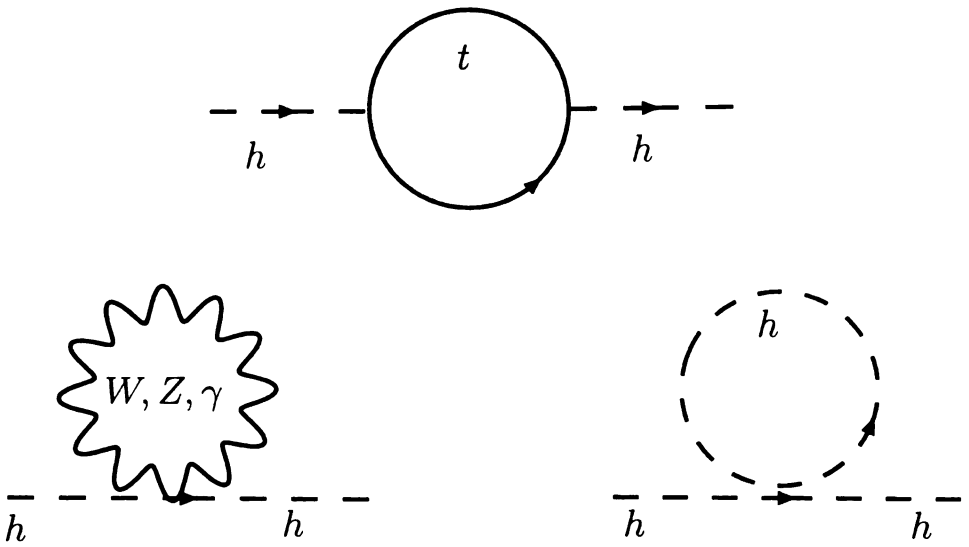

Figure 1.3: The quadratically divergent contributions to the Higgs mass from the top quark, gauge bosons and Higgs boson at one-loop level in the SM.

where λ_t is the top Yukawa coupling strength. Let's take some values of Λ to see how large δm_h^2 will be.

$$\delta m_h^2 \sim \begin{cases} -(200\,GeV)^2, \text{ if } \Lambda = 1\,\text{TeV}, \\ -4(200\,\text{GeV})^2, \text{ if } \Lambda = 2\,\text{TeV}, \\ -25(200\,\text{GeV})^2, \text{ if } \Lambda = 5\,\text{TeV}, \\ -100(200\,\text{GeV})^2, \text{ if } \Lambda = 10\,\text{TeV}. \end{cases}$$

The physical mass of the Higgs boson is

$$m_h^2 = m_{h0}^2 + \delta m_h^2,$$

where m_{h0}^2 is the bare mass parameter of the Higgs boson appearing in the Lagrangian, and we expect that m_h is at order of 100 GeV, say $m_h \sim 200$ GeV. Therefore, if the cutoff scale $\Lambda = 10$ TeV, we have to finely tune m_{h0}^2 at the level of one part in one hundred in order to have $m_h \sim 200$GeV. In other words, the fine-tuning for m_{h0} is

needed if the scale for new physics is high, compared to the weak scale ($\sim 246\,\mathrm{GeV}$). If we believe that the SM is valid up to GUT scale ($\gtrsim 10^{16}$ GeV) or even Plank scale (10^{19} GeV), a fine-tuning of about one part in $10^{26} \sim 10^{32}$ would be required. This is a well-known "fine-tuning problem" or the "hierarchy problem" in the Higgs sector of the SM. Therefore, we generally believe and expect that the new physics should naturally occur at energy scale Λ about 1 TeV or below, which also implies that there are new particles with masses at or below 1 TeV, if the new physics is a weakly coupled theory.

At the energy of weak scale, which is far below the scale of new physics, new particles can be "integrated out," and new physics effects would appear as a set of higher dimensional operators in terms of only the SM fields and the cutoff scale [25]. Since these higher dimensional operators can contribute to experimental observables at the weak scale, the new physics energy scale could be constrained by precision measurements. These operators can be categorized by the (approximate) symmetries which they break in the SM, such as baryon number, lepton number, CP, flavor and $SU(2)_C$ custodial symmetries. The experimental data currently put lower bounds on these operators to be $\gtrsim 5$ TeV [26–29]. This immediately generates the tension between the two scales: ~ 1 TeV , at which a new physics model is expected from the argument of quantum corrections to the Higgs boson mass, and ~ 5 TeV, below which there should be no new physics as mentioned above. Since the hierarchy of these two scales is not as big as that between weak and GUT or Planck scale, we call this as the "little hierarchy problem".

1.2 Possible Solutions

The hierarchy problem is one of the motivations for looking for the new physics beyond the SM. It is realized that the problem arises because the quantum corrections to the Higgs boson mass square are quadratically sensitive to the new physics scale. The most intuitive way is to cancel these corrections with the contributions from new particles. In this section, I will roughly introduce the cancellation in probably the most popular new physics model, the supersymmetric extension of the Standard Model, and explain in detail the Little Higgs model which is the focus of my work through this thesis.

1.2.1 Supersymmetric Extension of the Standard Model

Supersymmetry [30–33] is a symmetry that relates fermionic and bosonic degrees of freedom. It also predicts the existence of new particles which are supersymmetric partners of all the particles we have found. In addition, it requires that the total number of bosonic and fermionic degrees of freedom are equal. For example, the top quark has two supersymmetric partners, which are scalars and called top scalar-quark or *stop*, $\tilde{t}_L$ and $\tilde{t}_R$ that are corresponding to different chiralities of top quark, i.e. the left-handed state of the top quark t_L and the right-handed state t_R. The Higgs sector is extended to two Higgs doublets, and after the electroweak symmetry is broken, there exist five scalars, among which the lightest one is the SM-like Higgs boson. The quadratically divergent contribution of each diagram in Fig. 1.3 is exactly canceled by a diagram with the corresponding superpartner running in the loop, as shown in Fig. 1.4, where I only take only the top loop diagram as an illustration. The couplings for the Higgs boson to the SM particles and their supersymmetric partners are related by supersymmetry, and the cancellation happens because of the opposite

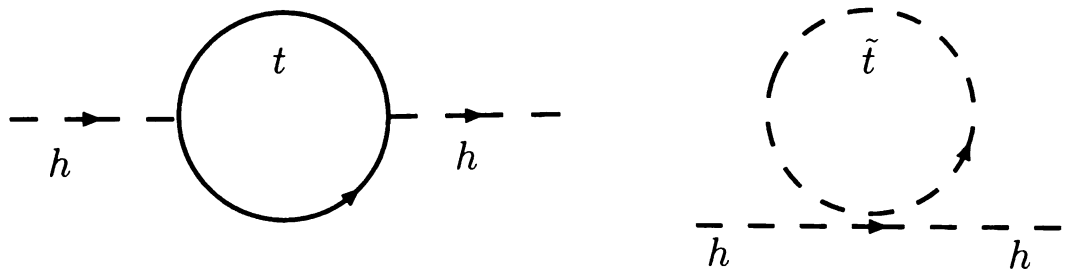

Figure 1.4: The cancellation in quadratically divergent contributions to the Higgs boson mass between top quark loop and top squark $\tilde{t}$ (superpartner of the top quark) loop in SUSY models.

spin statistics. For a review of the supersymmetry models, see [34–36] and references therein.

1.2.2 Little Higgs Model

The Little Higgs models provide an alternative way to cancel the quadratic divergences in quantum corrections to the Higgs boson mass. Unlike supersymmetry models, the cancellation in Little Higgs model happens between particles with the same spin statistics. I will explain in this section how the cancellation happens and introduce the "collective symmetry breaking" mechanism which is a crucial ingredient in the Little Higgs models.

For convenience, I take as an example the Littlest Higgs model [37], one of the most popular Little Higgs models discussed in the literature. The Littlest Higgs model is based on a $SU(5)/SO(5)$ non-linear sigma model. The global $SU(5)$ symmetry is broken down to $SO(5)$ at the scale f, therefore, 14 Nambu-Goldstone bosons are generated as a result of the spontaneous symmetry breaking. The Higgs boson is one of the Nambu-Goldstone bosons which are embedded in a Σ field. The kinetic term of the non-linear sigma field, which yields canonically normalized kinetic terms for

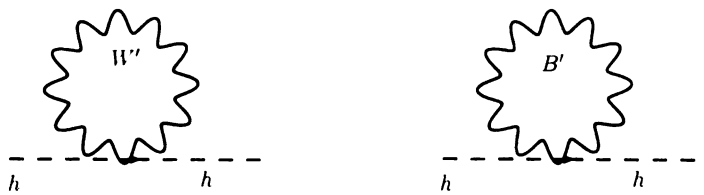

Figure 1.5: The one-loop diagrams of extra gauge bosons, W' and B', from the Littlest Higgs model, which cancel the quadratically divergent contributions to the Higgs boson mass from the SM gauge boson one-loop diagrams.

Nambu-Goldstone bosons, is given by

$$\mathcal{L}_{kin} = \frac{f^2}{8} Tr(D_\mu \Sigma)^\dagger (D^\mu \Sigma), \tag{1.1}$$

where the covariant derivative $D_\mu \Sigma$ and the explicit formula of Σ will be given in the next Chapter. Eq. (1.1) will generate interactions of the Higgs boson to gauge bosons as [37, 38]

$$\mathcal{L}_{kin} \supset \frac{g^2}{4} W_\mu^a W^{a\mu} hh + \frac{g'^2}{4} B_\mu B^\mu hh - \frac{g^2}{4} W_\mu'^a W'^{a\mu} hh - \frac{g'^2}{4} B'_\mu B'^\mu hh + \cdots, \tag{1.2}$$

where g and g' are weak and hypercharge coupling strength, respectively. It is easy to see that there exit two diagrams with new gauge bosons W' and B' in the loop, as shown in Fig. 1.5, which exactly cancel the quadratic divergences from SM gauge boson loop diagrams due to the same coupling strength for these two set of diagrams but with opposite sign as shown in Eq. (1.2).

In order to cancel the contribution form the top quark loop, one has to introduce a new heavy quark U related to the top quark. The couplings of the SM top quark and this heavy new quark to the Higgs boson can be obtained in the effective Lagrangian of the top sector [37]:

$$\mathcal{L}_{top} = -\frac{1}{2} \lambda_1 f \epsilon_{ijk} \epsilon_{xy} \bar{Q}_i \Sigma_{jx} \Sigma_{ky} u_R - \lambda_2 f \bar{U}_L U_R + h.c. \tag{1.3}$$

where $Q = (-ib_L,\, iu_L,\, U_L)^T$, the indies i, j, k run over the values 1, 2, 3 and x, y run over 4, 5, and b, u and U are weak eigenstates of the bottom, top and extra heavy

quarks, respectively. It is straightforward to expand Eq. (1.3) and get

$$\mathcal{L}_{top} \supset \frac{\sqrt{2}\lambda_1\lambda_2}{\sqrt{\lambda_1^2+\lambda_2^2}}\bar{t}_L t_R h + \frac{\sqrt{2}\lambda_1^2}{\sqrt{\lambda_1^2+\lambda_2^2}}\bar{t}_L T_R h + \frac{\lambda_1^2}{f\sqrt{\lambda_1^2+\lambda_2^2}}\bar{T}_L T_R hh$$

$$- \sqrt{\lambda_1^2+\lambda_2^2} f \bar{T}_L T_R + \cdots, \tag{1.4}$$

where $t_{L/R}$ and $T_{L/R}$ are mass eigenstates which are given as

$$t_L = u_L, \quad t_R = \frac{\lambda_2 u_R - \lambda_1 U_R}{\sqrt{\lambda_1^2+\lambda_2^2}},$$

$$T_L = U_L, \quad T_R = \frac{\lambda_1 u_R + \lambda_2 U_R}{\sqrt{\lambda_1^2+\lambda_2^2}}.$$

Note that, at this point, the top quark t is still massless and T quark gets its mass as

$$m_T = \sqrt{\lambda_1^2+\lambda_2^2} f.$$

Therefore, the diagrams which contribute to δm_h^2 form top sector interactions are shown in Fig. 1.6, and the contributions are

$$a) = -24\frac{\lambda_1^2\lambda_2^2}{\lambda_1^2+\lambda_2^2}\int \frac{d^4k}{(2\pi)^4}\frac{1}{k^2}$$

$$b) = -24\frac{\lambda_1^4}{\lambda_1^2+\lambda_2^2}\int \frac{d^4k}{(2\pi)^4}\frac{1}{k^2-m_T^2},$$

$$c) = +24\frac{\lambda_1^2}{f\sqrt{\lambda_1^2+\lambda_2^2}} m_T \int \frac{d^4k}{(2\pi)^4}\frac{1}{k^2-m_T^2}.$$

It can be shown that these three terms have quadratic divergences and the last two terms have also logarithmic divergences. Since $m_T = \sqrt{\lambda_1^2+\lambda_2^2} f$, it can be easily

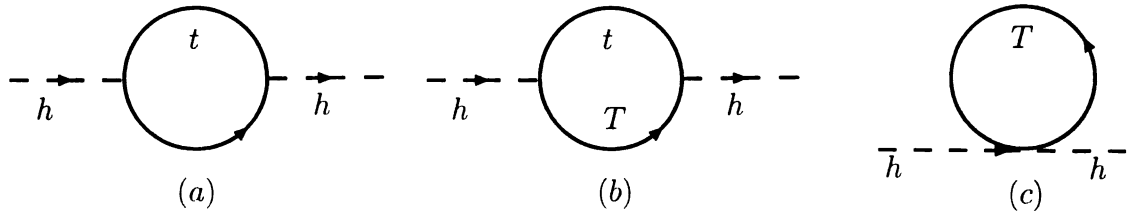

Figure 1.6: The cancellation in quadratically divergent contributions to the Higgs boson mass between top and the extra T quark in the Littlest Higgs model.

seen that the quadratic divergences cancel neatly because

$$-24\frac{\lambda_1^2\lambda_2^2}{\lambda_1^2+\lambda_2^2}-24\frac{\lambda_1^4}{\lambda_1^2+\lambda_2^2}+24\frac{\lambda_1^2}{f\sqrt{\lambda_1^2+\lambda_2^2}}m_T$$

$$=-24\lambda_1^2+24\frac{\lambda_1^2}{f\sqrt{\lambda_1^2+\lambda_2^2}}\sqrt{\lambda_1^2+\lambda_2^2}f=0.$$

However, the logarithmic terms are left over and contribute to the mass of the Higgs boson as

$$\delta m_h^2=-\frac{1}{16\pi^2}\frac{24\lambda_1^2\lambda_2^2}{\lambda_1^2+\lambda_2^2}m_T^2\ln\frac{\Lambda^2}{m_T^2}. \tag{1.5}$$

Like the situation in the SM, the contribution to δm_h^2 from top sector, i.e. Eq. (1.5), is the dominant one, and the negative sign provides an explanation to why electroweak symmetry is broken. Furthermore, if λ_1 or λ_2 vanishes, δm_h^2 from Fig. 1.6 is exactly zero, which means that the Higgs boson is an exact Nambu-Goldstone boson and stays massless. The mechanism which requires two or more couplings in the Lagrangian to break the symmetries that protect the Higgs boson mass is called " collective symmetry breaking". This is the general mechanism employed in Little Higgs models [39,40], and here I quote a statement of the "Little Higgs theory" from Ref. [40]:

The Higgs boson is a Nambu-Goldstone boson of a spontaneously broken symmetry. This symmetry is also explicitly broken but only "collectively", i.e. the symmetry is

broken when two or more couplings in the Lagrangian are non-vanishing. Setting any one of these couplings to zero restores the symmetry and therefore the masslessness of the Higgs boson.

Chapter 2

Model – The Littlest Higgs Model with T-parity

In Little Higgs models, the Higgs boson is embedded in the Nambu-Goldstone boson fields arising when a global symmetry G is spontaneously broken down to a subgroup H. Therefore, the Higgs boson is naturally light, because it is a pseudo-Nambu-Goldstone boson (pNGB). The idea of considering that Higgs is a pNGB was originally proposed by Georgi et al. [41–47] in 70's. Recently, a collective symmetry breaking mechanism [39] is introduced to make this old idea viable. The mass term of the Higgs boson is protected by several symmetries under which the Higgs boson is an exact Nambu-Goldstone boson. The Higgs boson gains its mass only when these symmetries are broken collectively, i.e. broken by two or more couplings in the Lagrangian. Therefore, there is no tree-level diagram which contributes to the mass of the Higgs boson. The Higgs potential can only be generated at loop level, which is Coleman-Weinberg potential. The most important contributions to the Coleman-Weinberg potential are from gauge boson loops and fermion loops. Furthermore, the sign of the induced quadratic term of the Higgs field is right (negative) to trigger electroweak symmetry breaking. Since the contributions to the Higgs boson mass are through loop diagrams, the Higgs boson mass is small due to the loop suppression. Since the

first Little Higgs model was proposed [39], it opened a "Little Higgs model building territory" [37,48–65]. In this chapter, I will discuss in detail the Littlest Higgs model with T-parity [54,57,59], which is an improved extension of the Littlest Higgs model, one of the most interesting Little Higgs models discussed in the literature.

The Littlest Higgs model [37] is an economical and predictable model. However, the original version of the Littlest Higgs model suffers from low energy electroweak precision tests, and the symmetry breaking scale f is forced to higher than about 4 TeV [66–71]. Since the cutoff scale Λ of the model is about $4\pi f$, this large Λ will reintroduce fine-tuning to the mass of the Higgs boson again. An elegant way to avoid the severe constraints from low energy electroweak precision tests is to introduce a symmetry, called T-parity [54, 57, 59], to forbid the existence of all the dangerous operators in which the SM fields and new fields mix at the tree level. As a result, the scale f as low as 500 GeV is allowed and makes the model very interesting and testable at the future colliders, such as the Large Hadron Collider (LHC) at CERN. Also, the Littlest Higgs model with T-parity provides a dark matter candidate which is the lightest T-odd particle, since it can not decay into any other particles and therefore is stable.

The Littlest Higgs model is based on a $SU(5)/SO(5)$ non-linear sigma model [37]. The global symmetry $SU(5)$ is broken down to $SO(5)$ by a vacuum expectation value (vev) of a $SU(5)$ symmetric tensor field Σ at the scale f, where

$$< \Sigma > \equiv \Sigma_0 = \begin{bmatrix} 0 & 0 & 0 & 1 & 0 \\ 0 & 0 & 0 & 0 & 1 \\ 0 & 0 & 1 & 0 & 0 \\ 1 & 0 & 0 & 0 & 0 \\ 0 & 1 & 0 & 0 & 0 \end{bmatrix}. \tag{2.1}$$

Under an $SU(5)$ transformation $V = \exp\{i\theta_a T_a\}$, the Σ field transforms as

$$\Sigma \to V \Sigma V^T.$$

Therefore, the 10 unbroken generators $\bar{T}_a$ of $SO(5)$ satisfy

$$\bar{T}_a \Sigma_0 + \Sigma_0 \bar{T} = 0,$$

and there are 14 broken generators $\hat{T}_a$ which satisfy

$$\hat{T}_a \Sigma_0 - \Sigma_0 \hat{T}_a = 0.$$

The expansion of Σ around its vev in broken directions has the form as

$$\Sigma = e^{i\pi_a \hat{T}_a / f} \Sigma_0 e^{i\pi_a \hat{T}_a^T / f} = e^{2i\pi_a \hat{T}_a / f} \Sigma_0 \equiv \xi^2 \Sigma_0, \tag{2.2}$$

where $\xi \equiv e^{i\pi_a \hat{T}_a / f}$, $a = 1 \sim 14$ and sum over index a is realized. We denote 14 Nambu-Goldstone boson fields as η, ω, H and ϕ, and the matrix $\pi_a \hat{T}_a$ could be written as

$$\Pi \equiv \pi_a \hat{T}_a = \begin{bmatrix} -\frac{w^0}{2} - \frac{\eta}{\sqrt{20}} & -\frac{w^+}{\sqrt{2}} & \frac{-i\pi^+}{\sqrt{2}} & -i\phi^{++} & -i\frac{\phi^+}{\sqrt{2}} \\ -\frac{w^-}{\sqrt{2}} & \frac{w^0}{2} - \frac{\eta}{\sqrt{20}} & \frac{v+h+i\pi^0}{2} & -i\frac{\phi^+}{\sqrt{2}} & \frac{-i\phi^0+\phi_p^0}{\sqrt{2}} \\ \frac{i\pi^-}{\sqrt{2}} & \frac{v+h-i\pi^0}{2} & \sqrt{\frac{4}{5}}\eta & \frac{-i\pi^+}{\sqrt{2}} & \frac{v+h+i\pi^0}{2} \\ i\phi^{--} & i\frac{\phi^-}{\sqrt{2}} & \frac{i\phi^+}{\sqrt{2}} & -\frac{w^0}{2} - \frac{\eta}{\sqrt{20}} & -\frac{w^-}{\sqrt{2}} \\ i\frac{\phi^-}{\sqrt{2}} & \frac{i\phi^0+\phi_p^0}{\sqrt{2}} & \frac{v+h-i\phi^0}{2} & -\frac{w^+}{\sqrt{2}} & \frac{w^0}{2} - \frac{\eta}{\sqrt{20}} \end{bmatrix}. \quad (2.3)$$

It should be also noticed that $SU(5)/SO(5)$ is also a symmetric space in which the unbroken and broken generators satisfy the commutation relations:

$$[\bar{T}_a, \bar{T}_b] \sim \bar{T}_c, \quad [\bar{T}_a, \hat{T}_b] \sim \hat{T}_c, \quad [\hat{T}_a, \hat{T}_b] \sim \bar{T}_c,$$

which has an automorphism: $\bar{T} \to \bar{T}$ and $\hat{T} \to -\hat{T}$, and it is this Z_2 automorphism that allow us to define T-parity consistency [57, 59].

2.1 Gauge Sector

A subgroup $[SU(2)_1 \times U(1)_1] \times [SU(2)_2 \times U(1)_2]$ of the $SU(5)$ is gauged, and the generators for $[SU(2) \times U(1)]_{1,2}$ are [37]

$$Q_1^a = \begin{pmatrix} \frac{\sigma^a}{2} & 0 & 0 & 0 \\ 0 & 0 & 0 & 0 \\ 0 & 0 & 0 & 0 \\ 0 & 0 & 0 & 0 \end{pmatrix}, \; Y_1 = \mathrm{diag}(3,\, 3,\, -2,\, -2,\, -2),$$

$$Q_2^a = \begin{pmatrix} 0 & 0 & 0 & 0 \\ 0 & 0 & 0 & 0 \\ 0 & 0 & 0 & 0 \\ 0 & 0 & 0 & \frac{-\sigma^{a*}}{2} \end{pmatrix}, Y_2 = \mathrm{diag}(2,\ 2,\ 2,\ -3,\ -3), \tag{2.4}$$

where σ^a is the Pauli matrix. Since the non-linear sigma field Σ transforms as $V\Sigma V^T$ under the $SU(5)$, the kinetic term of the non-linear sigma field, which yields canonically normalized kinetic terms for NGBs, is given by [37,38]

$$\mathcal{L}_{kin} = \frac{f^2}{8} Tr(D_\mu \Sigma)^\dagger (D^\mu \Sigma), \tag{2.5}$$

where the covariant derivative is [37]

$$D_\mu \Sigma = \partial_\mu \Sigma - i \sum_{j=1,2} [g_j W_{j\mu}^a (Q_j^a \Sigma + \Sigma Q_j^{aT}) + g_j' B_{j\mu} (Y_j \Sigma + \Sigma Y_j)], \tag{2.6}$$

where $W_{j\mu}^a$ $(a = 1 \sim 3)$ and $B_{j\mu}$ are the gauge boson fields, and g_j and g_j' are gauge couplings of $[SU(2) \times U(1)]_j$ $(j = 1, 2)$, respectively. Note that the linear combination of the gauged generators $\{Q_1^a - Q_2^a,\ Y_1 - Y_2\}$ is a set of broken generators of $SU(5)$ and $\{Q_1^a + Q_2^a,\ Y_1 + Y_2\}$ is a set of unbroken generators. Using the Z_2 inner automorphism of broken and unbroken generators, it is natural to define the T-parity transformation for the gauge fields as

$$W_1 \leftrightarrow W_2,$$

$$B_1 \leftrightarrow B_2.$$

The Eq. (2.5) will generate mass terms of the gauge bosons as

$$\frac{f^2}{8}(g_1^2 W_{\mu 1}^a W_1^{a\mu} + g_2^2 W_{\mu 2} W_2^{\mu} - 2g_1 g_2 W_{\mu 1}^a W_2^{a\mu})$$

$$+ \frac{1}{5}\frac{f^2}{8}(g_1' B_{\mu 1} B_1^{\mu} + g_2' B_{\mu 2} B_2^{\mu} - 2g_1' g_2' B_{\mu 1} B_2^{\mu}). \tag{2.7}$$

It is obvious that the relations $g_1 = g_2 = \sqrt{2}g$ and $g_1' = g_2' = \sqrt{2}g'$ have to hold in order to have a T-parity invariant (for $W_1 \leftrightarrow W_2$ and $B_1 \leftrightarrow B_2$) effective Lagrangian, where g and g' are the weak and hypercharge couplings in the SM, respectively. Defining

$$W_L = \frac{W_1 + W_2}{\sqrt{2}},\ W_H = \frac{W_1 - W_2}{\sqrt{2}}, \tag{2.8}$$

$$B_L = \frac{B_1 + B_2}{\sqrt{2}},\ B_H = \frac{B_1 - B_2}{\sqrt{2}}, \tag{2.9}$$

therefore, one can check that under T-parity transformation, $W_L \to W_L$ and $W_H \to -W_H$, i.e. W_L is a "even" and W_H is "odd" under T-parity. From Eq. (2.7) and the definitions of W_L and W_H, we have

$$f^2 g^2 W_{\mu H}^+ W_H^{\mu -} + \frac{f^2 g^2}{2} W_{\mu H}^3 W_H^{\mu 3} + \frac{1}{2}\frac{f^2 g'^2}{5} B_{\mu H} B_H^{\mu}, \tag{2.10}$$

from which masses for heavy gauge bosons W_H and B_H are read as

$$m_{W_H^3} = m_{W_H^{\pm}} = gf,$$

$$m_{B_H} = \frac{g'}{\sqrt{5}} f, \tag{2.11}$$

where $W_H^{\pm} \equiv (W_H^1 \mp i W_H^2)/\sqrt{2}$, while W_L and B_L are still massless. After shifting $h \to h + v$ and electroweak symmetry is spontaneously broken, Eq. (2.5) will generate

the mass terms of W_L and B_L and mixing terms between $W_{L/H}$ and $B_{L/H}$ as

$$f^2g^2(1-\frac{1}{4}\frac{v^2}{f^2})W^+_{\mu H}W^{\mu-}_H+\frac{f^2g^2}{2}(1-\frac{1}{4}\frac{v^2}{f^2})W^3_{\mu H}W^{\mu 3}_H$$

$$+\frac{gg'}{4}\frac{v^2}{f^2}W^3_{\mu H}B^\mu_H+\frac{1}{2}\frac{f^2g'^2}{5}(1-\frac{5}{4}\frac{v^2}{f^2})B_{\mu H}B^\mu_H$$

$$+W^+_\mu W^{-\mu}\left[\frac{1}{4}g^2v^2(1-\frac{v^2}{6f^2})\right]+\frac{1}{2}W^3_{\mu L}W^{3\mu}_L\left[\frac{1}{4}g^2v^2(1-\frac{v^2}{6f^2})\right]$$

$$+\frac{1}{2}B_{\mu L}B^\mu_L\left[\frac{1}{4}g'^2v^2(1-\frac{v^2}{6f^2})\right]-W^3_{\mu L}B^\mu_L\left[\frac{1}{4}gg'v^2(1-\frac{v^2}{6f^2})\right], \tag{2.12}$$

where $W^\pm\equiv(W^1_L\mp iW^2_L)/\sqrt{2}$ are the SM $W^\pm$ bosons with a mass

$$m_{W^\pm}\sim\frac{gv}{2}(1-\frac{1}{12}\frac{v^2}{f^2}), \tag{2.13}$$

and the mass of $W^\pm_H$ is shifted slightly, and becomes

$$m_{W^\pm_H}=fg(1-\frac{1}{8}\frac{v^2}{f^2}).$$

After rotating $(W^3_\mu,\ B_\mu)$ into their mass eigenstates $(Z_\mu,\ A_\mu)$

$$\begin{pmatrix} W^3_H \\ B_H \end{pmatrix}=\begin{pmatrix} \cos\theta_H, & -\sin\theta_H \\ \sin\theta_H, & \cos\theta_H \end{pmatrix}\begin{pmatrix} Z_H \\ A_H \end{pmatrix},$$

and

$$\begin{pmatrix} W^3_L \\ B_L \end{pmatrix}=\begin{pmatrix} \cos\theta_W, & \sin\theta_W \\ -\sin\theta_W, & \cos\theta_W \end{pmatrix}\begin{pmatrix} Z \\ A \end{pmatrix}.$$

one can get masses for all the neutral gauge bosons and mixing angles,

$$
\begin{aligned}
m_{Z_H} &= fg(1-\frac{1}{8}\frac{v^2}{f^2}),\\
m_{A_H} &= \frac{g'}{\sqrt{5}}f(1-\frac{5}{8}\frac{v^2}{f^2}),\\
m_Z &= \frac{\sqrt{g^2+g'^2}}{2}v(1-\frac{1}{12}\frac{v^2}{f^2}) = \frac{m_W}{\cos\theta_W},\\
m_A &= 0,
\end{aligned}
\tag{2.14}
$$

and

$$
\begin{cases}
\cos\theta_H & \simeq 1\\
\sin\theta_H & \simeq \frac{5gg'}{4(5g^2-g'^2)}\frac{v^2}{f^2}
\end{cases},
\tag{2.15}
$$

$$
\begin{cases}
\cos\theta_W &= g/\sqrt{g^2+g'^2}\\
\sin\theta_W &= g'/\sqrt{g^2+g'^2}
\end{cases}.
\tag{2.16}
$$

In principle, Eq. (2.13) can be written in terms of arbitrary order of v/f. If we define the mass of W-boson as

$$m_W = \frac{1}{2}gv_{SM},$$

the relation between v and v_{SM} is

$$v_{SM} = v(1-\frac{1}{12}\frac{v^2}{f^2}+\mathcal{O}(\frac{v^3}{f^3})),
\tag{2.17}$$

where $v_{SM} \sim 246$ GeV. Through the rest of this thesis, all the physical quantities will be expressed in terms of v_{SM} instead of using v, and the subscript SM will be omitted. The masses of T-odd heavy gauge bosons, $W_H^{\pm}$, Z_H and A_H, only depend on the symmetry breaking scale f which can be obtained by measuring the mass of

one of the T-odd gauge bosons. Also note that the ρ parameter which is defined as

$$\rho \equiv \frac{m_W^2}{m_Z^2 \cos^2\theta_w},$$

is equal to 1 at the tree level.

2.2 T-odd Fermion Sector

To implement T-parity in the fermion sector, one has to introduce two $SU(2)$ doublets $q_{1,2}$ for each SM fermion flavor. The T-even combination is the SM fermion field, while the other one is T-odd partner of the SM fermion. To generate the heavy T-odd fermion mass, one introduces the interactions [57, 59, 72]

$$\mathcal{L}^f_{T-odd} = -\kappa f(\bar{\psi}_2 \xi \psi_c + \bar{\psi}_1 \Sigma_0 \Omega \xi^\dagger \Omega \psi_c) + h.c., \tag{2.18}$$

where

$$\psi_1 = \begin{bmatrix} q_1 \\ 0 \\ 0 \\ 0 \end{bmatrix}_L, \quad \psi_2 = \begin{bmatrix} 0 \\ 0 \\ 0 \\ q_2 \end{bmatrix}_L, \quad \psi_c = \begin{bmatrix} q_c \\ \chi_c \\ \tilde{q}_c \end{bmatrix}_R,$$

$$q_i = -\sigma_2 \begin{bmatrix} u_i \\ d_i \end{bmatrix}, \; i = 1,\, 2,\, c,$$

$\Omega = \mathrm{diag}(1,\, 1,\, -1,\, 1,\, 1)$ and ξ is defined in Eq. (2.2). Here, the $SU(2)$ doublet q_i is embedded in an incomplete $SU(5)$ multiplet, and the flavor $u\,(d)$ means $u\,(d)$, $c\,(s)$, $t\,(b)$ for quarks as well as $\nu_e\,(e)$, $\nu_\mu\,(\mu)$ and $\nu_\tau(\tau)$ for leptons. Under the T-parity transformation, $\psi_1 \leftrightarrow -\Sigma_0 \psi_2$ and $\xi \rightarrow \Omega \xi^\dagger \Omega$. From Eq. (2.18), we can see that the

	q_1	q_2	U_{L1}	U_{L2}	U_{R1}	U_{R2}	u_R	d_R
Y_1	1/30	2/15	8/15	2/15	8/15	2/15	1/3	$-1/6$
Y_2	2/15	1/30	2/15	8/15	2/15	8/15	1/3	$-1/6$

Table 2.1: $U(1)_{1,2}$ charges for fermions. . The SM hypercharge is given by $Y = Y_1 + Y_2$.

T-odd fermion, $q_- \equiv (q_1 + q_2)/\sqrt{2}$ will get a Dirac mass term with $\tilde{q}_c$ and leads to the masses of T-odd fermions as

$$m_{d_-} = \sqrt{2}\kappa f, \;\; m_{u_-} \simeq \sqrt{2}\kappa f(1 - \frac{1}{8}\frac{v^2}{f^2}). \tag{2.19}$$

The κ in Eq. (2.18) in general contains flavor indices, and large flavor mixings can cause flavor-changing-neutral-current problems [73], however, for all the studies in this these, I will take the κ to be flavor universal for quarks and leptons individually. Usually, κ is taken to be of order unity, however, we should keep in mind that it is actually an arbitrary parameter and can only be determined from the mass of T-odd particle and the scale f, cf. Eq. (2.19). If the masses of T-odd fermions are order of 1 TeV, the effect of T-odd fermions to high energy collider phenomenology will not be negligible. Actually it is quantitatively important as we will discuss in both Chapter 4 and Chapter 5.

For q_c and χ_c, we simply assume Dirac mass terms for them, as suggested in Ref. [54, 59]. Furthermore, we assume that their Dirac masses are so large (as large as about 3 TeV) that these extra T-odd fermions are decoupled, but remains to be small enough not to generate the naturalness problem in the Higgs mass parameter. Thus, we will not consider any effects induced by these extra T-odd fermions.

The $U(1)_{1,2}$ charges $Y_{1,2}$ for all fermion fields are listed in Table 2.1. Those charges are determined by the gauge invariance Yukawa interactions which we will

discuss later. The T-odd fermions also interact with their SM partner fermions and the heavy gauge boson as follows:

$$\begin{aligned}\mathcal{L} = & \frac{g}{\sqrt{2}} W^{+}_{H\mu}(\bar{u}_L \gamma^\mu d_{L-} + \bar{u}_{L-} \gamma^\mu d_L) \\ & + \sum_{f=u,d} \left[(g c_H T_{3f} + g' s_H Y') Z_{H\mu} \right. \\ & \left. + (-g s_H T_{3f} + g' c_H Y') A_{H\mu} \right] \bar{f}_L \gamma^\mu f_{L-} + h.c.,\end{aligned}$$

where $Y' = -1/10$, and $s_H(c_H) \equiv \sin\theta_H(\cos\theta)$ which is shown in Eq. (2.15).

2.3 Top Sector

In top sector, singlet fields U_{L1} and U_{L2} are introduced and embedded together with the q_1 and q_2 doublets into the following multiplets

$$Q_1 = \begin{bmatrix} q_1 \\ U_1 \\ 0 \\ 0 \end{bmatrix}_L \quad \text{and} \quad Q_2 = \begin{bmatrix} 0 \\ 0 \\ U_2 \\ q_2 \end{bmatrix}_L .$$

For the top-Yukawa interaction, one can write down the following T-parity invariant Lagrangian [54, 57, 59]

$$\begin{aligned}\mathcal{L}_{top} &= -\frac{\lambda_1}{2\sqrt{2}} f \epsilon_{ijk} \epsilon_{xy} \left[(\bar{Q}_1)_i \Sigma_{jx} \Sigma_{ky} - (\bar{Q}_2 \Sigma_0)_i \tilde{\Sigma}_{jx} \tilde{\Sigma}_{ky} \right] u_R \\ &- \lambda_2 f (\bar{U}_{L1} U_{R1} + \bar{U}_{L2} U_{R2}) + h.c., \end{aligned} \tag{2.20}$$

where ϵ_{ijk} and ϵ_{xy} are antisymmetric tensors, and i, j, k run over $1-3$ and x, y run over $1-2$; $\tilde{\Sigma}$ is the image of Σ under T-parity. Under the T-parity, these fields

transform as

$$\begin{aligned} Q_1 \leftrightarrow -\Sigma_0 Q_2 \quad &\Rightarrow \quad q_1 \leftrightarrow -q_2,\ U_{L1} \leftrightarrow -U_{L2}, \\ \Pi \rightarrow -\Omega\Pi\Omega \quad &\Rightarrow \quad \Sigma \rightarrow \tilde{\Sigma} = \Sigma_0\Omega\Sigma^\dagger\Omega\Sigma_0, \\ U_{R1} \leftrightarrow -U_{R2} \quad &, \quad u_R \leftrightarrow u_R. \end{aligned}$$

Therefore, the Eq. (2.20) will generate the mass terms as

$$\begin{aligned} -\lambda_1 v(1-\frac{v^2}{4f^2})\bar{u}_{L+}u_{R+} - \lambda_1 f(1-\frac{v^2}{2f^2})\bar{U}_{L+}u_{R+} \\ -\lambda_2 f(\bar{U}_{L+}U_{R+} + \bar{U}_{L-}U_{R-}) + h.c., \end{aligned} \tag{2.21}$$

where we have defined the fields as follows:

$$\begin{aligned} u_{L\pm} &= \frac{q_1 \mp q_2}{\sqrt{2}}, \\ U_{L\pm} &= \frac{U_{L1} \mp U_{L2}}{\sqrt{2}}, \\ U_{R\pm} &= \frac{U_{R1} \mp U_{R2}}{\sqrt{2}}, \end{aligned}$$

the subscript "$\pm$" means the quantum number "even/odd" under T-parity. The T-odd particle, U_-, gets a Dirac mass term $\lambda_2 f$, and we denote this T-odd field as T_- hereafter, i.e. $m_{T_-} = \lambda_2 f$. From Eq. (2.21), we see that in order to calculate masses of the T-even particles, we have to diagonalize the mass matrix

$$\mathbf{M} = \begin{bmatrix} \lambda_1 v_{SM}(1-\frac{v^2}{4f^2}) & 0 \\ \lambda_1 f(1-\frac{v^2}{2f^2}) & \lambda_2 f \end{bmatrix}. \tag{2.22}$$

The relation between mass eigenstates $(t,\ T_+)_{L,R}$ and gauge eigenstates $(u_+,\ U_+)_{L,R}$ are related by rotation matrices as

$$\begin{bmatrix} t_L \\ T_{L+} \end{bmatrix} = L \begin{bmatrix} u_{L+} \\ U_{L+} \end{bmatrix} \equiv \begin{bmatrix} \cos\beta & -\sin\beta \\ \sin\beta & \cos\beta \end{bmatrix} \begin{bmatrix} u_{L+} \\ U_{L+} \end{bmatrix}, \text{ and}$$

$$\begin{bmatrix} t_R \\ T_{R+} \end{bmatrix} = R \begin{bmatrix} u_{R+} \\ U_{R+} \end{bmatrix} \equiv \begin{bmatrix} \cos\alpha & -\sin\alpha \\ \sin\alpha & \cos\alpha \end{bmatrix} \begin{bmatrix} u_{R+} \\ U_{R+} \end{bmatrix}.$$

After diagonalizing the mass matrix $\mathbf{M}$, the mixing angles β and α can be derived as

$$\begin{cases} \sin\beta \simeq & \frac{\lambda_1^2}{\lambda_1^2+\lambda_2^2}\frac{v}{f}(1-\frac{\lambda_1^4+3\lambda_2^4-2\lambda_1^2\lambda_2^2}{4(\lambda_1^2+\lambda_2^2)^2}\frac{v^2}{f^2}) \\ \cos\beta \simeq & 1-\frac{\lambda_1^4}{2(\lambda_1^2+\lambda_2^2)^2}\frac{v^2}{f^2} \end{cases} \tag{2.23}$$

$$\begin{cases} \sin\alpha \simeq & \frac{\lambda_1}{\sqrt{\lambda_1^2+\lambda_2^2}}(1-\frac{\lambda_2^2(\lambda_2^2-\lambda_1^2)}{2(\lambda_1^2+\lambda_2^2)^2}\frac{v^2}{f^2}) \\ \cos\alpha \simeq & \frac{\lambda_2}{\sqrt{\lambda_1^2+\lambda_2^2}}(1-\frac{\lambda_1^2(\lambda_1^2-\lambda_2^2)}{2(\lambda_1^2+\lambda_2^2)^2}\frac{v^2}{f^2}). \end{cases} \tag{2.24}$$

The masses of t and T_+ quarks are therefore

$$m_t \simeq \frac{\lambda_1\lambda_2}{\sqrt{\lambda_1^2+\lambda_2^2}}v(1-\frac{\lambda_1^4+\lambda_2^4}{4(\lambda_1^2+\lambda_2^2)^2}\frac{v^2}{f^2}), \tag{2.25}$$

$$m_{T+} \simeq \sqrt{\lambda_1^2+\lambda_2^2}f(1-\frac{\lambda_1^2\lambda_2^2}{2(\lambda_1^2+\lambda_2^2)^2}\frac{v^2}{f^2}). \tag{2.26}$$

Note that the mass of the T-even $T_+(m_{T+})$ is always heavier than the T-odd $T_-(m_{T-})$ quark. The model parameters in the top sector are λ_1, λ_2 and f. However, λ_1 and λ_2 could be related by the top quark mass, i.e. Eq. (2.25) .

2.4 Light Quark Sector

The top quark mass is already introduced in the previous section. For light up-type quarks of the first two generations, the Lagrangian is similar to top Yukawa interactions (cf. Eq. (2.20)), but without including singlet fields, U_1 and U_2, because the contributions from the first two generations to the mass of the Higgs boson are negligible, and there is no need to add new fields.

For down-type quarks, one of the possible effective Lagrangian of Yukawa interactions is given by [74, 75]

$$\mathcal{L}_d = i\frac{\lambda_d}{2\sqrt{2}} f \epsilon_{ij}\epsilon_{xyz}\left[(\bar{\Psi}'_2)_x \Sigma_{iy}\Sigma_{jz} X - (\bar{\Psi}'_1)_x \tilde{\Sigma}_{iy}\tilde{\Sigma}_{jz}\tilde{X}\right] d_R, \tag{2.27}$$

where $\tilde{X}$ is the T-parity transformation of X, and

$$\Psi'_1 = \begin{bmatrix} -\sigma_2 q_1 \\ 0 \\ 0 \\ 0 \end{bmatrix}, \quad \Psi'_2 = \begin{bmatrix} 0 \\ 0 \\ 0 \\ -\sigma_2 q_2 \end{bmatrix}.$$

The form of X depends on how we build up the model, and the only requirement of X is that it should be a singlet field under $SU(2)_{1,2}$ with its charge under $U(1)_{1,2}$ (Y_1, Y_2) fixed to be (1/10, −1/10). One of the possible choice for X is $\Sigma_{33}^{\pm 1/4}$, and I refer $\Sigma_{33}^{1/4}$ to Case A and $\Sigma_{33}^{-1/4}$ to Case B for latter studies.

2.5 Higgs Sector

As we have shown, there are $SU(2)_L$ doublet and triplet Higgs bosons in the low energy effective theory. The gauge and Yukawa interactions break the global symmetry, so these Higgs bosons receive masses from radiative corrections via fermion

and gauge boson loops. Because of the collective symmetry breaking mechanism, the doublet Higgs boson does not receive large quadratic divergence in its mass parameter, and hence the natural mass scale of the doublet Higgs boson is of the order of weak scale. On the other hand, the triplet Higgs boson mass is not protected by such a mechanism, therefore, its mass scale is naturally of the order of f. Calculating the dominant quadratically divergent top- and gauge-loop corrections to the effective Higgs potential, one gets [37,38]

$$\begin{aligned}
\mathcal{L}_{eff} &= a_t\lambda_1^2 f^4 \epsilon^{wx}\epsilon_{yz}\epsilon^{ijk}\epsilon_{klm}(\Sigma_{iw}\Sigma_{jx}\Sigma^{*my}\Sigma^{*lz} + \tilde{\Sigma}_{iw}\tilde{\Sigma}_{jx}\tilde{\Sigma}^{*my}\tilde{\Sigma}^{*lz}) \\
&\quad + a_g f^4 \left[g^2 \mathrm{Tr} \sum_{r=1,2} (Q_r^a \Sigma)(Q_r^a \Sigma)^* + g'^2 \mathrm{Tr} \sum_{r=1,2} (Y_r \Sigma)(Y_r \Sigma)^* \right] \\
&\simeq -M_\phi^2 (\mathrm{Tr}\Phi^\dagger \Phi) + \cdots
\end{aligned} \tag{2.28}$$

where a_t and a_g are constants of the order of 1, Φ is a $SU(2)$ triplet scalar field, whose form is given as

$$\Phi = \begin{bmatrix} -i\phi^{++} & -i\phi^+/\sqrt{2} \\ -i\phi^+/\sqrt{2} & (-i\phi^0 + \phi_P^0)/\sqrt{2} \end{bmatrix}.$$

Note that because of the collective symmetry breaking mechanism, the doublet Higgs boson does not receive quadratically divergent corrections at one-loop level, however, it receives the logarithmically divergent one-loop and quadratically divergent two-loop corrections, even though we don't show them explicitly in Eq. (2.28). As shown in Eq. (2.28), the coefficient of the $\mathrm{Tr}\Phi^\dagger\Phi$ term is $-M_\Phi^2$. Hence, the mass of the triplet Higgs boson is related to the quartic coupling of the doublet Higgs boson. Consequently, there is a relation between the triplet and doublet Higgs boson masses, which is approximately expressed as

	Standard Model Particles	New Particles
quark	$\begin{pmatrix} u \\ d \end{pmatrix}, \begin{pmatrix} c \\ s \end{pmatrix}, \begin{pmatrix} t \\ b \end{pmatrix}$	$\begin{pmatrix} u_- \\ d_- \end{pmatrix}, \begin{pmatrix} c_- \\ s_- \end{pmatrix}, \begin{pmatrix} t_- \\ b_- \end{pmatrix}, T_+, T_-$
lepton	$\begin{pmatrix} \nu_e \\ e^- \end{pmatrix}, \begin{pmatrix} \nu_\mu \\ \mu^- \end{pmatrix}, \begin{pmatrix} \nu_\tau \\ \tau^- \end{pmatrix}$	$\begin{pmatrix} \nu_{e_-} \\ e_-^- \end{pmatrix}, \begin{pmatrix} \nu_{\mu_-} \\ \mu_-^- \end{pmatrix}, \begin{pmatrix} \nu_{\tau_-} \\ \tau_-^- \end{pmatrix}$
gauge boson	gluon, $W^\pm$, Z, γ	$W_H^\pm$, Z_H, A_H
scalar	h	$\phi^{\pm\pm}$, $\phi^\pm$, ϕ^0, ϕ_p^0

Table 2.2: The particle spectrum in the Littlest Higgs model with T-parity.

$$M_\Phi \simeq \frac{\sqrt{2} m_h f}{v}.$$

In summary, I list the particle spectrum of the Littlest Higgs model with T-parity in Table 2.2. Typically, A_H is the lightest T-odd particle in most of the parameter space and is a dark matter candidate. The free model parameters are f, κ_q, κ_ℓ, λ_1, λ_2 and m_h, which can be translated to physical masses of new particles and gauge couplings, as shown in the Table 2.3.

Parameter	Particle mass	Relation
f	$m_{W_H} \simeq gf$	$f \simeq m_{W_H}/g$
κ_q	$m_{q_-} \simeq \sqrt{2}\kappa_q f$	$\kappa_q \simeq m_{q_-} g/(\sqrt{2}m_{W_H})$
κ_ℓ	$m_{\ell_-} \simeq \sqrt{2}\kappa_\ell f$	$\kappa_\ell \simeq m_{\ell_-} g/(\sqrt{2}m_{W_H})$
λ_2	$m_{T_-} = \lambda_2 f$	$\lambda_2 \simeq m_{T_-} g/m_{W_H}$
λ_1	$m_t = \lambda_1\lambda_2 v/\sqrt{\lambda_1^2+\lambda_2^2}$ $m_{T_+} \simeq \sqrt{\lambda_1^2+\lambda_2^2} f$	$\lambda_1 \simeq \frac{g m_{T_-} m_t}{(g^2 m_{T_-}^2 v^2 - m_t^2 m_{W_H}^2)^{1/2}}$
m_h	$m_{\phi^{\pm\pm},\phi^{\pm},\phi^0,\phi_p^0} \simeq \sqrt{2} m_h f/v$	$m_h \simeq m_\phi v g/(\sqrt{2}m_{W_H})$

Table 2.3: The Lagrangian parameters and their relations to particle masses in the Littlest Higgs model with T-parity, where g is the weak coupling strength, m_i denotes the mass of particle i, q_- represents a T-odd quark, ℓ_- denotes a T-odd lepton and v is the vev.

Chapter 3

Constraints on Parameter Space

The electroweak sector of the Standard Model has already been precisely tested by the experimental data, especially in LEP and SLD experiments. Any new model beyond the Standard Model, generally, will shift the predictions of the electroweak observables due to the tree level mixings between the Standard Model particle fields and new particle fields or/and due to the loop contributions from new particles. As a result, the corrections to the electroweak observables could be written in terms of parameters in the new models, and the allowed parameter space would be constrained by the current experimental data. In the Littlest Higgs Model with T-parity, the free parameters are f, λ_1, λ_2, κ_ℓ, κ_q and the Higgs boson mass m_h. However, the λ_1 and λ_2 are connected by the top quark mass, we could choose either one to be the input parameter. In this Chapter, I will discuss and review how to constrain the parameters in the Littlest Higgs Model with T-parity from the theoretical argument about the unitarity and experimental data.

3.1 Global Fit

In Ref. [76], the dominant one-loop corrections to the precision electroweak observables are calculated, and the authors also perform a global fit to constrain the param-

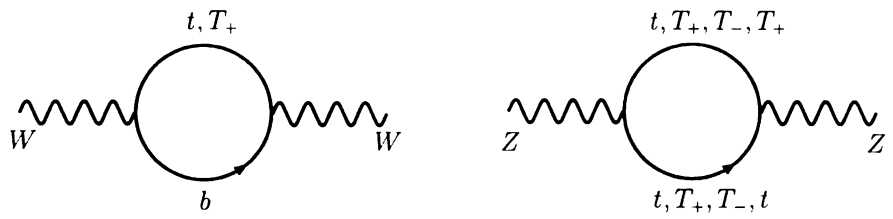

Figure 3.1: The diagrams of the most significant contribution to the oblique corrections from the top t, T_+ and T_- quarks.

eters of the Littlest Higgs Model with T-parity. In this section, I will briefly review this paper.

The electroweak observables receive contributions from the T-even T_+ quark as well as the T-odd particles. As studied in Ref. [76], the largest corrections to precision electroweak observables are induced by the one-loop diagrams involving the T-even T_+ quark, as shown in Fig. 3.1.

These oblique corrections are described in terms of the Peskin-Takeuchi S, T and U parameters [77] and the results are [76]

$$S = \frac{s_\beta^2}{2\pi}\left[\left(\frac{1}{3} - c_\beta^2\right)\ln x_t + \frac{(1+x_t)^2}{(1-x_t)^2} + \frac{2x_t^2(3-x_t)}{(1-x_t)^3}\ln x_t - \frac{8}{3}\right], \tag{3.1}$$

$$T = \frac{3}{16\pi}\frac{s_\beta^2}{s_w^2 c_w^2}\frac{m_t^2}{m_Z^2}\left[\frac{s_\beta^2}{x_t} - 1 - c_\beta^2 - \frac{2c_\beta^2}{1-x_t}\ln x_t\right], \tag{3.2}$$

$$U = -\frac{s_\beta^2}{2\pi}\left[s_\beta^2\ln x_t + \frac{(1+x_t)^2}{(1-x_t)^2} + \frac{2x_t^2(3-x_t)}{(1-x_t)^3}\ln x_t - \frac{8}{3}\right], \tag{3.3}$$

where $x_t \equiv m_t^2/m_{T_+}^2$; $s_\beta = \sin\beta$ and $c_\beta = \cos\beta$, where β is the left-handed $t - T_+$ mixing angle given in Eq. (2.23); $s_w = \sin\theta_w$ and $c_w = \cos\theta_w$, where θ_w is the weak mixing angle. If we take $x_t \ll 1$ limit, the Eqs. (3.1), (3.2) and (3.3) could be

simplified as

$$S = \frac{1}{3\pi}\left(\frac{\lambda_1}{\lambda_2}\right)^2 \frac{m_t^2}{m_{T_+}^2}\left[-\frac{5}{2} + \ln\frac{m_{T_+}^2}{m_t^2}\right], \tag{3.4}$$

$$T = \frac{3}{8\pi}\frac{1}{s_w^2 c_w^2}\left(\frac{\lambda_1}{\lambda_2}\right)^2 \frac{m_t^4}{m_{T_+}^2 m_Z^2}\left[\ln\frac{m_{T_+}^2}{m_t^2} - 1 + \frac{1}{2}\left(\frac{\lambda_1}{\lambda_2}\right)^2\right], \tag{3.5}$$

$$U = \frac{5}{6\pi}\left(\frac{\lambda_1}{\lambda_2}\right)^2 \frac{m_t^2}{m_{T_+}^2}. \tag{3.6}$$

It is obvious that the T parameter is much larger than both S and U parameters due to the enhanced factors $1/(s_w^2 c_w^2) \sim 5.6$ and $m_t^2/m_Z^2 \sim 3.7$ for the contributions from the top sector. As a result, the T parameter is about 20 times of the S parameter.

After EWSB, there is a mass splitting of the T-odd gauge bosons, $W_H^{\pm}$ and Z_H. And the contributions to the T parameter is [76]

$$T_{W_H} = -\frac{9}{16\pi s_w^2 c_w^2 m_Z^2}\frac{g^2}{8}\frac{v^4}{f^2}\ln\frac{\Lambda^2}{m_{W_H}^2},$$

where g is the weak coupling. Since the Littlest Higgs model with T-parity is non-renormalizable, it should not be surprising that the result depends on the UV cutoff scale Λ. As argued in Ref. [57], a counterterm operator of form

$$\mathcal{L}_c = \delta_c \frac{g^2}{16\pi^2} f^2 \sum_{i,a} Tr\left[\left(Q_i^a D_\mu \Sigma\right)\left(Q_i^a D^\mu \Sigma\right)^*\right],$$

where δ_c is an order-one coefficient whose exact value depends on the details of the UV physics, should be included. Therefore, the total contribution from the T-odd gauge bosons is [76]

$$T_{T-odd\,gauge} = -\frac{1}{4\pi s_w^2}\frac{v^2}{f^2}\left(\delta_c + \frac{9}{4}\ln\frac{4\pi}{g}\right),$$

where $\Lambda = 4\pi f$ is assumed. Furthermore, the T-parity partners of the SM fermions also contribute to T parameter. The contribution from each T-odd doublet fermion is given by [76]

$$T_{T-odd\,fermion} = -\frac{\kappa^2}{192\pi^2\alpha}\frac{v^2}{f^2},$$

where $\alpha \equiv e^2/(4\pi)$. Note that κ is assumed to be universal for all the T-odd fermions in the calculations. In addition to the oblique corrections, the correction to the vertex of Z boson, bottom and anti-bottom quarks, $Zb\bar{b}$, from the top quark loop is the most important one. In the Littlest Higgs model with T-parity, there are two kinds of contributions. The first one is the correction to the couplings of the top quark to the Z boson. The second one is due to the existence of additional T-even T_+ quark. In the heavy T_+ and top quark limit, the correction in additional to the SM one-loop correction is [76]

$$\delta g_L^{Zb\bar{b}} = \frac{g}{c_w}\frac{\alpha}{8\pi s_w^2}\frac{m_t^4}{m_W^2 m_{T_+}^2}\frac{\lambda_1^2}{\lambda_2^2}\ln\frac{m_{T_+}^2}{m_t^2},$$

where $\delta g_L^{Zb\bar{b}}$ denotes the correction to the left-handed coupling of the Z boson to bottom and anti-bottom quarks, $Zb_L\bar{b}_L$. However, as studied in Ref. [76], this contribution to the global fit is not significant. Using 21 experimental data determined in the Z pole [78], deviations from the SM predictions could be written in terms of the oblique parameters and $\delta g_L^{Zb\bar{b}}$ [79]. The Fig. 3.2 shows the two dimensional contour of the χ^2 fit, taking $\delta_c = 0$ and neglecting the contributions of the T-odd fermions to the T parameter. It is clear that the symmetry breaking scale f could be as low as 500 GeV. As a result, the typical mass spectrum is about or below 1 TeV, which is relatively light and makes the model phenomenologically interesting at the LHC.

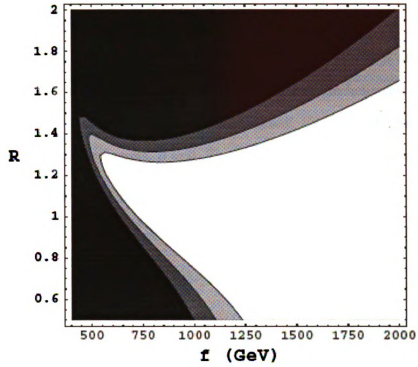

Figure 3.2: Exclusion contours of the parameter $R = \lambda_1/\lambda_2$ and f. The contributions of the T-odd fermions to the T parameter is neglected. From the lightest to the darkest, the contours correspond to the 95, 99 and 99.9 confidence level exclusion.

3.2 Unitarity and Top Quark Mass

The parameters λ_1 and λ_2 in the top sector are related by the top quark mass, cf. Eq. (2.25). If one of them is known, we could use the top quark mass to derive another. In this section, we define another parameter $R \equiv \lambda_1/\lambda_2$ and consider the untarity of a set of scattering processes that include the third generation quarks (t, b, T_+), gauge bosons ($W^\pm$, Z) and the Higgs boson, in which R is involved. The amplitudes for $t\bar{t} \to t\bar{t}$, $T_+\bar{T}_+$, $b\bar{b}$, WW, and Zh processes and their inverse processes contribute to $J = 1$ partial wave amplitude matrix in this coupled system. The $J = 1$

partial wave amplitudes are given by

$$a^1_{\mu\mu'} = \frac{1}{32\pi}\int_{-1}^{1} d(\cos\theta) d^1_{\mu\mu'}(\theta) T_{\mu\mu'}.$$

Here $d^1_{\mu\mu'}(\theta)$ is the well-known Wigner d-function. For fermions, μ and μ' are defined by $\mu = (\lambda - \bar{\lambda})/2$ and $\mu' = (\lambda' - \bar{\lambda}')/2$, where λ's are the helicities of the fermions: $\lambda\,(\bar{\lambda})$ for the initial state fermion (anti-fermion) and $\lambda'\,(\bar{\lambda}')$ for the final state fermion (anti-fermion), and for bosons, $\mu = 0$. $T_{\mu\mu'}$ is a helicity amplitude with μ and μ'.

Writing the channels in the order $t_+\bar{t}_-$, $(T_+)_+(\bar{T}_+)_-$, W^+W^-, hZ, $t_-\bar{t}_+$ and $b_-\bar{b}_+$, where the subscripts "$\pm$" denote the helicity states, the $J = 1$ partial wave amplitude matrix a^1 is given by

$$a^1 = \frac{\sqrt{2}m_t^2}{16\pi v}$$

$$\begin{pmatrix} 0 & 0 & -1 & -i & -1/\sqrt{2} & 1 \\ 0 & 0 & -R^2 & -iR^2 & R^2/\sqrt{2} & R^2/\sqrt{2} \\ -1 & -R^2 & 0 & 0 & 0 & (1+R^2) \\ i & iR^2 & 0 & 0 & i(1+R^2) & 0 \\ -1/\sqrt{2} & R^2/\sqrt{2} & 0 & -i(1+R^2) & 0 & 0 \\ 1/\sqrt{2} & R^2/\sqrt{2} & (1+R^2) & 0 & 0 & 0 \end{pmatrix}. \quad (3.7)$$

Here we have assumed that the center-of-mass energy $\sqrt{s}$ is much larger than masses of particles considered here, and only couplings in top sector are relevant, and gauge couplings and all other Yukawa couplings are taken to be zero. We have not shown explicitly the color indices in Eq. (3.7), however all color neutral channels should be taken into account. Thus the $J = 1$ partial wave amplitude matrix in this system is 14×14. Note that the parameter R is the only unknown parameter in Eq. (3.7), and the absolute value of the largest eigenvalue of the $J = 1$ partial wave amplitude

matrix increases as R gets larger. The requirement that the absolute value of the largest eigenvalue be less than a half ($|a^1_{\rm max}| < 1/2$) yields the upper bound on the parameter R as

$$R < 3.3, \text{ for } m_t = 175\,\text{GeV}.$$

In terms of $s_\alpha (= \sin\alpha)$, this bound corresponds to

$$s_\alpha < 0.96,$$

since $R = s_\alpha/c_\alpha$. This bound generates a upper bound on λ_1

$$\lambda_1 = \frac{m_t}{v\sqrt{1-s_\alpha^2}} < 2.5, \tag{3.8}$$

for $m_t = 175$ GeV.

On the other hand, the experimental value of the top quark mass m_t gives the relation between λ_1 and s_α as

$$\lambda_1 = \frac{m_t}{v}\frac{1}{\sqrt{1-s_\alpha^2}} \geq 0.71, \tag{3.9}$$

for $s_\alpha^2 \geq 0$ and $m_t = 175$ GeV. Therefore, combining Eqs. (3.8) and (3.9), we have the range for λ_1 as

$$0.71 \lesssim \lambda_1 \lesssim 2.5. \tag{3.10}$$

We could also discuss the "naturalness" constraint on these parameters. If we calculate the one-loop contribution to the Higgs mass parameter (m_h) induced by the top sector, the correction is described by

$$\Delta m_h^2 = c\frac{y_t^2}{16\pi^2} m_{T_+}^2 \equiv a_H m_h^2,$$

where $y_t = \sqrt{2}m_t/v$ and c is a constant of $\mathcal{O}(1)$. This correction should not be much larger than the Higgs boson (on-shell) mass squared m_h^2, otherwise fine-tuning

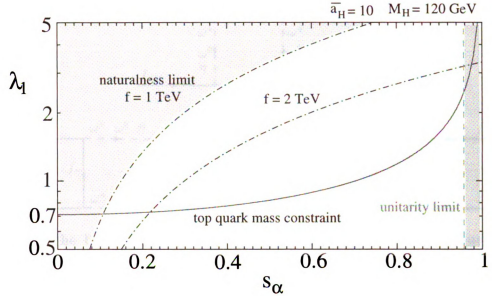

Figure 3.3: Allowed region of parameters λ_1 and s_α. Solid line (red) represents a relation between λ_1 and s_α required by top quark mass ($m_t = 175$ GeV). Dashed line (green) shows an upper limit on s_α from the unitarity bound on the $J = 1$ partial wave amplitude in the coupled system of $(t\bar{t},\ T_+\bar{T}_+,\ b\bar{b},\ WW,\ Zh)$ states, as expressed in Eq. (3.8). Dash-dotted lines (blue) show that naturalness consideration puts lower limit on s_α (or equivalently lower limit on λ_1), as shown in Eq. (3.11), and the shaded region in upper-left area of the figure is excluded for $f = 1$ TeV. For $f = 2$ TeV, the excluded region is extended to the dash-dotted line with $f = 2$ TeV. Here we have assumed $\bar{a}_H = 10$ and $m_h = 120$ GeV.

is needed. Thus the coefficient a_H is a measure of the "naturalness" of the Higgs mass correction. If we take $\bar{a}_H (= a_H/2c)$ to be smaller than 10, we get the upper limit on m_{T_+} as

$$m_{T_+} \leq 6.7\,\text{TeV}\sqrt{\frac{\bar{a}_H}{10}}\left(\frac{m_h}{120\,GeV}\right).$$

In other words, using the mass relation $m_{T_+} \simeq m_t f/(s_\alpha c_\alpha v)$, we have

$$s_\alpha \geq 0.11\sqrt{\frac{10}{\bar{a}_H}}\left(\frac{120\,\text{GeV}}{m_h}\right)\left(\frac{f}{1\,\text{TeV}}\right). \tag{3.11}$$

We summarize these constraints on the parameters of the top sector in Fig. 3.3.

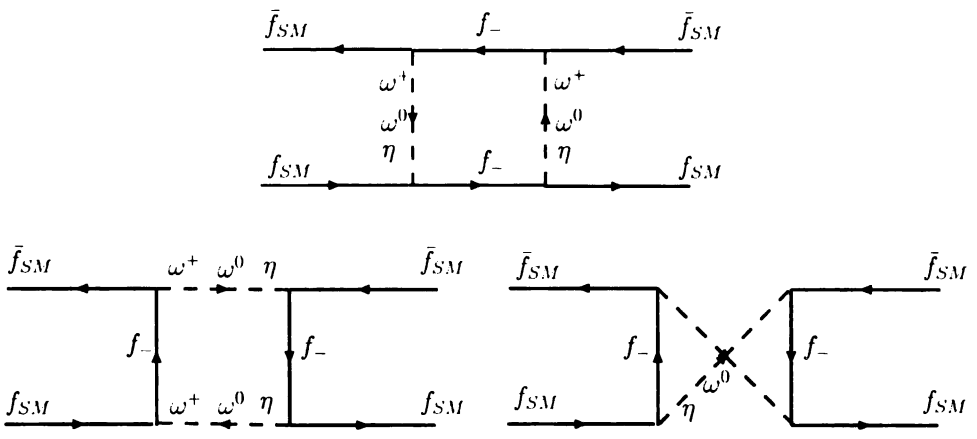

Figure 3.4: The box diagrams which give large contributions to the four-fermion operators for fixed f in the Littlest Higgs model with T-parity.

3.3 Four-Fermion Interactions

Because of the existence of the T-odd fermions, there are box diagrams which will contribute to four-fermion operators. Among them, the diagrams involving NGBs and T-odd fermions in the loop may be dangerous, as shown in Fig. 3.4, because the contributions will not vanish if we take the heavy mass limit for T-odd fermion for a fixed f. After integrating these T-odd particles out, we will have effective four-fermion contact interactions whose corrections to the SM predictions will be constrained by experimental, and as a result, the masses of T-odd fermions will be bounded.

The most general chirality invariant form of the four fermion interaction reads

$$\frac{g^2}{2\Lambda^2}\bar{\psi}_L\gamma^\mu\psi_L\bar{\psi}_L\gamma_\mu\psi_L,$$

where Λ is the new physics scale. One then can determine the scale Λ unambiguously from the unitarity condition by setting $g^2(\Lambda)/4\pi = 1$ for the new strong interaction coupling. For example, $\Lambda(eeee) > 10.3\,\text{TeV}$, $\Lambda(eedd) > 26.4\,\text{TeV}$, and $\Lambda(uudd) > 2.4\,\text{TeV}$ at 95% confidence level [29]. Using these limits, we can calculate the upper bound on T-odd fermion masses. If we assume the universal mass for T-odd lepton (ℓ_-) and quark (q_-), i.e. $\kappa_\ell = \kappa_q = \kappa$, the strongest constraint is from $O(eedd)$ [76],

which leads to

$$\kappa_\ell = \kappa_q \leq 3.4 \frac{f}{\text{TeV}} . \tag{3.12}$$

However, there is no physical reason to believe that the lepton and quark sectors will share the same κ. Here, I will consider the case that κ is different in quark and lepton sectors. As a result, the masses of the T-odd leptons will differ from the masses of the T-odd quarks. In order to avoid problems of flavor changing neutral current (FCNC), we further assume κ_ℓ and κ_q are universal individually. Under this assumption, we obtain the constraints on κ_ℓ and κ_q separately from $O(eeee)$ and $O(uudd)$ as follows:

$$\kappa_\ell \leq 8.6 \frac{f}{\text{TeV}}$$
$$\kappa_q \leq 37.1 \frac{f}{\text{TeV}}$$

However, κ_q and κ_ℓ are correlated by the $O(eedd)$ which leads to

$$\frac{\kappa_\ell^2 \kappa_q^2}{\kappa_\ell^2 - \kappa_q^2} \ln(\frac{\kappa_\ell}{\kappa_q}) \leq \frac{128\pi^3 f^2}{(26.4\,\text{TeV})^2}. \tag{3.13}$$

Note that if we take the $\kappa_q = \kappa_\ell$ limit, Eq. (3.13) will reproduce the result of Eq. (3.12). Fig. 3.5 shows the correlation of Eq. (3.13) for various values of f. The region below each curve is the allowed parameter space of κ_ℓ and κ_q for the corresponding f. The constraint is tight for small f: when $f = 500\,\text{GeV}$, large κ_q prefers smaller κ_ℓ and vice versa, for example, $\kappa_q > 4$ requires $\kappa_\ell < 1$. This constraint becomes quite loose when f becomes large.

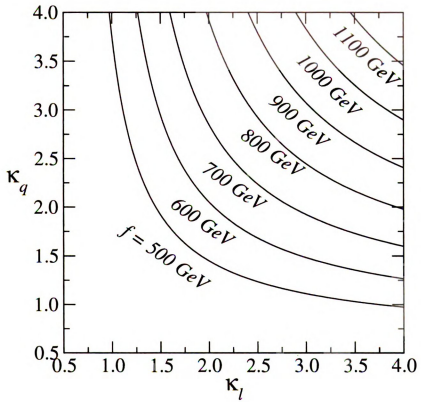

Figure 3.5: Allowed region of κ_ℓ and κ_q for various values of f. The region below each curve is allowed.

Chapter 4

Indirect Search at the LHC

The Standard Model describes the current experimental data amazingly well, therefore, the effects of new models to the precisely measured observables must be small in order not to have any contradiction. Since the predictions of these observables will be written in terms of parameters of new models, the experimental data will constraint on allowed parameter space of models, which have been reviewed in the previous chapter. For observables which are predicted by the SM but have not yet been measured, or not precisely measured, they could be used for indirect search of new models, if there exist notable differences between the new model and the SM predictions. In this Chapter, I will focus on the Littlest Higgs model with T-parity effects in top quark physics, including single-top quark and top-antitop quark pair studies, and the Higgs boson physics at the LHC.

4.1 Single Top Production at the LHC

The existence of the T-even T_+ quark will affect the coupling of the W boson to top and bottom quarks, which is refer to be Wtb coupling hereafter. The couplings of $W_\mu^+ \bar{t} b$ and $W_\mu^+ \bar{T}_+ b$ in the Littlest Higgs model with T-parity are

$$iV_{tb}\frac{g}{\sqrt{2}}c_\beta \gamma^\mu P_L, \qquad \text{and} \qquad iV_{tb}\frac{g}{\sqrt{2}}s_\beta \gamma^\mu P_L \simeq iV_{tb}\frac{g}{\sqrt{2}}s_\alpha^2 \frac{v}{f}\gamma^\mu P_L,$$

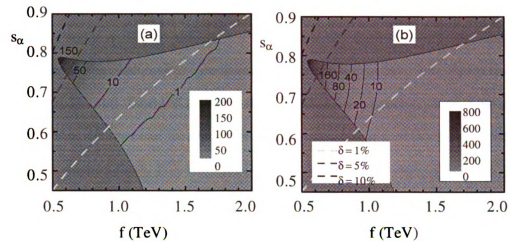

Figure 4.1: The contour of δ, mass of the T-even T_+ quark m_{T_+} and the T-odd T_- quark m_{T_-} in the $s_\alpha - f$ plan.

where V_{tb} is the value of the $(t,\ b)$ element of the Cabibbo-Kobayashi-Maskawa (CKM) matrix, $c_\beta \equiv \cos\beta$, $s_\beta \equiv \sin\beta$ and $s_\alpha \equiv \sin\alpha$ whose definitions are already shown in Eqs. (2.23) and (2.24), and $P_L = \frac{1-\gamma_5}{2}$ is the left-handed projection operator. Note that the $V_{tb}c_\beta = V_{tb}\sqrt{1-s_\beta^2}$ in the above equation is denoted as the effective CKM matrix element, V_{tb}^{eff}, which is determined from the low energy processes. Therefore the prediction of the single top quark production, which will be precisely measured at the LHC, will be different from that in the SM. In this section, I will review the study of the single-top quark production in the Littlest Higgs model with T-parity that is done in Ref. [80].

Since the strength of the Wtb coupling in the Littlest Higgs Model with T-parity is always smaller than in the SM, the single top quark production rate at the Tevatron and the LHC will be smaller than the prediction in the SM. The deviations from the

SM can be expressed in terms of s_α and the symmetry breaking scale f, as [80]

$$\delta \equiv \frac{\sigma_{SM} - \sigma_{LHT}}{\sigma_{SM}} = s_\alpha^2 \frac{v^2}{f^2} + \mathcal{O}\left(\frac{v^4}{f^4}\right).$$

Fig. 4.1 shows the contour of δ in the $s_\alpha - f$ plan, and the dark region is the 95% exclusion region from the electroweak precision test mentioned in Sec. 3.1. Since the mass of the T-even T_+ and T-odd T_- quarks only depend on s_α and f, their masses are also shown in Fig. 4.1 and can be related to δ. For example, if $\delta \lesssim 2\%$ (the region right to the yellow dashed line), $f \gtrsim 780$ GeV, $m_{T_+} \gtrsim 1.1$ TeV and $m_{T_-} \gtrsim 830$ GeV; if $2\% \lesssim \delta \lesssim 5\%$(the region between the yellow and red dashed lines), $600\,\text{GeV} \lesssim f \lesssim 1.1\,\text{TeV}$, $870\,\text{GeV} \lesssim m_{T_+} \lesssim 1.6\,\text{TeV}$ and $580\,\text{GeV} \lesssim m_{T_-} \lesssim 950\,\text{GeV}$; if $5\% \lesssim \delta \lesssim 8\%$(the region between red and blue dashed lines) , $550\,\text{GeV} \lesssim f \lesssim 680\,\text{GeV}$, $800\,\text{GeV} \lesssim m_{T_+} \lesssim 1\,\text{TeV}$ and $500\,\text{GeV} \lesssim m_{T_-} \lesssim 620\,\text{GeV}$. Furthermore, single top quark events are produced via s-channel ($q\bar{q}' \to W^* \to t\bar{b}$), t-channel ($qb \to q't$) and Wt associated channel ($gb \to Wt$). In the Littlest Higgs Model with parity, the deviations from the SM predictions on these three channels are the same at the tree level, i.e. $\delta_{s-channel} = \delta_{t-channel} = \delta_{Wt}$. This could provide a test for the T-parity, since the deviation is only due to the mixing between the top quark and the T-even T_+ quark, while there exit additional mixings between the SM gauge bosons and the heavy gauge bosons in models without T-parity.

4.2 Top Pair Production at Hadron Colliders

The top quark is a special quark in the SM due to its large mass. As the top quark mass is close to the electroweak symmetry breaking (EWSB) scale, $m_t \sim 170.9$ GeV [81], studying the top quark physics might shed lights on the mechanism of EWSB. At the Tevatron, the top quark pair is mainly produced via the quark-antiquark annihilation, whereas at the CERN Large Hadron Collider (LHC) it is

produced mainly through gluon-gluon fusion. The LHC will be a true top factory, producing hundreds of millions of top quarks every year. With such a large rate, it becomes possible to accurately measure the total cross section of the top quark pair production, which provides a good probe of searching for new physics. The new physics effects can modify the $gt\bar{t}$ coupling via quantum corrections. The non-SM one-loop corrections to the top quark pair production at hadron colliders have been studied within the general two-Higgs-doublet model (2HDM) [82–85] and the minimal supersymmetric Standard Model (MSSM) [84–98]. Within these corrections, the Yukawa electroweak radiative correction is especially interesting because of the existence of the large enhancement to the Yukawa couplings in the 2HDM [99] and MSSM [34, 35]. Significant effects indeed were found on both total cross section and differential cross section distributions, as compared to the one-loop electroweak corrections in the SM [82, 100–104]. In this section, we shall examine the leading electroweak corrections to the top quark pair production in the Littlest Higgs model with T-parity (LHT) [54, 57, 59].

Since the symmetry breaking scale f could be as low as 500 GeV, the masses of the new particles are at the order of TeV, and they may cause large quantum corrections to the top quark pair production at high energy colliders. Here, we will calculate the *leading* electroweak (EW) radiative corrections to the anomalous $gt\bar{t}$ couplings by applying the Goldstone-boson equivalence theorem (ET) [105–120]. We also examine their effects in the $q\bar{q} \to g \to t\bar{t}$ processes at the LHC. The one-loop leading EW corrections to the anomalous $gt\bar{t}$ coupling are given in terms of the Passarino-Veltman scalar functions [121], which are evaluated using the library LOOPTOOLS (FF) [122–124].

4.2.1 Form Factors of $gt\bar{t}$ and One-loop Electroweak Corrections

We shall apply the ET to calculate the leading electroweak Yukawa contributions and adopt the following notations: $\pi^0(\pi^\pm)$ is the Goldstone boson eaten by the Z-boson (W-boson); $\omega^0(\omega^\pm, \eta)$ is the Goldstone boson eaten by Z_H (W_H, A_H) *. The T-odd heavy quarks which contribute to the $gt\bar{t}$ coupling are t_-, b_- and T_-, which are T-parity partners of the SM top, bottom quarks and heavy T-even T_+ quark, respectively. The interactions between the SM top quark, the T_+ quark, scalars (the Higgs boson and Goldstone bosons), and T-odd quarks could be found by expanding the effective Lagrangian, Eq. (2.20) and Eq. (2.18). For completeness, we show them again below

$$\begin{aligned}\mathcal{L}_{top} = &-\frac{\lambda_1}{2\sqrt{2}} f \epsilon_{ijk}\epsilon_{xy}\left[(\bar{Q}_1)_i \Sigma_{jx}\Sigma_{ky} - (\bar{Q}_2\Sigma_0)_i \tilde{\Sigma}_{jx}\tilde{\Sigma}_{ky}\right] u_R \\ &- \lambda_2 f(\bar{U}_{L1}U_{R1} + \bar{U}_{L2}U_{R2}) + h.c.,\end{aligned}$$

and

$$\mathcal{L}^f_{T-odd} = -\kappa f(\bar{\psi}_2 \xi \psi_c + \bar{\psi}_1 \Sigma_0 \Omega \xi^\dagger \Omega \psi_c) + h.c..$$

The relevant couplings of the SM top quark and new heavy particles, which contribute to the loop corrections, are shown in Table 4.1 †. The coupling of the $\bar{t}FS$ interaction relevant to our calculations is given as $i(g_V + g_A\gamma_5)$, where F (S) denotes the heavy fermion (scalar). There also exist couplings between T-odd $SU(2)$ triplet scalars ϕ to the top quark, but they are neglected in this work since they are at the $\mathcal{O}(v/f)$. Since we perform our calculations in the 't Hooft-Feynman gauge, the mass of the would-be Goldstone boson is the same as its corresponding gauge boson. The

*There is an order of v^2/f^2 mixing between $\omega^\pm$ and the $SU(2)$ triplet T-odd scalars $\phi^\pm$ [76], which is neglected in our calculation.

†These Feynman rules coincide with the results in Refs. [72,125,126], up to the $\mathcal{O}(v/f)$ accuracy.

masses of the heavy particles are given as follows:

$$m_t \sim \frac{\lambda_1\lambda_2}{\sqrt{\lambda_1^2+\lambda_2^2}}v,\ m_{T_+} \sim \sqrt{\lambda_1^2+\lambda_2^2}f,\ m_{T_-} = \lambda_2 f,$$

$$m_{\omega^{\pm,0}} \sim gf,\ m_\eta \sim \frac{g'f}{\sqrt{5}},\ m_{t_-} \simeq m_{b_-} \sim \sqrt{2}\kappa f$$

where g (g') is the weak (hypercharge) gauge coupling strength, and $v \simeq 246$ GeV.

Following the parametrization in Ref. [82], the effective matrix element of $gt\bar{t}$, including the one-loop corrections, can be written as

$$-ig_s T^a \bar{u}_t \Gamma^\mu v_{\bar{t}}, \tag{4.1}$$

with

$$\Gamma^\mu = (1+\alpha)\gamma^\mu + i\beta\sigma^{\mu\nu}q_\nu + \xi\left(\gamma^\mu - \frac{2m_t}{\hat{s}}q^\mu\right)\gamma_5, \tag{4.2}$$

where the loop-induced form factors α, β and ξ are usually refered to the chromo-charge, chromo-magnetic-dipole and chromo-anapole form factors, respectively. Here, g_s is the strong coupling strength, T^a are the color generators, $q = p_t + p_{\bar{t}}$, and $\hat{s} = (p_t + p_{\bar{t}})^2$. After summing over the final state and averaging over the initial state colors and spins, the constituent total cross section of $q\bar{q} \to g \to t\bar{t}$ is [82]

$$\hat{\sigma} = \frac{8\pi\alpha_s^2}{27\hat{s}^2}\sqrt{1-\frac{4m_t^2}{\hat{s}}}\left\{\hat{s}+2m_t^2+2\Re\left[(\hat{s}+2m_t^2)\alpha+3m_t\hat{s}\,\beta\right]\right\}, \tag{4.3}$$

where $\alpha_s \equiv g_s^2/(4\pi)$ and $\Re$ denotes taking its real part. Note that ξ does not contribute as a result of the interference with the Born matrix element, but for completeness we will present the analytical expressions of those three form factors in the LHT model below.

At the one-loop level, the $gt\bar{t}$ coupling receives two kinds of quantum corrections: one is the triangle-loop correction (Fig. 4.2 a), the other is the self-energy correction

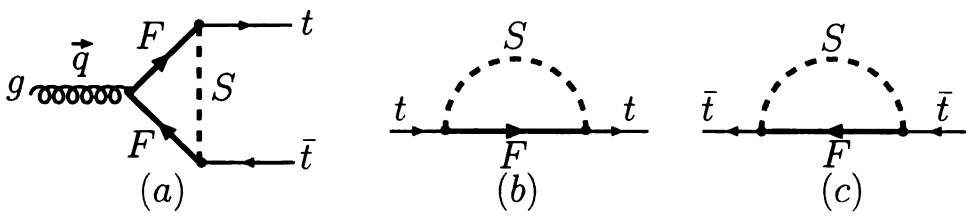

Figure 4.2: Feynman diagrams of the one-Loop corrections to the $gt\bar{t}$ coupling in the LHT model: (a) the vertex correction; (b) and (c) the wave function renormalization.

	$\bar{t}T_+h$	$\bar{t}T_+\pi^0$	$\bar{t}t_-\omega^0$	$\bar{t}t_-\eta$	$\bar{t}b_-\omega^-$	$\bar{t}T_-\eta$
g_V	$-\frac{\lambda_1^2}{2\sqrt{\lambda_1^2+\lambda_2^2}}$	$i\frac{\lambda_1^2}{2\sqrt{\lambda_1^2+\lambda_2^2}}$	$i\frac{\sqrt{2}}{4}\kappa$	$-i\frac{\sqrt{10}}{20}\kappa$	$i\frac{1}{2}\kappa$	$-i\frac{\sqrt{5}}{5}\frac{\lambda_1\lambda_2}{\sqrt{\lambda_1^2+\lambda_2^2}}$
g_A	$-\frac{\lambda_1^2}{2\sqrt{\lambda_1^2+\lambda_2^2}}$	$i\frac{\lambda_1^2}{2\sqrt{\lambda_1^2+\lambda_2^2}}$	$i\frac{\sqrt{2}}{4}\kappa$	$-i\frac{\sqrt{10}}{20}\kappa$	$i\frac{1}{2}\kappa$	$i\frac{\sqrt{5}}{5}\frac{\lambda_1\lambda_2}{\sqrt{\lambda_1^2+\lambda_2^2}}$

Table 4.1: The relevant couplings to the calculations of the leading electroweak one-loop corrections to $q\bar{q} \to g \to t\bar{t}$.

to the external top quark lines (Fig. 4.2 b) and (Fig. 4.2 c). For simplicity, we use the particles running inside the loop to represent the corresponding loop correction diagram. For example, Fig. 4.2 (a) is denoted as (F, F, S). In the LHT model, the diagrams contributing to the anomalous $gt\bar{t}$ coupling are given by $(T_+, T_+, h/\pi^0)$, $(t_-, t_-, \eta/\omega^0)$, $(b_-, b_-, \omega^\pm)$ and (T_-, T_-, η). The couplings of the $gF\bar{F}$ vertex are just the usual strong coupling while the $\bar{t}FS$ couplings are given in Table 4.1.

We use dimensional regularization to regulate the ultraviolet divergences and adopt the on-mass-shell renormalization scheme. In this scheme, the wave function renormalization corrections of the external top quark legs are canceled by the corresponding counterterms. We will regularize the ultraviolet divergences in our calculation by dimensional regularization with the regulator defined by

$$\Delta = \frac{1}{\epsilon} - \gamma_E + \ln 4\pi,$$

where $2\epsilon \equiv 4 - n$, n is the dimensionality of space-time and γ_E is the Euler constant.

As we are calculating the leading EW corrections to the $gt\bar{t}$ coupling, we do not need introduce the counterterm for the strong coupling. By introducing appropriate counterterms, one can easily deduce the renormalized vertex of $gt\bar{t}$ as

$$-ig_s T^a \bar{u}_t \left(\gamma^\mu + \delta\Gamma^\mu_{\rm ren}\right) v_t,$$

where

$$\begin{aligned}\delta\Gamma^\mu_{ren} &= \gamma^\mu \left(\frac{1}{2}\delta Z_V^{t*} + \frac{1}{2}\delta Z_A^{t*}\gamma_5 + \frac{1}{2}\delta Z_V^{\bar{t}} + \frac{1}{2}\delta Z_A^{\bar{t}}\gamma_5\right) + \delta\Gamma^\mu_{vertex} \\ &= \gamma^\mu \left(\delta Z_V^t + \delta Z_A^t \gamma_5\right) + \delta\Gamma^\mu_\triangle \end{aligned} \tag{4.4}$$

Here, $\delta Z^{t,\bar{t}}_{V,A}$ denote the wave function renormalization constants of the external top quark lines, defined by $Z_{t,\bar{t}} \equiv 1 + \delta Z_{t,\bar{t}} = 1 + \delta Z_V^{t,\bar{t}} + \delta Z_A^{t,\bar{t}}\gamma_5$, while $\delta\Gamma_\triangle$ denotes the triangle loop corrections to the vertex. Clearly, the δZ_V counterterms only contribute to the form factor α, the δZ_A counterterms only contribute to the form factor ξ, but the vertex corrections $\delta\Gamma_\triangle$ contribute to all three form factors. We thus write the form factors as follows,

$$\alpha = \alpha_\triangle + \delta Z_V, \qquad \beta = \beta_\triangle, \qquad \xi = \xi_\triangle + \delta Z_A \tag{4.5}$$

where $\alpha_\triangle$, $\beta_\triangle$ and $\xi_\triangle$ denote the coefficients of the γ^μ, $\sigma^{\mu\nu}q_\nu$ and $\gamma^\mu\gamma_5$ terms in $\delta\Gamma^\mu_\triangle$, respectively. Note that there is an additional term $q^\mu\gamma_5$ in $\delta\Gamma^\mu_\triangle$. After adding the δZ_A counterterms, we can write the combination of $\gamma^\mu\gamma_5$ and $q^\mu\gamma_5$ in a compact form as the ξ term in Eq. (4.2).

Consider the renormalization constants. The wave function renormalization constants can be determined from the top quark self-energy, see Figs. 4.2 (b, c), which can be decomposed as follows:

$$\Sigma(\not{p}) = \not{p}\left[\Sigma_V\left(p^2\right) + \Sigma_A\left(p^2\right)\gamma_5\right] + m_t\Sigma_S\left(p^2\right). \tag{4.6}$$

In the on-shell scheme, the finite parts of the counterterms are determined by the requirement that the residue of the fermion propagator is equal to one, which fixes the wave function renormalization constants by

$$\delta Z_V = -\Sigma_V\left(p^2 = m_t^2\right) - 2m_t^2 \frac{\partial}{\partial p^2}\left(\Sigma_V + \Sigma_S\right)|_{p^2=m_t^2}, \tag{4.7}$$

$$\delta Z_A = -\Sigma_A\left(p^2 = m_t^2\right). \tag{4.8}$$

In the LHT model, they are given by

$$\begin{aligned}\delta Z_V = {} & \frac{1}{16\pi^2}\frac{g_V^2 + g_A^2}{2m_t^2}\left\{A_0\left(m_S^2\right) - A_0\left(m_F^2\right) + \left(m_F^2 - m_S^2 - m_t^2\right)B_0\left(m_t^2\right)\right\} \\ & + \frac{1}{16\pi^2}\left[g_V^2\left(-m_t^2 + m_S^2 - m_F^2 - 2m_t m_F\right)\right. \\ & \left. + g_A^2\left(-m_t^2 + m_S^2 - m_F^2 + 2m_t m_F\right)\right]B_0'\left(m_t^2\right),\end{aligned} \tag{4.9}$$

$$\delta Z_A = \frac{1}{16\pi^2}\frac{g_V g_A}{m_t^2}\left\{A_0\left(m_S^2\right) - A_0\left(m_F^2\right) + \left(m_F^2 - m_S^2 + m_t^2\right)B_0\left(m_t^2\right)\right\}, \tag{4.10}$$

where A_0 and B_0 are the well-known one-point and two-point scalar functions [121]. For completeness, their definitions are given in the Appendix. We also introduce the following shorthand notations,

$$B_0\left(m_t^2\right) \equiv B_0\left(m_t^2; m_S^2, m_F^2\right), \qquad B_0'\left(m_t^2\right) \equiv \frac{\partial}{\partial p^2} B_0\left(p^2; m_S^2, m_F^2\right)\Big|_{p^2=m_t^2}.$$

Now consider the vertex corrections $\delta\Gamma_{\triangle}^{\mu}$, which we decompose into the form factors $\alpha_{\triangle}$, $\beta_{\triangle}$ and $\xi_{\triangle}$ listed below. The form factor $\alpha_{\triangle}$ is given by

$$\begin{aligned}\alpha_{\triangle} = {} & -\frac{g_V g_V^*}{16\pi^2}\left\{\alpha_1 + \alpha_2 B_0\left(\hat{s}\right) + \alpha_3 B_0\left(m_t^2\right) + \alpha_4 C_0\right\} \\ & - \frac{g_A g_A^*}{16\pi^2}\left\{\alpha_1' + \alpha_2' B_0\left(\hat{s}\right) + \alpha_3' B_0\left(m_t^2\right) + \alpha_4' C_0\right\},\end{aligned} \tag{4.11}$$

where

$$\alpha_1 = \frac{\hat{s}}{2\left(\hat{s}-4m_t^2\right)} + \frac{2}{\hat{s}-4m_t^2}\left[-A_0(m_S^2)+A_0(m_F^2)\right], \tag{4.12}$$

$$\alpha_2 = \frac{1}{2(\hat{s}-4m_t^2)^2}\Big[-16m_t^4 - 32m_F m_t^3 + (-16m_F^2+16m_S^2+14\hat{s})m_t^2 + 8m_F\hat{s}m_t - \hat{s}^2 - 2m_F^2\hat{s} + 2m_S^2\hat{s}\Big], \tag{4.13}$$

$$\alpha_3 = \frac{1}{2(\hat{s}-4m_t^2)^2}\Big[32m_F m_t^3 + (32m_F^2 - 32m_S^2 - 6\hat{s})m_t^2 - 8m_F\hat{s}m_t - 2\hat{s}(m_F^2-m_S^2)\Big], \tag{4.14}$$

$$\begin{aligned}\alpha_4 = \frac{1}{2(\hat{s}-4m_t^2)^2}\Big[&16m_t^6 + 32m_F m_t^5 + (32m_F^2 - 32m_S^2 - 6\hat{s})m_t^4 \\ &+ (32m_F^3 - 32m_F m_S^2 - 24m_F\hat{s})m_t^3 \\ &+ (16m_F^4 + 16m_S^4 - 32m_F^2m_S^2 + 2\hat{s}^2 - 28m_F^2\hat{s} + 20m_S^2\hat{s})m_t^2 \\ &+ (4m_F\hat{s}^2 - 8m_F^3\hat{s} + 8m_F m_S^2\hat{s})m_t + 2m_F^2\hat{s}^2 + 2m_F^4\hat{s} + 2m_S^4\hat{s} - 4m_F^2m_S^2\hat{s}\Big],\end{aligned} \tag{4.15}$$

and

$$\alpha_1' = \alpha_1, \qquad \alpha_{2,3,4}' = \alpha_{2,3,4}\Big|_{m_F\to -m_F}.$$

Here we introduce the following shorthand notations,

$$B_0(\hat{s}) \equiv B_0\left(\hat{s}; m_t^2, m_t^2\right), \qquad C_0 \equiv C_0\left(m_t^2, \hat{s}; m_S^2, m_F^2, m_F^2\right),$$

where $C_0(...)$ is the usual three-point scalar function [121]. The form factor $\beta_\triangle$ is given by

$$\begin{aligned}\beta_\triangle = &\frac{g_V g_V^*}{16\pi^2}\left\{\beta_1 + \beta_2 B_0(\hat{s}) + \beta_3 B_0\left(m_t^2\right) + \beta_4 C_0\right\} \\ &+ \frac{g_A g_A^*}{16\pi^2}\left\{\beta_1' + \beta_2' B_0(\hat{s}) + \beta_3' B_0\left(m_t^2\right) + \beta_4' C_0\right\},\end{aligned} \tag{4.16}$$

where

$$\beta_1 = \frac{m_t}{\hat{s} - 4m_t^2} + \frac{1}{m_t(\hat{s} - 4m_t^2)} \left[-A_0(m_S^2) + A_0(m_F^2) \right], \tag{4.17}$$

$$\beta_2 = \frac{1}{(\hat{s} - 4m_t^2)^2} \left[2m_t^3 - 8m_F m_t^2 + (-6m_F^2 + 6m_S^2 + \hat{s})m_t + 2m_F \hat{s} \right], \tag{4.18}$$

$$\begin{aligned} \beta_3 = \frac{1}{m_t(\hat{s} - 4m_t^2)^2} \Big[& -2m_t^4 + 8m_F m_t^3 + (10m_F^2 - 10m_S^2 - \hat{s})m_t^2 \\ & - 2m_F \hat{s} m_t + (m_S^2 - m_F^2)\hat{s} \Big], \end{aligned} \tag{4.19}$$

$$\begin{aligned} \beta_4 = \frac{-2}{(\hat{s} - 4m_t^2)^2} \Big[& m_t^5 + 4m_F m_t^4 + (2m_F^2 + 2m_S^2 - \hat{s})m_t^3 \\ & - m_F(4m_F^2 - 4m_S^2 + \hat{s})m_t^2 \\ & + \left(-3m_F^4 + m_F^2(6m_S^2 + \hat{s}) - 3m_S^4 - 2m_S^2 \hat{s} \right) m_t + m_F(m_F^2 - m_S^2)\hat{s} \Big], \end{aligned} \tag{4.20}$$

$$\tag{4.21}$$

and

$$\beta_1' = \beta_1, \qquad \beta_{2,3,4}' = \beta_{2,3,4}\Big|_{m_F \to -m_F}.$$

Finally, the form factor $\xi_\triangle$ is given by

$$\xi_\triangle = -\frac{g_V g_A^*}{16\pi^2} \left\{ -1 + \xi_1 B_0(\hat{s}) + \xi_2 B_0\left(m_t^2\right) + \xi_3 C_0 \right\}, \tag{4.22}$$

where

$$\xi_1 = \frac{1}{\hat{s} - 4m_t^2} \left[2m_t^2 - 2m_S^2 + 2m_F^2 + \hat{s} \right], \tag{4.23}$$

$$\xi_2 = \frac{-2}{\hat{s} - 4m_t^2} \left[m_F^2 - m_S^2 + 3m_t^2 \right], \tag{4.24}$$

$$\xi_3 = \frac{-2}{\hat{s} - 4m_t^2} \left[m_t^4 - (2m_F^2 + 2m_S^2 + \hat{s})m_t^2 + m_S^4 + m_F^4 - 2m_F^2 m_S^2 + m_F^2 \hat{s} \right].$$

$$\tag{4.25}$$

Since only B_0 and A_0 scalar functions contain the ultra-violet (UV) divergence,

$$B_0 = \frac{1}{\epsilon} + finite, \qquad A_0\left(q^2\right) = \frac{q^2}{\epsilon} + finite,$$

one can easily check that the UV divergences in $\delta\Gamma^{\mu}_{\triangle}$ indeed cancel with those in the counterterms.

4.2.2 Numerical result

The model parameters for the numerical evaluation are λ_1, λ_2, κ and f. As λ_1 and λ_2 are related by the mass of the top quark, cf. Eq. (2.25), we could choose either one as the input parameter, and in this study λ_1 is chosen. As pointed out from the partial wave study in Sec. 3.2, λ_1 should be bounded in the region $0.71 \lesssim \lambda_1 \lesssim 2.51$. Furthermore, if κ is not universal for quark and lepton sectors, as shown in Sec. 3.3, the upper bound for κ of the quark sector from the constrains of four-fermion operators could be quite loose even for a low f value, say $f \sim 500$ GeV. For illustration, we choose the values of the parameters as follows:

$$\lambda_1 = 2.5, \qquad \kappa = 5, \qquad f = 500\,\text{GeV}, \qquad m_t = 175\,\text{GeV},$$
$$m_W = 80.4\,\text{GeV}, \qquad m_Z = 91.2\,\text{GeV}, \qquad m_h = 120(500)\,\text{GeV},$$

where m_W, m_Z and m_h denote masses of the W boson, Z boson and Higgs boson, respectively, and the bottom quark is considered massless throughout this study. With the chosen parameters, the masses of new heavy particles are given by

$$m_{T_+} = 1302\,\text{GeV}, \quad m_{T_-} = 364\,\text{GeV},$$

$$m_{t_-} \simeq m_{b_-} = 3536\,\text{GeV}, \quad m_{\omega^{\pm,0}} = 327\,\text{GeV}, \quad m_\eta = 78\,\text{GeV}.$$

Since, as a result of the interference with the Born matrix element, ξ does not contribute, we need only the form factors α and β, which depend on both the couplings

(g_V and g_A) and the masses of the scalars and fermions flowing in the loops. We split the form factors in the LHT, α_{LHT} and β_{LHT}, as follows:

$$\alpha_{LHT} = \alpha_{SM} + \alpha_{HEAVY}, \qquad \beta_{LHT} = \beta_{SM} + \beta_{HEAVY},$$

where the subscript *SM* and *HEAVY* denote contributions to form factors which are induced by the SM loops and the new heavy particle loops, respectively. In Figs. 4.3(a) and (c), we present the values of form factors α and β as a function of the invariant mass of the top quark pair system, respectively. In order to investigate the dependence of the SM Higgs boson mass, we also choose two different Higgs boson masses: $m_h = 120\,\text{GeV}$ and $m_h = 500\,\text{GeV}$. We note a few interesting points listed as follows:

- For $m_{t\bar{t}} > 500\,\text{GeV}$, α_{SM} is negative but α_{HEAVY} is positive. Furthermore, in the region of $400\,\text{GeV} < m_{t\bar{t}} < 2000\,\text{GeV}$, $\alpha_{HEAVY} \simeq |\alpha_{SM}|$. Therefore, their sum, α_{LHT}, is around zero. The small kink in α_{HEAVY} near $m_{t\bar{t}} \sim 2m_{T_-}\,\text{GeV}$ is due to the threshold effect from producing the $T_-\bar{T}_-$ pair. However, in the large $m_{t\bar{t}}$ region, e.g. $m_{t\bar{t}} > 2500\,\text{GeV}$, α_{HEAVY} receives a large corrections from the $(T_+, T_+, h/\pi^0)$ loops, and is much larger than $|\alpha_{SM}|$. In particular, α_{HEAVY} reaches its maximum around the threshold region, i.e. $m_{t\bar{t}} \sim 2m_{T_+}$. As a result, α_{LHT} is positive and much larger than α_{SM} in the large $m_{t\bar{t}}$ region, see the (black) solid line ($m_h = 120\,\text{GeV}$) and the (blue) dotted line ($m_h = 500\,\text{GeV}$) in Fig. 4.3(a). In the small $m_{t\bar{t}}$ region, i.e. $m_{t\bar{t}} < 500\,\text{GeV}$, α_{HEAVY} is negligible and $\alpha_{LHT} \simeq \alpha_{SM}$.

- The form factor β_{HEAVY} is always negative, see the (black) solid line (LHT) and the (red) dashed line (SM) in Fig. 4.3(d). In the large $m_{t\bar{t}}$ region, both β_{LHT} and β_{SM} are negligible. Note that the chromo-magnetic-dipole form

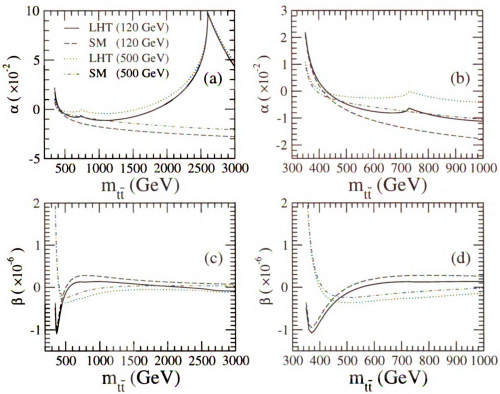

Figure 4.3: Dependence of the form factors on the invariant mass of the top quark pair in both the LHT and SM: (a) and (b) α; (c) and (d) β. (b) and (d) is the same as (a) and (c), respectively, but focusing on $m_{t\bar{t}} < 1\,\text{TeV}$ region.

factor β can contribute to the branching ratio of $b \to s\gamma$ process [127–130], and our numerical results are consistent with the current bounds [129].

Below, we will examine the effects of the leading EW corrections on the top quark pair production at the LHC. For that, we calculate the differential cross section, $d\sigma/dm_{t\bar{t}}$, given by

$$\frac{d\sigma}{dm_{t\bar{t}}} = \int dx_1 dx_2 \left\{ f_{q/p}(x_1, Q)\, f_{\bar{q}/p}(x_2, Q)\, \frac{d\hat{\sigma}}{dm_{t\bar{t}}}(q\bar{q} \to t\bar{t}) + (x_1 \leftrightarrow x_2) \right\},$$

where $\hat{\sigma}$ labels the hard process cross section, and $f_{q/p}(x, Q)$ denotes the parton distribution function of finding the parton q in the colliding proton with the momentum fraction x. Q is the factorization scale of the hard scattering process. In our calculations, we use the CTEQ 6.1 parton distribution functions [131]. We note that

at the LHC, the dominant mechanism for top quark pair production is via gluon-gluon fusion, i.e., $gg \to t\bar{t}$. Nevertheless, in this work, we focus on the new physics effect predicted by the LHT to top quark pair production cross section in the quark and anti-quark scattering processes. To examine in detail the effect of leading EW corrections, we calculate the relative corrections defined as

$$\frac{\Delta\sigma}{\sigma^0} \equiv \left(\frac{d\sigma}{dm_{t\bar{t}}} - \frac{d\sigma_0}{dm_{t\bar{t}}}\right) / \frac{d\sigma_0}{dm_{t\bar{t}}},$$

where σ_0 denotes the tree-level SM cross section. Fig. 4.4(a) shows our numerical results, while Fig. 4.4(b) reveals the details of the small $m_{t\bar{t}}$ region of Fig. 4.4(a). It is clear that the relative corrections are dominated by α, because α is much larger than β. Again, we find that the negative EW corrections in the SM are almost canceled by the positive EW corrections from the new heavy particle loops in the LHT model in the region of $m_{t\bar{t}} < 2000\,\text{GeV}$. In the large $m_{t\bar{t}}$ region, the leading EW corrections in the LHT model could increase the cross section by about 20%. However, such a deviation might hardly be recognized as the cross section drops rapidly with increasing $m_{t\bar{t}}$. Moreover, bearing in mind that the top quark pair production at the LHC is predominately via the gluon-gluon fusion process, a systematic study including the $gg \to t\bar{t}$ process should be one of the future projects needed to be done.

4.3 Production and Decay of the Higgs Boson

In Little Higgs models, one of the characteristic features is to introduce a vector-like quark with a specific coupling to the Higgs boson so that the contribution from this new particle to the mass of the Higgs boson at one-loop level will exactly cancel the contribution from the top quark. Since the most severe quadratically divergent correction is removed, the Higgs boson is naturally light without a serious fine-tuning. In the Littlest Higgs Model with T-parity (LHT), the T-even T_+ quark plays such a

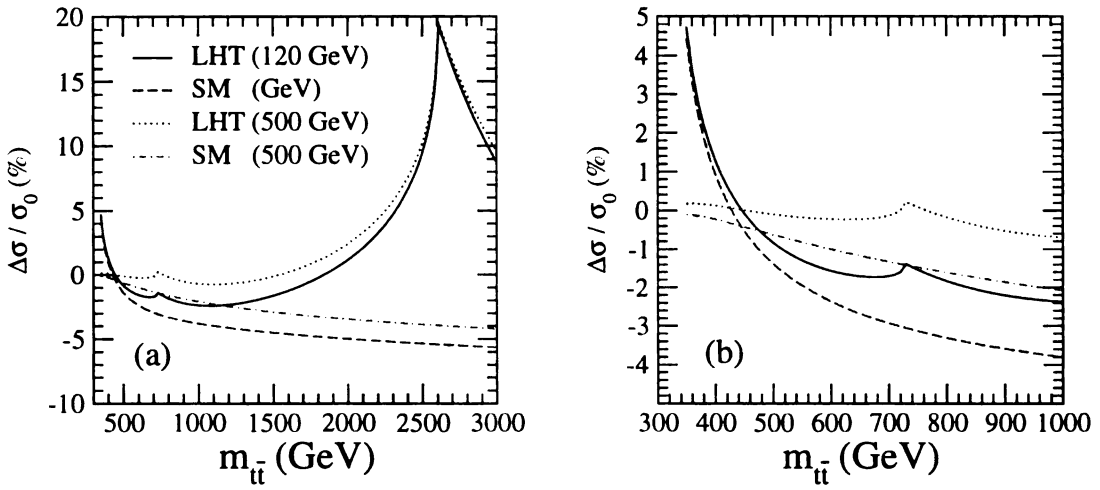

Figure 4.4: The ratio of the one-loop leading EW correction to the Born level total cross section of $q\bar{q} \to g \to t\bar{t}$ at the LHC. (b) is the same as (a) but focusing on the small $m_{t\bar{t}}$ region.

role. The cancellation between the T_+ and the top quark is shown in the Fig. 1.6. As mentioned before, the T-parity requires a set of T-odd particles which are the T-parity partners of the SM particles, these new particles will also have quadratic divergence contribution to the Higgs boson mass. Fortunately, the cancellation happens neatly between these T-odd particles.

One interesting picture of the self-energy diagram of the Higgs boson is that, if we attach two gluon lines to the fermion loop, as shown in Fig. 4.5, and one of the Higgs takes its vev, we will see immediately that the diagram becomes the Higgs boson production via the gluon-gluon fusion process. In the SM, the Higgs boson production at the LHC is dominated by the gluon-gluon fusion process with the top quark in the loop because of the large top quark Yukawa coupling and the existence of a non-decoupling effect in heavy top quark limit. In the LHT model, both the T-even T_+ quark and almost all the T-odd particles will contribute to the total cross section of the Higgs boson production. In the rest of this section, I will discuss in detail how large the effects from new particles are and how the result will affect the

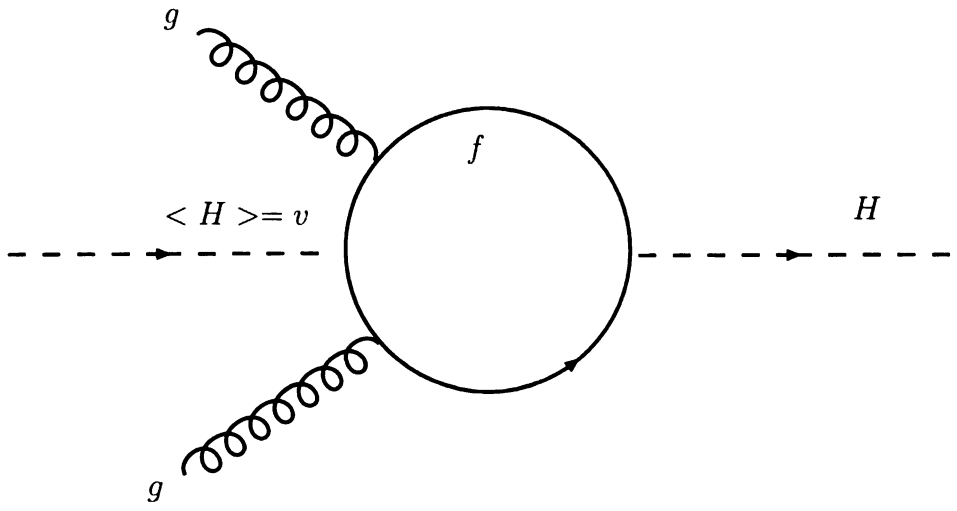

Figure 4.5: Illustration of the Higgs boson production via gluon-gluon fusion process.

strategy of searching for the Higgs boson at the LHC.

4.3.1 Yukawa Couplings of the Top and T_+ quarks

The large top Yukawa coupling generates a quadratically divergent correction to the Higgs boson mass. In order to cancel this divergence, one introduces $SU(2)$ singlet fields U_1 and U_2, which are embedded into the following multiplets:

$$Q_1 = \begin{pmatrix} q_1 \\ U_1 \\ 0 \\ 0 \end{pmatrix}, \; Q_2 = \begin{pmatrix} 0 \\ 0 \\ U_2 \\ q_2 \end{pmatrix},$$

and constructs the T-parity invariant Lagrangian [59,72,76], as mentioned in Sec. 2.3:

$$\begin{aligned} \mathcal{L}_{\sqcup} = & -\frac{\lambda_1}{2\sqrt{2}} f \epsilon_{ijk}\epsilon_{xy} \left[(\bar{Q}_1)_i \Sigma_{jx} \Sigma_{ky} - (\bar{Q}_2 \Sigma_0)_i \tilde{\Sigma}_{jx} \tilde{\Sigma}_{ky} \right] u_R \\ & - \lambda_2 f (\bar{U}_1 U_{R_1} + \bar{U}_2 U_{R_2}) + \text{h.c.}, \end{aligned} \tag{4.26}$$

here ϵ_{ijk} and ϵ_{xy} are antisymmetric tensors, and i, j and k run over $1 \sim 3$ and x and y over $4 \sim 5$. Under T-parity, these fields transform as

$$Q_1 \leftrightarrow -\Sigma_0 Q_2,\ U_{R_1} \leftrightarrow -U_{R_2} \text{ and } u_R \to u_R.$$

The above Lagrangian contains the following neutral Higgs boson interactions

$$\mathcal{L}_t \simeq -\lambda_1 f \left(\frac{s_\Sigma}{\sqrt{2}} \bar{u}_{L_+} u_R + \frac{1+c_\Sigma}{2} \bar{U}_{L_+} u_R - \lambda_2 f \left(\bar{U}_{L_+} U_{R_+} + \bar{U}_{L_-} U_{R_-} \right) \right)$$

$$- \lambda_2 f \left(\bar{U}_{L_+} U_{R_+} + \bar{U}_{L_-} U_{R_-} \right) + \text{h.c.}\,, \tag{4.27}$$

where $c_\Sigma \equiv \cos(\frac{\sqrt{2}(v+h)}{f})$ and $s_\Sigma \equiv \sin(\frac{\sqrt{2}(v+h)}{f})$ which are originated from the non-linear sigma model field Σ. As shown in Sec. 2.3, one T-odd fermion T_- gets a mass $m_{T'_-} = \lambda_2 f$ (cf. Eq. (2.21)), and note that T_- does not interact with the Higgs boson at tree level, and thus it does not contribute to the gluon fusion process at the one-loop order. The left-handed (right-handed) top quark and T_+ quark are linear combinations of u_{L_+} and U_{L_+} (u_R and U_{R+}) with masses $m_t \simeq \lambda_1\lambda_2/\sqrt{\lambda_1^2+\lambda_2^2}\, v$ and $m_{T_+} \simeq \sqrt{\lambda_1^2+\lambda_2^2} f$, as shown in Sec. 2.3.

From Eq. (4.27), we find that the Higgs boson interactions are approximately given by

$$-\mathcal{L} = g^{LHT}_{h\bar{t}t} h \bar{t}_L t_R + g^{LHT}_{h\bar{T}T} h \bar{T}_L T_R + \text{h.c.},$$

where

$$g^{LHT}_{h\bar{t}t} \simeq \frac{m_t}{v} \left\{ 1 - \frac{3+2R^2+3R^4}{4(1+R^2)^2} \frac{v^2}{f^2} + \cdots \right\} \tag{4.28}$$

$$= g^{SM}_{h\bar{t}t} \left\{ 1 - \frac{3+2R^2+3R^4}{4(1+R^2)^2} \frac{v^2}{f^2} + \cdots \right\}, \tag{4.29}$$

$$g^{LHT}_{h\bar{T}T} \simeq -\frac{m_t}{v} \frac{R}{1+R^2} \frac{v}{f} + \cdots = -g^{SM}_{h\bar{t}t} \frac{R}{1+R^2} \frac{v}{f} + \cdots, \tag{4.30}$$

with $R = \lambda_1/\lambda_2$ and $v \simeq 246$ GeV , and $g^{SM}_{h\bar{t}t}$ is the top quark Yukawa coupling in the SM. It is important to note that the relation between the top mass and its Yukawa coupling is modified in this model: the top Yukawa coupling is reduced, compared to that in the SM. In addition, the heavy T_+ quark also has a Yukawa interaction, but its sign is opposite to that of the top Yukawa coupling. The modification of top Yukawa coupling and the new Yukawa interaction of T_+quark will be important for studying the Higgs boson production rate via gluon fusion process and the decay branching ratio of the Higgs boson into a di-photon mode.

4.3.2 Yukawa Couplings of Light Up- and Down-type Quarks

Here we summarize other Higgs interactions that are important when we consider Higgs boson decays. Yukawa couplings of up-type quarks for the first and second generations are given by the similar Lagrangian for the top quark (see Sec. 2.4), but without introducing extra singlet fields U_i and U_{R_i} $(i = 1 - 2)$ in Eq. (2.20). The Yukawa couplings $g^{LHT}_{h\bar{u}u}$ (where u denotes the up or charm quark) are modified from those in the SM. Their ratios are approximately given as follows:

$$\frac{g^{LHT}_{h\bar{u}u}}{g^{\rm SM}_{h\bar{u}u}} = 1 - \frac{3}{4}\frac{v^2}{f^2} - \frac{5}{32}\frac{v^4}{f^4} + \cdots = \begin{cases} 0.90 \text{ for } f = 700\,\text{GeV}, \\ 0.95 \text{ for } f = 1 \quad \text{TeV}, \end{cases} \tag{4.31}$$

For down-type quark Yukawa couplings, one of the possible effective Lagrangians [74, 75] is given by Eq. (2.27). The corrections of the Yukawa couplings compared with that in the SM are given as

$$\frac{g^{LHT}_{h\bar{d}d}}{g^{\rm SM}_{h\bar{d}d}} = 1 - \frac{1}{4}\frac{v^2}{f^2} + \frac{7}{32}\frac{v^4}{f^4} + \cdots = \begin{cases} 0.97 \text{ for } f = 700\,\text{GeV}, \\ 0.99 \text{ for } f = 1 \quad \text{TeV}, \end{cases} \quad \text{for Case A}, \tag{4.32}$$

$$= 1 - \frac{5}{4}\frac{v^2}{f^2} - \frac{17}{32}\frac{v^4}{f^4} + \cdots = \begin{cases} 0.84 \text{ for } f = 700\,\text{GeV}, \\ 0.92 \text{ for } f = 1 \quad \text{TeV}, \end{cases} \quad \text{for Case B.} \tag{4.33}$$

Note that the down-type quark Yukawa couplings could be significantly suppressed in Case B. We also consider the same Yukawa structures in lepton sector, as in quark sector. Thus, the charged lepton Yukawa couplings are also suppressed in the same way as the down-type quark Yukawa couplings.

4.3.3 Yukawa Couplings of the T-odd Particles

The effective Lagrangian given by Eq. (2.18) in Sec. 2.2 leads to the following interactions which contain the couplings between the Higgs boson and T-odd up-type quarks,

$$\mathcal{L}_\kappa = -\sqrt{2}\kappa f \left[\bar{d}_{L\_} \tilde{d}_c + \frac{1+c_\xi}{2} \bar{u}_{L\_} \tilde{u}_c - \frac{s_\xi}{\sqrt{2}} \bar{u}_{L\_} \chi_c - \frac{1-c_\xi}{2} \bar{u}_{L\_} u_c \right] + \text{h.c.} \cdots . \tag{4.34}$$

Here we only show the fermion mass terms and a few interaction terms with the Higgs boson. $c_\xi (\equiv \cos\frac{v+h}{\sqrt{2}f})$ and $s_\xi (\equiv \sin\frac{v+h}{\sqrt{2}f})$ are originated from the non-linear sigma model field ξ which contains the Higgs boson. $u_{L\_}$ and u_{L_+} are T-odd and T-even eigenstates, respectively, as defined by $u_{L_\pm} = (u_{L_1} \mp u_{L_2})/\sqrt{2}$. The same definition also applies to the down-type quark.

We stress that the Higgs boson interactions in $\mathcal{L}_\kappa$ provide $O(1)$ Yukawa-type interactions for $\kappa \sim O(1)$, so that these individual interactions could contribute to the quadratic divergences of Higgs boson mass. However, all the quadratic divergences, induced by the individual field introduced in Eq. (2.18), cancel in the limit of $v \to 0$, as long as Ψ_c forms a complete $SO(5)$ multiplet. Hence, the set of Higgs boson inter-

actions introduced in $\mathcal{L}_\kappa$ is consistent with the absence of large quadratic divergences to the Higgs mass parameter.

4.3.4 Other Higgs interactions

The interactions of the Higgs boson to the SM gauge bosons can be derived from Eq. (1.1). Similarly, the couplings g_{hVV}^{LHT} (where $V = Z, W$) are also slightly suppressed:

$$\frac{g_{hVV}^{LHT}}{g_{hVV}^{\rm SM}} = 1 - \frac{1}{4}\frac{v^2}{f^2} - \frac{1}{32}\frac{v^4}{f^4}\cdots \simeq \begin{cases} 0.97 \text{ for } f = 700\,\text{GeV}, \\ 0.98 \text{ for } f = 1 \quad \text{TeV}. \end{cases} \tag{4.35}$$

In addition, there are interactions of the Higgs boson with T-odd heavy W_H boson which should be taken into account in $h \to \gamma\gamma$ decay branching ratio, the couplings are:

$$g_{hW_H^+W_H^-} = -g_{hW^+W^-}^{LHT}.$$

4.3.5 Higgs Boson Production

Due to the new Higgs boson interactions in $\mathcal{L}_\kappa$ of Eq. (4.34), the T-odd fermions can contribute to the Higgs boson production via the gluon-gluon fusion process at one-loop level, as shown in Fig. 4.6 (b).

From the structure of the mass matrix and the Higgs boson interactions for the T-odd fermions, we find that $h\bar{u}_{L\_}\tilde{u}_c$ interaction provides the dominant T-odd fermion contribution to $\sigma_{gg\to h}$ and the result is not sensitive to the masses m_q and m_χ, as long as the T-odd fermion masses are much larger than half of the Higgs boson mass. The ratio of the amplitude induced by the T-odd fermions to the one by the SM

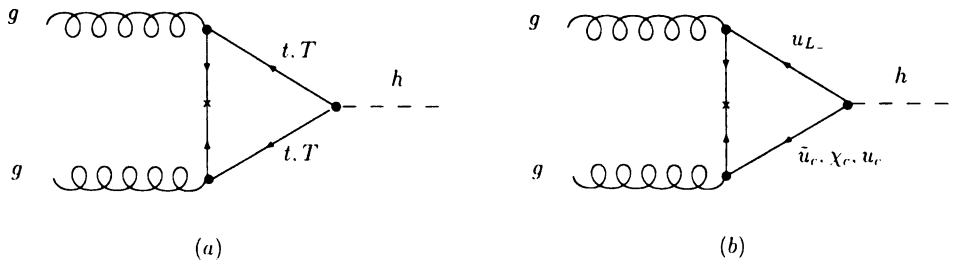

Figure 4.6: Contributions to the Higgs boson production via gluon-gluon fusion process $gg \to h$, induced by (a) top-quark and T-even partner T_+, and (b) T-odd fermions.

top-quark, which is the dominant contribution in the SM, is approximately expressed as

$$\frac{A_{gg\to h}(\text{T-odd fermion})}{A_{gg\to h}(\text{top in SM})} \simeq -\frac{1}{4}\frac{v^2}{f^2} + \cdots \simeq \begin{cases} -3\% \text{ for } f = 700 \text{ GeV}, \\ -1.5\% \text{ for } f = 1 \text{ TeV}. \end{cases} \tag{4.36}$$

Here, we have assumed that the fermions in the loop are much heavier than half of the Higgs boson, so that the one-loop vertex diagram in Fig. 4.6 can be approximated as a three-point vertex after shrinking the heavy internal lines into a point [132]. The negative sign of the ratio is originated from the positive sign of $h\bar{u}_{L\_}\tilde{u}_C$ interaction term in Eq. (4.34) after fixing the correct negative sign for the $\bar{u}_{L\_}\tilde{u}_C$ mass term. Note that as shown in Eq. (4.36) the leading order contribution, in terms of v/f, does not explicitly depend on the parameter κ. Namely, κ term generates a "non-decoupling" contribution to $\sigma_{gg\to h}$ which does not vanish as $\kappa f \to \infty$ with a fixed f value. Since the interaction shown in Eq. (2.18) is needed for each fermion generation to generate mass terms for all the T-odd partners, the parameter κ has a generation index in general [73]. Since the result in Eq. (4.36) does not depend on κ, the sum over all three generations of this type of corrections to the $gg \to h$ amplitude will be three times of the result shown in Eq. (4.36). (As shown in Eq. (4.34), there are no equivalent Higgs couplings to down-type quarks in $\mathcal{L}_\kappa$.) Hence, the correction

$\delta\sigma_{gg\to h}$ to the production cross section of $gg \to h$ induced by the T-odd fermions is approximately given by

$$\frac{\delta\sigma_{gg\to h}}{\sigma^{\rm SM}_{gg\to h}} \simeq -3\frac{v^2}{f^2} + \cdots \simeq \begin{cases} -37\% \text{ for } f = 700\,\text{GeV}, \\ -18\% \text{ for } f = 1 \ \ \text{TeV}, \end{cases} \tag{4.37}$$

for three generation case. Therefore, we find that the effect of the T-odd fermion mass terms on the Higgs boson production rate via gluon fusion could be significant, especially when f is below 1 TeV.

In the SM, the most important contribution to the Higgs boson production via the gluon-gluon fusion process comes from top-quark loop, as shown in Fig. 4.6 (a). As we have discussed, the top-Yukawa coupling is modified in the LHT model, and hence the contribution to the gluon fusion process is also modified. Furthermore, there is also new contribution induced at one-loop level by the partner of top-quark, the T-even heavy quark T_+. The ratios of the amplitudes to the top contribution in the SM are given as follows:

$$\frac{A_{gg\to h}(\text{top in LHT})}{A_{gg\to h}(\text{top in SM})} \simeq 1 - \frac{3+2R^2+3R^4}{4(1+R^2)^2}\frac{v^2}{f^2} + \cdots \tag{4.38}$$

$$\frac{A_{gg\to h}(T_+ \text{ in } LHT)}{A_{gg\to h}(\text{top in SM})} \simeq -\frac{m_t^2}{m_{T_+}^2} + \cdots = -\frac{R^2}{(1+R^2)^2}\frac{v^2}{f^2} + \cdots, \tag{4.39}$$

where we have assumed $m_t,\, m_{T_+} \gg m_h/2$. Therefore, the cross section of the Higgs boson production via the gluon-gluon fusion in the LHT model is modified by the T-even top sector (including both top and T contributions). As compared to that in the SM,

$$\frac{\delta\sigma_{gg\to h}(\text{T-even top sector})}{\sigma_{gg\to h}(\text{top in SM})} \simeq -\frac{3}{2}\frac{v^2}{f^2} + \cdots \simeq \begin{cases} -19\% \text{ for } f = 700\,\text{GeV}, \\ -9\% \text{ for } f = 1 \ \ \text{TeV}. \end{cases} \tag{4.40}$$

We note that although contributions from the top quark and T_+ separately depend on R, the sum of them does not. This suggests that even if λ_2 is large, and therefore T_+ quark is heavy, the T_+ contribution does not decouple as long as the scale f is about 1 TeV. In case of the Littlest Higgs model without T-parity, the authors in Ref. [133] had reached a similar conclusion on the contribution from top and heavy T-even top partner which is rather common in any Littlest Higgs models[‡]. Since the T-odd fermion contribution discussed in the previous section is as large as the one induced by the T-even top-quark sector, the correction to $\sigma_{gg\to h}$ in the LHT model is largely enhanced by the T-odd fermion contributions as compared to that in the Littlest Higgs model without T-parity.

When we sum over all the contributions discussed above, the deviation ($\delta\sigma_{gg\to h} \equiv \sigma^{\rm LH}_{gg\to h} - \sigma^{\rm SM}_{gg\to h}$) of the Higgs boson production cross section via the gluon-gluon fusion process in the LHT model ($\sigma^{\rm LH}_{gg\to h}$) from the SM prediction ($\sigma^{\rm SM}_{gg\to h}$) is approximately given by

$$\frac{\delta\sigma_{gg\to h}}{\sigma^{\rm SM}_{gg\to h}} \simeq -3\frac{v^2}{f^2} + \cdots \simeq \begin{cases} -37\% \text{ for } f = 700\,\text{GeV}, \\ -18\% \text{ for } f = 1\ \ \text{TeV}, \end{cases} \tag{4.41}$$

where we have assumed that the Higgs mass is smaller than the fermion masses in the loop. It is clear that the extra contributions in the LHT model significantly suppress the Higgs boson production cross section via gluon fusion process.

In Fig. 4.7, we show a numerical result of the deviation ($\delta\sigma_{gg\to h}$) of the Higgs boson production cross section via $gg \to h$ in the LHT model from the SM prediction, normalized by the SM prediction ($\delta\sigma_{gg\to h}/\sigma^{\rm SM}_{gg\to h}$). Here, we assumed that $\kappa = 3$,

[‡]Since in the Little Higgs model without T-parity, the ρ parameter at tree level is not one [66], the model has a stronger constraint on the scale f. Therefore, one expects that the effect on the Higgs boson production via gluon fusion in the model without T-parity will be much smaller than what is expected in the Littlest Higgs model with T-parity.

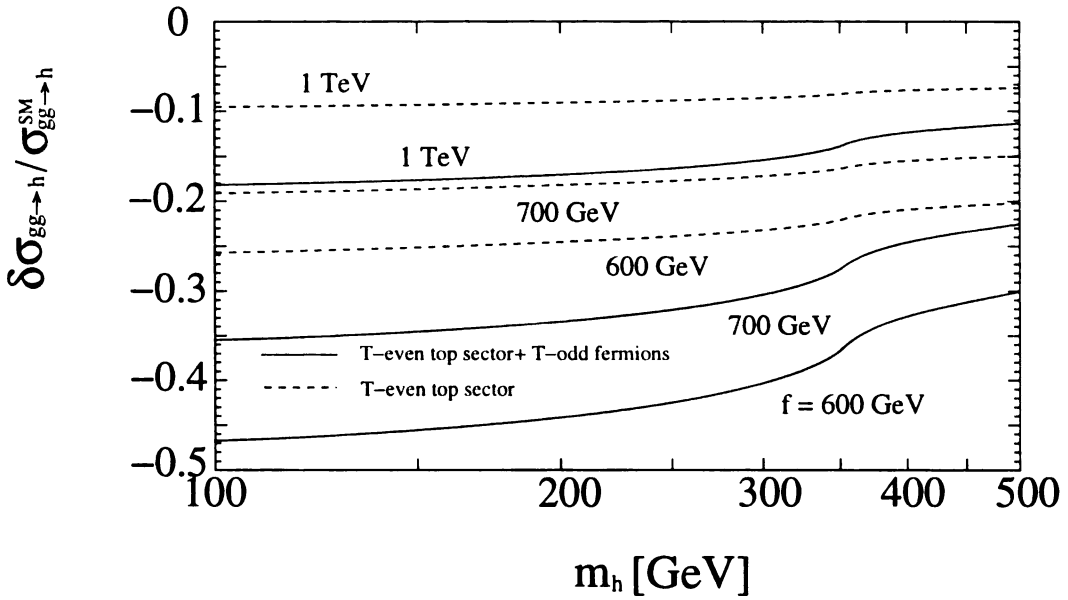

Figure 4.7: Deviations ($\delta\sigma_{gg\to h} = \sigma^{\rm LH}_{gg\to h} - \sigma^{\rm SM}_{gg\to h}$) of the Higgs boson production cross section via gluon fusion process in the LHT model ($\sigma^{\rm LH}_{gg\to h}$) from that in the SM ($\sigma^{\rm SM}_{gg\to h}$), normalized by $\sigma^{\rm SM}_{gg\to h}$, as a function of Higgs mass m_h. We have taken $\kappa = 3$, $m_q = m_\chi = 5f$ and $R = 1$, though our result is not sensitive to their specific values as long as m_q, $m_\chi \gg m_h/2$. Dashed lines show the effect induced by the T-even top sector only. Solid lines include the contributions from T-odd fermions in addition to T-even top sector. In each case, the results for $f = 600$ GeV, 700 GeV and 1 TeV are shown. Here, the complete one-loop calculation was used in our numerical analysis.

$m_q = m_\chi = 5f$ and $R = 1$, but we have checked that our result does not strongly depend on these parameters as long as m_q and m_χ are much larger than $m_h/2$. For our numerical analysis, we adapted a public code, HDECAY [134], for the SM calculation, and modified the code with a complete one-loop calculation in accordance with the effective Lagrangian described in the previous section for the LHT model calculation. Dashed lines show the corrections induced by the T-even top sector only (assuming there are no other corrections), and solid lines include the contributions from T-odd fermions in addition to T-even top sector. One sees that the approximate results in

Eqs. (4.37), (4.40) and (4.41) well describe the numerical result in Fig. 4.7 when the Higgs boson is light. Fig. 4.7 shows that, if the scale f is smaller than about 1 TeV, the production cross section via the gluon-gluon fusion is largely suppressed in all range of Higgs mass, but especially in small Higgs mass region. For example, the deviation from the SM prediction can be more than 40% (30%) for $m_h < 300$ GeV and $f < 600\,(700)$ GeV if we take into account all the corrections discussed above. This large suppression will be important especially when the Higgs mass is relatively small because the gluon-gluon fusion process is one of the main discovery modes for detecting a light SM Higgs boson.

We note that as suggested by the naive dimensional analysis [135] in low energy effective theory, one may write down the operator, $\sum_{i=1,2} \frac{g_s^2 f^2}{\Lambda^2} \Sigma_{3i}^\dagger \Sigma_{3i} G^A_{\mu\nu} G^{A,\mu\nu} \sim \frac{g_s^2 h^\dagger h}{\Lambda^2} G^A_{\mu\nu} G^{A,\mu\nu}$, with an $O(1)$ coefficient, where $G^A_{\mu\nu}$ is the field strength tensor of the gluon field and g_s is the strong coupling. In that case, this operator will induce a counterterm for $hG^A_{\mu\nu}G^{A,\mu\nu}$ coupling with its coefficient at the order of $g_s^2 v/(16\pi^2 f^2)$, which has the same magnitude as the one-loop contribution calculated above. However, due to the Little Higgs mechanism, we expect the coefficient for the operator $\Sigma_{3i}^\dagger \Sigma_{3i}$, which generates Higgs boson mass term, to be suppressed by a two-loop suppression factor of $v^2/\Lambda^2 \simeq (1/16\pi^2)^2$ as compared to the naive dimensional analysis (with a coefficient f^2/Λ^2). It is likely the same suppression factor $(1/16\pi^2)^2$ also applies to the above operator $\Sigma_{3i}^\dagger \Sigma_{3i} G^A_{\mu\nu} G^{A,\mu\nu}$ and yields a much smaller coefficient as compared to the genuine one-loop contributions. Therefore, we expect the one-loop contributions discussed above well represent the dominant contributions to $\sigma_{gg\to h}$.

4.3.6 Other Production Channels and Decay Modes

In the LHT model, the Higgs boson interactions are modified through the interactions of the non-linear sigma model field with other particles, as shown in Eqs. (4.28), (4.31),

(4.32), (4.33) and (4.35).

Because of the slight suppression of the Higgs couplings with the gauge bosons and the top quark, the Higgs boson production rates via the gauge boson fusion processes ($VV \to h$), the associated Wh and $\bar{t}th$ processes are also slightly suppressed.

Furthermore, the modification of the Higgs couplings also affects the decay branching ratios of the Higgs boson. In Fig. 4.8 (a), we show the ratios of the total decay width of the Higgs boson in the LHT model to that in the SM, $\Gamma_h^{\rm LH}/\Gamma_h^{\rm SM}$ for $f = 700$ GeV, in Case A and B of the down-type quark Yukawa interactions, cf. Eq. (2.27). In Case A, partial decay widths for main decay modes of the Higgs boson such as $b\bar{b}$, $\tau\tau$ and $VV\,(V = W, Z)$ are almost equally suppressed by about $(0.97)^2 = 0.94$ for $f = 700$ GeV. Therefore, the total decay width of Higgs boson is almost uniformly suppressed in the whole range of Higgs mass. Consequently, the branching ratios of most of the Higgs decay modes are very close to the SM predictions. Thus, in Case A, the only sizable change from the SM prediction is the gluon fusion cross section $\sigma_{gg\to h}$, as discussed in the previous section.

On the other hand, in Case B, both bottom and tau Yukawa couplings are significantly suppressed, and hence the total decay width of the Higgs boson is largely reduced in the small Higgs mass region where $h \to b\bar{b}$ and $\tau\tau$ decay modes dominate, as seen in Fig. 4.8 (a). For m_h larger than $2m_W$, the Higgs boson mostly decays into gauge bosons, ZZ and WW, and the suppression factor of the total decay width is about $(0.97)^2 = 0.94$ for $f = 700$ GeV.

An interesting effect in Case B is that because of the largely reduced total decay width in small Higgs mass region, some of the Higgs boson decay branching ratios are increased even though the corresponding partial decay widths are reduced. We have

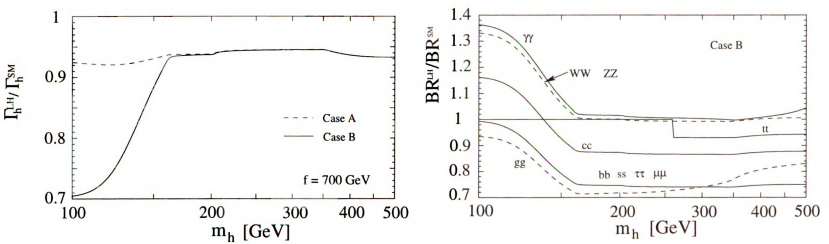

Figure 4.8: (a) A ratio of the total Higgs decay width in the LHT model $\Gamma_h^{\rm LH}$ to one in the SM $\Gamma_h^{\rm SM}$ GeV in Case A and B for the down-type quark Yukawa couplings. (b) Ratios of the Higgs decay branching ratios in the LHT model $\Gamma_h^{\rm LH}$ to those in the SM $\Gamma_h^{\rm SM}$ for $f = 700$ GeV in Case B.

also calculated the di-photon decay width $\Gamma(h \to \gamma\gamma)$ at one-loop level[§]. Similar to the fact that the W-boson contribution dominates over the top-quark contribution to $\Gamma(h \to \gamma\gamma)$ for small Higgs mass region in the SM, the effect of the extra-fermions in the di-photon decay mode is less important than that in the gluon fusion process. Furthermore, the extra-boson contributions tend to cancel the extra-fermion contributions in di-photon decay mode, and therefore the partial decay width of $h \to \gamma\gamma$ does not change very much, as compared to the SM prediction. As a result, in contrast to Case A, the decay branching ratio of $h \to \gamma\gamma$ is enhanced by about 35 % for a 100 GeV Higgs boson in Case B, for the total decay width of Higgs boson is reduced by about 30 %.

In Fig. 4.8 (b), we show a numerical result on ratios of Higgs decay branching ratio in the LHT model to that in the SM, $\mathrm{BR}^{\mathrm{LH}}/\mathrm{BR}^{\mathrm{SM}}$, for a few main Higgs decay modes in Case B. Here we have again taken f to be 700 GeV. We see that especially $\gamma\gamma$ and VV ($V = W, Z$) decay branching ratios are largely enhanced in the small Higgs mass region.

Since the production cross section via gluon fusion is strongly suppressed, the discovery modes of the Higgs boson will be changed significantly. In Table 4.2, $R_\sigma \times R_{\mathrm{BR}}$ is listed for various production and decay processes in cases for $m_h = 120$ GeV and 200 GeV. Here, we define $R_{\sigma(X)}(\equiv \sigma^{\mathrm{LH}}_{(X)}/\sigma^{\mathrm{SM}}_{(X)})$ as the ratio of the Higgs boson production cross section in the LHT model ($\sigma^{\mathrm{LH}}_{(X)}$) to that in the SM ($\sigma^{\mathrm{SM}}_{(X)}$) for each production process X. The subscripts gg, VV, $t\bar{t}h$, and Vh represent the gluon-gluon fusion ($gg \to h$), weak boson fusion ($VV \to h$, with $V = W, Z$), $t\bar{t}h$ and Vh associated productions, respectively. $R_{\mathrm{BR}(Y)} \equiv \mathrm{BR}^{\mathrm{LH}}_{(Y)}/\mathrm{BR}^{\mathrm{SM}}_{(Y)}$ for $h \to Y$ decay modes, where $Y = \gamma\gamma$, $\tau\tau$, $b\bar{b}$ and VV.

In the SM, the $\gamma\gamma$ decay mode of the Higgs boson produced via gluon fusion is

[§]See Ref. [133] for the study of $h \to \gamma\gamma$ in the Littlest Higgs model without T-parity.

$m_h = 120$ GeV	$R_{BR(\gamma\gamma)}$	$R_{BR(\tau\tau)}$	$R_{BR(b\bar{b})}$	$R_{BR(VV)}$
$R_{\sigma(gg)}$ (Case A)	0.57, 0.68, 0.84	0.56, 0.67, 0.83	–	0.55, 0.66, 0.83
(Case B)	0.81, 0.86, 0.93	0.51, 0.63, 0.81	–	0.78, 0.84, 0.92
$R_{\sigma(VV)}$ (Case A)	0.97, 0.98, 0.99	0.95, 0.96, 0.98	–	0.94, 0.96, 0.98
(Case B)	1.34, 1.22, 1.09	0.84, 0.89, 0.95	–	1.30, 1.19, 1.08
$R_{\sigma(t\bar{t}h)}$ (Case A)	–	0.87, 0.90, 0.95	0.87, 0.90, 0.95	–
(Case B)	–	0.77, 0.83, 0.92	0.77, 0.83, 0.92	–
$R_{\sigma(Vh)}$ (Case A)	0.97, 0.98, 0.99	–	0.95, 0.96, 0.98	–
(Case B)	1.34, 1.22, 1.09	–	0.84, 0.89, 0.95	–
$m_h = 200$ GeV	$R_{BR(\gamma\gamma)}$	$R_{BR(\tau\tau)}$	$R_{BR(b\bar{b})}$	$R_{BR(VV)}$
$R_{\sigma(gg)}$ (Case A)	–	–	–	0.55, 0.67, 0.83
(Case B)	–	–	–	0.56, 0.67, 0.83
$R_{\sigma(VV)}$ (Case A)	–	–	–	0.90, 0.94, 0.97
(Case B)	–	–	–	0.90, 0.94, 0.97

Table 4.2: $R_\sigma \times R_{\rm BR}$ for $f = (600, 700, 1000)$ GeV. Here $R_{\sigma(X)} (\equiv \sigma^{\rm LH}_{(X)}/\sigma^{\rm SM}_{(X)})$ is defined as a ratio of the Higgs boson production cross section in the little Higgs model ($\sigma^{\rm LH}_{(X)}$) to one in the SM ($\sigma^{\rm SM}_{(X)}$) for each Higgs boson production process X.

The subscripts gg, VV, $t\bar{t}h$, and Vh represent gluon fusion ($gg \to h$), weak boson fusion ($VV \to h$ where $V = W, Z$), $t\bar{t}h$ and Vh associated productions, respectively. $R_{\rm BR(Y)} \equiv {\rm BR}^{\rm LH}_{(Y)}/{\rm BR}^{\rm SM}_{(Y)}$ for each Higgs decay mode $h \to Y$, where $Y = \gamma\gamma$, $\tau\tau$, $b\bar{b}$ and VV.

one of the important discovery channels for a light Higgs boson with mass around 100 GeV. However, in the LHT model that we study here, this mode would be strongly suppressed. For example, $R_{\sigma(gg)} \times R_{\mathrm{BR}(\gamma\gamma)} = 0.68\,(0.86)$ for $m_h = 120$ GeV and $f = 700$ GeV in Case A (Case B), as shown in Table 4.2. Note that since the $h \to \gamma\gamma$ decay branching ratio is enhanced in Case B, $R_{\sigma(gg)} \times R_{\mathrm{BR}(\gamma\gamma)}$ is not suppressed as largely as in Case A. The similar conclusion also holds for the $h \to VV$ mode. On the other hand, $\gamma\gamma$ and VV decay modes of Higgs boson produced via weak boson fusion will be quite different from that via gluon fusion since the weak boson fusion process is not largely suppressed. In Case A, $R_{\sigma(VV)} \times R_{\mathrm{BR}(\gamma\gamma)}$ is very close to the SM prediction. In Case B, however, it could be significantly enhanced because of the enhancement of the $\gamma\gamma$ decay branching ratio. The decay branching ratio to $\tau\tau$ decay mode and the Higgs boson production rate via weak boson fusion do not change in either Case A or Case B. Thus, $R_{\sigma(VV)} \times R_{\mathrm{BR}(\tau\tau)}$ is close to the SM prediction.

When Higgs mass is relatively heavy ($m_h > 160$ GeV), the decay mode to gauge bosons ($h \to VV$, ($V = W, Z$)) becomes important. Since in both Case A and Case B the branching ratio for $h \to VV$ ($V = W, Z$) is almost the same as the SM prediction, the VV decay mode via gluon fusion production is significantly suppressed, but that via weak boson fusion is not. Therefore, typically the discovery modes of Higgs boson produced via weak boson fusion processes will become more important in the LHT model than in the SM. Since these effects could be larger than the experimental uncertainties ($10\% - 20\%$) [136–140] on the measurement of the Higgs boson production cross sections times the branching ratios, they could be observable at the LHC[¶].

We note that when the scale f is around 1 TeV, the T-odd heavy gauge boson

[¶]We stress that the further improvement of the theoretical calculation will be important to observe these effects.

masses can be of $O(100)$ GeV. For example, for $f = 700$ GeV, the T-odd $U(1)$ (A_H) and $SU(2)$ (W_H and Z_H) gauge boson masses are $m_{A_H} \simeq 100$ GeV and $m_{W_H,Z_H} \simeq 450$ GeV, respectively. When the Higgs mass is larger than twice of these masses, Higgs boson can decay into a heavy gauge boson pair. We have checked that in that case the decay branching ratios of the heavy gauge boson pair are less than 10^{-2} for $f \geq 700$ GeV. Therefore, the extra Higgs decay modes does not significantly change the branching ratios of the SM Higgs boson decay modes.

As discussed in previous sections, the Higgs boson production rate via $gg \rightarrow h$ process in the Littlest Higgs model with T-parity strongly depends on the mechanism to give T-odd particles (and other additional extra-particles) heavy masses. Thus the prediction may be sensitive to new physics above the cutoff scale, and our result shows that the effect could be quite large and become observable at the LHC. Therefore, searching for the Higgs boson in various detection modes at the LHC is very important, and the measurement of the relative event rates in multi-channels could reveal the mechanism which provides the cancellation of the quadratic divergence of the Higgs mass parameter and the origin of mass terms for the extra heavy fermions in the LHT model.

Chapter 5

Direct Search at Colliders

With the allowed low mass scale f, the new particles are at order of TeV and could be copiously produced at the LHC, and several studies about the collider phenomenology have been presented in the literature [72,80,125,141–145].In this chapter, I will study the direct search for these new particles. I will first discuss the crucial role of the T-odd fermions in unitarizing the $q\bar{q} \to W_H^+ W_H^-$ scattering process. Then I will calculate the total cross sections of all of the interesting $2 \to 2$ processes for producing new particles at the LHC. In order to study the collider phenomenology of the new particles, we have to know about their decay branching ratios. Moreover, there are some processes in the SM which could generate the same final state signatures as that predicted by the LHT model. We should study how to separate the LHT signatures from the background.

5.1 Unitarity of $u\bar{u} \to W_H^+ W_H^-$

Before we present a detailed study on the collider phenomenology of the LHT model, we stress in this section the importance of the T-odd $SU(2)$ doublet fermion contributions to high energy processes. To illustrate the important role of the T-odd $SU(2)$ doublet fermions in high energy processes, we discuss the high energy behavior of

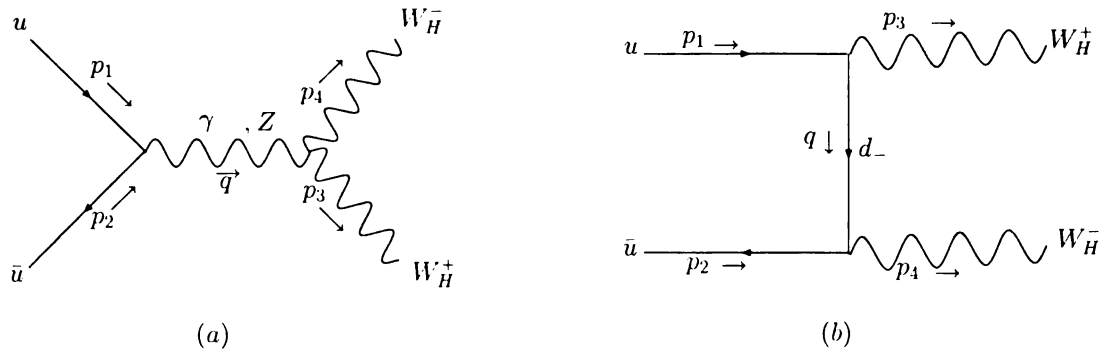

Figure 5.1: Tree-level Feynman diagrams for $u\bar{u} \to W_H^+ W_H^-$.

$u\bar{u} \to W_H^+ W_H^-$.

The tree-level diagrams for this process are given in Fig. 5.1 which includes s-channel and t-channel. The amplitudes of the s-channel process with a photon and a Z boson exchanged are expressed by A^γ and A^Z, respectively, and the amplitude of the t-channel process with a T-odd down-quark d_- exchanged is A^{d_-}. For the scattering process $u(p_1)\bar{u}(p_2) \to W_H^+(p_3) W_H^-(p_4)$, we have

$$\begin{aligned} A^\gamma &= \frac{2e^2}{3s}\bar{v}(p_2)\{(-\not{p}_3 + \not{p}_4)\varepsilon^*(p_3)\cdot\varepsilon^*(p_4) \\ &\quad -2p_4\cdot\varepsilon^*(p_3)\not{\varepsilon}^*(p_4) + 2p_3\cdot\varepsilon^*(p_4)\not{\varepsilon}^*(p_3)\}u(p_1), \end{aligned} \tag{5.1}$$

$$\begin{aligned} A^Z &= \frac{e^2}{2\sin^2\theta_W}\frac{1}{s - M_Z^2}\bar{v}(p_2)\{(-\not{p}_3 + \not{p}_4)\varepsilon^*(p_3)\cdot\varepsilon^*(p_4) \\ &\quad -2p_4\cdot\varepsilon^*(p_3)\not{\varepsilon}^*(p_4) + 2p_3\cdot\varepsilon^*(p_4)\not{\varepsilon}^*(p_3)\}(L+R)u(p_1), \end{aligned} \tag{5.2}$$

$$A^{d_-} = -\frac{g^2}{2}\frac{1}{t - M_{d_-}^2}\bar{v}(p_2)\not{\varepsilon}^*(p_4)P_L(\not{t} - M_{d_-})\not{\varepsilon}^*(p_3)P_L u(p_1), \tag{5.3}$$

where $L \equiv (1 - \frac{4}{3}\sin^2\theta_w)P_L$, $R = -\frac{4}{3}\sin^2\theta_W P_R$, and θ_W is the weak mixing angle, $P_L = \frac{1-\gamma_5}{2}$ ($P_R = \frac{1+\gamma_5}{2}$) is the left-handed (right-handed) projection operator. In the center-of-mass frame of $W_H^+ W_H^-$, the 4-momenta of the particles can be chosen

to be

$$\begin{aligned} p_1 &= (E,\, 0,\, 0,\, E),\ p_2 = (E,\, 0,\, 0,\, -E), \\ p_3 &= (E,\, p\sin\theta,\, 0,\, p\cos\theta),\ p_4 = (E,\, -p\sin\theta,\, 0,\, -p\cos\theta), \end{aligned} \tag{5.4}$$

where E is the energy of incoming and outgoing particles, p is the momentum of outgoing heavy gauge bosons and θ is the scattering angle. In the high energy limit, $E \gg M_{W_H}$, the polarization state of W_H boson is dominated by its longitudinal mode. In order to check the high energy behavior of the scattering process, we consider the case that both the heavy gauge bosons W_H^+ and W_H^- are longitudinally polarized, therefore we take

$$\epsilon^\mu(p_3) = \epsilon_0^\mu(p_3) = \frac{1}{M_{W_H}}(p,\ E\sin\theta,\ 0,\ E\cos\theta),$$

$$\epsilon^\mu(p_4) = \epsilon_0^\mu(p_4) = \frac{1}{M_{W_H}}(p,\ -E\sin\theta,\ 0,\ -E\cos\theta).$$

Since the incoming fermion u and anti-fermion $\bar{u}$ have opposite helicities, the helicity amplitudes of s-channel and t-channel processes can be easily found to be

$$A^\gamma(-+) = \frac{8e^2Ep(p^2-3E^2)}{3sM_{W_H}^2}\sin\theta,$$

$$A^Z(-+) = (1-\frac{4}{3}s_W^2)\frac{e^2}{s_W^2(s-M_Z^2)}\frac{2Ep(p^2-3E^2)}{M_{W_H}^2}\sin\theta,$$

$$A^{d_-}(-+) = \frac{e^2}{s_W^2(t-M_{d_-}^2)}\frac{E(2E^3\cos\theta+p^3-3pE^2)}{M_{W_H}^2}\sin\theta,$$

where $s_W \equiv \sin\theta_W$, $(-+)$ are the helicities of $(u,\, \bar{u})$, the Mandelstam variables $s \equiv (p_1+p_2)^2$ and $t \equiv (p_1-p_3)^2$, and M_Z, M_{W_H} and M_{d_-} are the masses of

Z-boson, heavy T-odd W-boson and heavy T-odd down-quark, respectively. As we take the high energy limit, i.e. $\sqrt{s} \gg M_X$ ($X = Z, W_H$ and d_-), each amplitude behaves as follows:

$$A^{\gamma}(-+) = -\frac{s_W^2 \sin\theta}{3f^2} s,$$

$$A^{Z}(-+) = -(1 - \frac{4}{3}s_W^2)\frac{\sin\theta}{4f^2} s,$$

$$A^{d-}(-+) = \frac{\sin\theta}{4f^2} s.$$

It is evident that each term diverges as energy goes to infinity, but their sum is zero because of the cancellation between the s-channel and t-channel contributions. Therefore, we conclude that it is essential to include the contribution from the T-odd down-quark to warrant a good high energy behavior of the scattering process $u\bar{u} \to W_H^+ W_H^-$. This can be illustrated by the partial-wave analysis, as to be given below.

The $J = 1$ partial-wave amplitude (denoted as $a^{J=1}$) of the $u\bar{u} \to W_H^+ W_H^-$ process, for producing longitudinal W_H's, consists of two contributions: one from s-channel, another from t-channel. We find

$$a^{J=1}_{\text{s-channel}} = \frac{\alpha s}{48\sqrt{2}s_W^2 M_{W_H}^2}\beta(3 - \beta^2),$$

$$a^{J=1}_{\text{t-channel}} = \frac{\alpha s}{64\sqrt{2}s_W^2 M_{W_H}^2}\int_{-1}^{1} \frac{\sin^2\theta(2\cos\theta + \beta^3 - 3\beta)}{1 - \beta\cos\theta + \frac{2M_{d_-}^2}{s}} d\cos\theta,$$

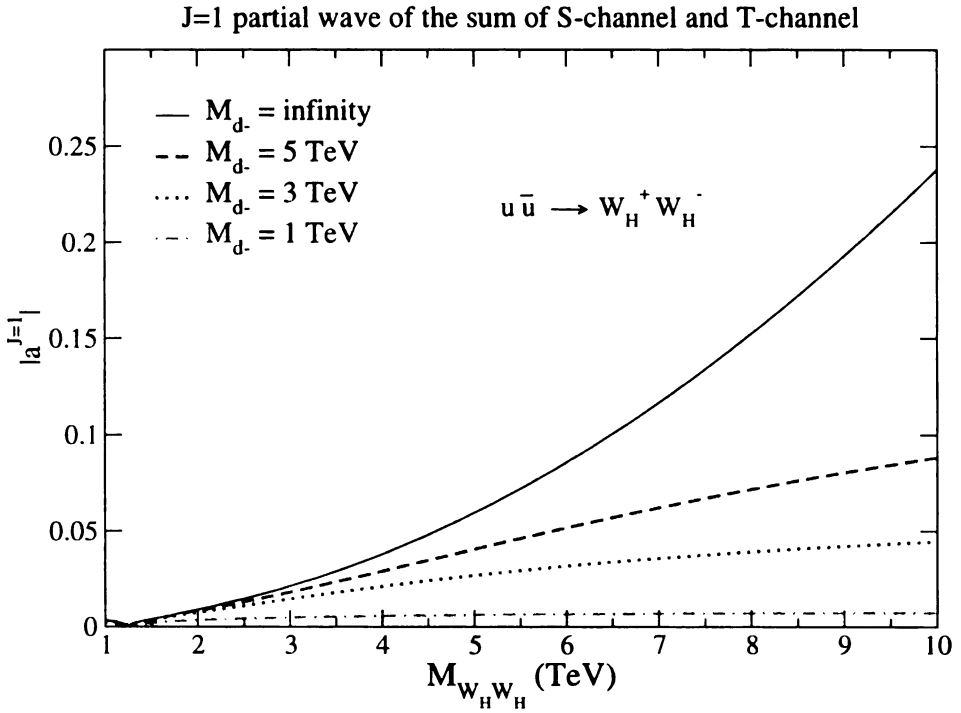

Figure 5.2: J=1 partial wave for $u\bar{u} \to W_H^+ W_H^-$ scattering process.

where $\alpha = \frac{e^2}{4\pi}$ and $\beta \equiv \sqrt{1 - 4M_{W_H}^2/s}$. ($e$ is the unit of electric charge.) When $s \gg M_{W_H}^2$ and $s \gg M_{d\_}^2$, we have

$$a^{J=1}_{\text{s-channel}} = -a^{J=1}_{\text{t-channel}} = \frac{\alpha s}{24\sqrt{2}s_W^2 M_{W_H}^2}.$$

In Fig. 5.2, we show the $J = 1$ partial-wave amplitude of the $u\bar{u} \to W_H^+ W_H^-$ process, as a function of the invariant mass $M_{W_H W_H}$ of the $W_H^+ W_H^-$ pair, for cases with $M_{d\_} = 1$, 3, 5 TeV and ∞. We found that the unitarity is not violated up to about 15 TeV in the decoupling limit of the T-odd down quark. On the other hand, as we learn in Sec. 3.3, the constraint on the four-fermion operator contributing to the $e^+e^- \to q\bar{q}$ scattering sets an important upper limit on the T-odd fermion mass. Since the masses of the T-odd $SU(2)$ doublet fermions cannot be too heavy, they can be copiously produced at the LHC. Therefore, in following sections, we study the collider phenomenology of the LHT model with emphasis on the contributions of the

T-odd fermions to the productions of the heavy particles (either bosons or fermions) at the LHC.

5.2 Productions of New Particles at the LHC

In this section, we first discuss the productions of these heavy T-odd fermions, either produced in pairs or in association with heavy T-odd gauge bosons at the LHC. Then, we discuss the impact of T-odd fermion contribution to the production of heavy T-odd gauge boson pairs. As discussed in the previous section, it is necessary to include the contribution from these heavy T-odd fermions to yield an unitary scattering amplitude. For completeness, we will also discuss the production of heavy T-odd triplet Higgs bosons.

Given the model described in Chapter 2, we can calculate the direct production rates of non-SM fermions, gauge bosons and triplet Higgs bosons. In our numerical results, we have used CTEQ6M parton distribution functions [131] with the renormalization and factorization scales being chosen to be the invariant mass of the constituent process. Only the leading order results are reported here. For our phenomenological analysis we have implemented the complete LHT model into CalcHEP package [146] and used it in our analysis. To check our analytical derivation of the effective Lagrangian for the implementation of the LHT model into CalcHEP, we applied LanHEP package [147] for automatic generations of Feynman rules for the CalcHEP. The parameters used in numerical calculations in this section are as follows,

$$\lambda_1 = \lambda_2 \simeq 1, \quad \kappa_q = \kappa_\ell = 1,$$

$$m_t = 175\,\text{GeV}, \quad m_h = 120\,\text{GeV}, \quad m_Z = 91.18\,\text{GeV}.$$

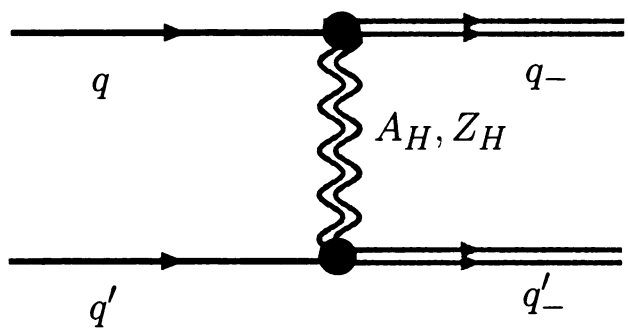

Figure 5.3: Representative Feynman diagram for $pp \to q_- q_-^{(\prime)}$ via t-channel exchange of the T-odd photon A_H and T-odd Z-boson Z_H.

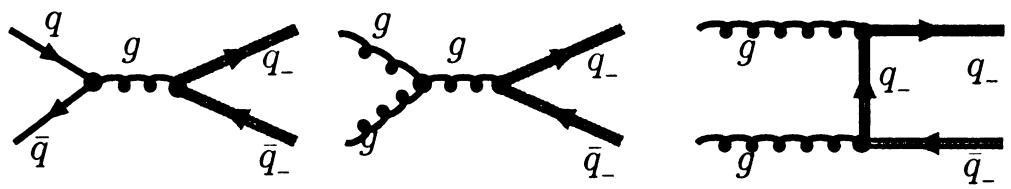

Figure 5.4: QCD Feynman diagrams for the $pp \to q_- \bar{q}_-$ process.

5.2.1 The First and Second Generation T-odd Quark Pair Production

The LHC is a proton-proton hadron collider, so that a heavy T-odd quark, denoted as q_-, can be copiously produced in pairs as long as its mass is not too large. There are two main mechanisms of the T-odd quark pair production. Firstly, $q_- q'_-$, same-sign-charge quarks can be produced via exchanging the T-odd heavy photon and Z-boson (A_H and Z_H) in t- (or u-) channel processes initiated by same-sign-charge light quarks. A respective Feynman diagram corresponding to this process is shown in Fig. 5.3. Secondly, the $q_- q'_-$ pair production takes place via both electroweak and obviously dominating QCD processes. The respective QCD Feynman diagrams for this process are shown in Fig. 5.4.

In Fig. 5.5, we present pair production rates of the first and second generation heavy T-odd quarks versus f values, organized by their electric charges.

The solid curve presents the production cross section of heavy quark pairs with

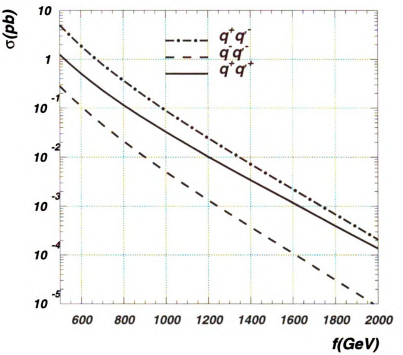

Figure 5.5: The first and second generation T-odd quark productions at the LHC.

positive charges, $q_-^+q_-^+$, which includes, for example, u_-u_-, $\bar{d}_-\bar{d}_-$ and $u_-\bar{d}_-$ pairs. The dashed curve is for the production of heavy quark pairs with negative charges, $q_-^-q_-^-$, which includes, for example, $\bar{u}_-\bar{u}_-$, d_-d_- and $d_-\bar{u}_-$ pairs. The dot-dashed curve is for the production of heavy quark pairs with opposite-sign charges, $q_-^+q_-^-$, which includes, for example, u_-d_- and $\bar{u}_-\bar{d}_-$ pairs. It is evident that the heavy T-odd quark pair production rates are sizable. The production rate of positive charge pairs is larger than that of the negative charge pairs because of the larger parton density associated with positive charge pair production in proton-proton collision. One should notice that the electroweak $q_-^+q_-^+$ production is comparable with the essentially QCD $q_-^+q_-^-$ production process. This happens because the production of heavy quark pairs with positive charges is initiated by both valence quarks in the

proton which have higher parton density than that contributing to either QCD or EW $q_-^+ q_-^-$ production. Furthermore, $q_-^+ q_-^+$ ($q_-^- q_-^-$) production becomes even more sizable as compared to $q_-^+ q_-^-$ production when f (and so the T-odd quark mass) increases, since the contribution from valence quarks becomes more important in the large x-value region. This is an important result because the $q_-^+ q_-^+$ ($q_-^- q_-^-$) production can provide an exciting experimental signatures at the LHC, as we shall discuss together with their detection strategies later.

5.2.2 The Third Generation Quark Production

In Fig. 5.6, we present various production rates of heavy T-even and T-odd top quark pairs as well as the rate of single T-even heavy top quark associatively produced with SM light quarks as a function of f. The T-odd bottom quark pair production rate is also given.

The T-odd heavy singlet top quark pair ($T_-\bar{T}_-$) has the largest cross section (solid curve) because, in the LHT model considered here, the T-odd heavy singlet top quark (T_-) is lighter than the T-even heavy top (T_+). Note that the mass of T-odd doublet quarks is determined by the choice of κ value which is taken to be 1 in this study. In this case T-odd heavy doublet top quark (t_-) mass is larger than the T_- mass and is about the same as the T_+ mass.

As f increases, both T_- and T_+ become heavier, and the single-T_+ production in association with light quarks ($\bar{q}T_+ + q\bar{T}_+$) (long-dash curve) rate becomes larger than the $T_-\bar{T}_-$ rate. This is because of the phase space suppression in the $T_-\bar{T}_-$ pair production, for producing two heavy particles, as compared to producing only one heavy particle in single-T_+ event. Furthermore, the single-T_+ production mechanism is dominated by longitudinal W-boson fusion with the incoming bottom quark in the t-channel production process, similar to the SM t-channel single-top production [148–

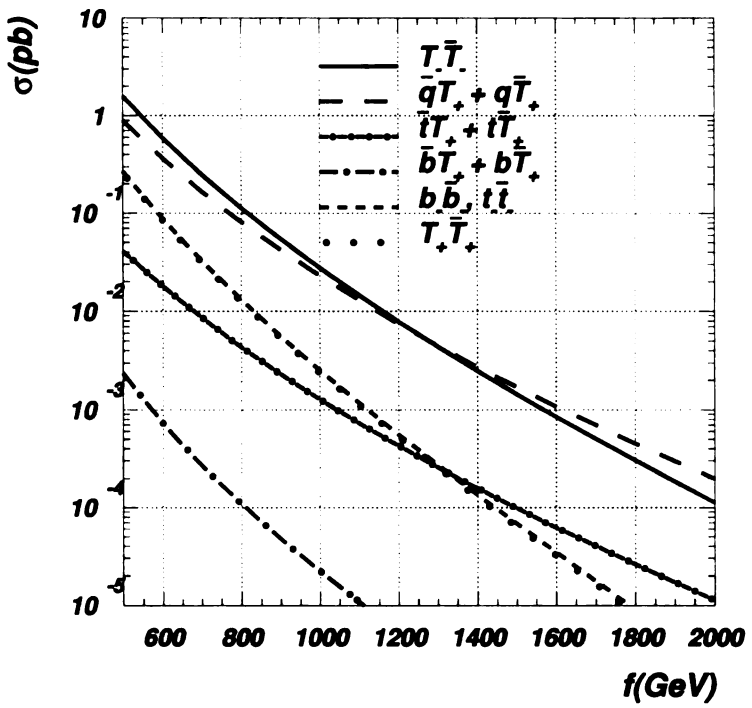

Figure 5.6: The third generation heavy T-odd and T-even quark productions at the LHC.

156]. Due to the collinear enhancement for the light quark emitting a W-boson in the high energy region, the constituent cross section of single-T_+ process does not drop as fast as that of pair production process. In Fig. 5.6, we also show the production rates of the T-odd $t_-\bar{t}_-$ and $b_-\bar{b}_-$ pairs (short-dash curve), where t_- and b_- are originated from the T-odd $SU(2)$ doublet quark fields, and their masses are generated from the κ term of the effective Lagrangian. One can see that $T_+\bar{T}_+$ and $t_-\bar{t}_-$ (or $b_-\bar{b}_-$) production cross sections are very close to each other because of the same production mechanism and the similar masses of T_+ and t_- (b_-) (for this particular choice of model parameters). Fig. 5.6 also presents cross sections for the associate tT_+ (short dot-dash line) and bT_+ (long dot-dash line) productions. The tT_+ production rate dominates over the bT_+ rate because the diagram with t-channel

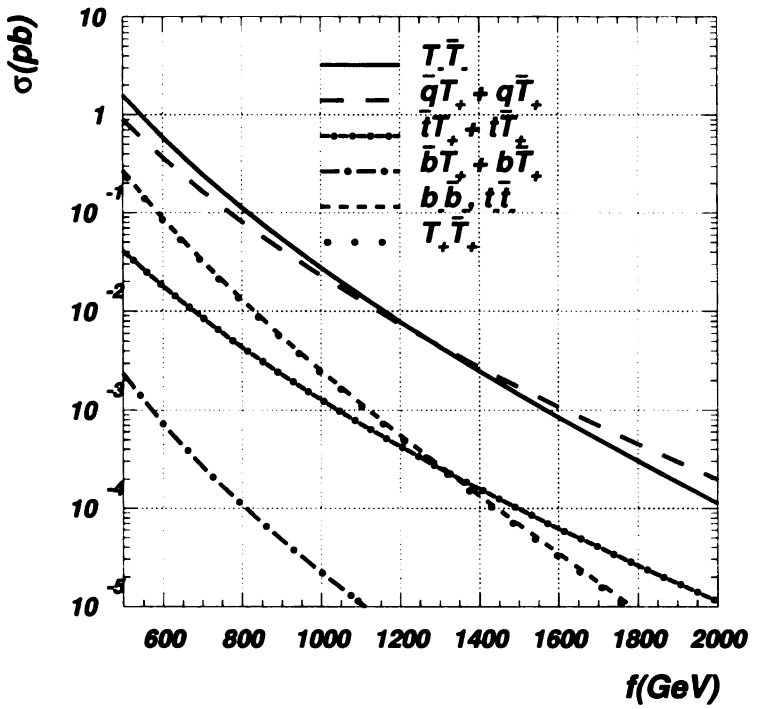

Figure 5.6: The third generation heavy T-odd and T-even quark productions at the LHC.

156]. Due to the collinear enhancement for the light quark emitting a W-boson in the high energy region, the constituent cross section of single-T_+ process does not drop as fast as that of pair production process. In Fig. 5.6, we also show the production rates of the T-odd $t_-\bar{t}_-$ and $b_-\bar{b}_-$ pairs (short-dash curve), where t_- and b_- are originated from the T-odd $SU(2)$ doublet quark fields, and their masses are generated from the κ term of the effective Lagrangian. One can see that $T_+\bar{T}_+$ and $t_-\bar{t}_-$ (or $b_-\bar{b}_-$) production cross sections are very close to each other because of the same production mechanism and the similar masses of T_+ and t_- (b_-) (for this particular choice of model parameters). Fig. 5.6 also presents cross sections for the associate tT_+ (short dot-dash line) and bT_+ (long dot-dash line) productions. The tT_+ production rate dominates over the bT_+ rate because the diagram with t-channel

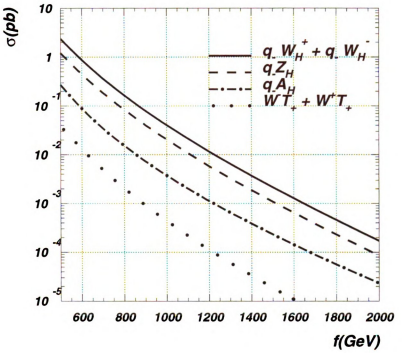

Figure 5.7: Quark gauge boson associated productions at the LHC.

W-boson exchange plays the leading role for the tT_+ production, and the similar diagram for bT_+ production is suppressed by Cabibbo-Kobayashi-Maskawa (CKM) matrix elements. For example, it is suppressed by V_{cb} in the $cb \to bT_+$ production process.

5.2.3 Quark Gauge Boson Associated Production

Another production mechanism for heavy T-odd quarks in the LHT model is via associated production with heavy T-odd gauge bosons. Since the initial state of the scattering process is T-even, the final state has to be a pair of T-odd particles. For example, the $d\_W_H^+$ pair can be produced via the $ug \to d\_W_H^+$ production . In Fig. 5.7, the solid curve shows the associated production rates of heavy charged T-

odd gauge bosons with all possible T-odd heavy quarks and anti-quarks, including the T-odd heavy top (anti-) quark and heavy bottom (anti-) quark, as a function of f. One can see that $q_- W_H$ (solid line) associate production is the dominant one, $q_- Z_H$ (dashed line) production rate is about a factor of 2 smaller, due to the $|g_{qq_-W_H}/g_{qq_-Z_H}| \simeq \sqrt{2}$ coupling ratio, and $q_- A_H$ (dot-dashed line) production is suppressed even more due to $|g_{qq_-W_H}/g_{qq_-A_H}| \simeq 5\sqrt{2}\cot\theta_W$.

We note that due to T-parity, the T-even heavy top quark T_+ can be produced associatively with the SM (hence, T-even) gauge bosons, not the T-odd heavy gauge bosons, whose production rates are also given in Fig. 5.7 (dotted line). Since bT_+W coupling is suppressed as v/f one can see that T_+W^- ($\bar{T}_+W^+$) rate is significantly smaller than the $q_- W_H$ rate, and this suppression obviously grows with the increase of f value.

5.2.4 T-odd Gauge Boson Pair Production

As discussed in the previous section, the presence of the T-odd heavy quarks in the model is essential for unitarizing the scattering amplitudes of $qq \to V_H V_H$ processes, where V_H denotes T-odd heavy electroweak gauge bosons. In Fig. 5.8, we show all possible T-odd heavy gauge boson pair production cross sections versus f value.

We note that due to the destructive effect from the t-channel T-odd heavy quark exchange diagram, which is needed to respect unitarity in high energy region, the predicted T-odd gauge boson pair production rates are smaller than those reported in Ref. [72] where the important T-odd heavy quark exchange diagram was not included in the calculations. Moreover, it is not a constant suppression factor in every production channel such that the relative difference between the $Z_H W_H^\pm$ and $W_H^+ W_H^-$ rates is much smaller than that reported in Ref. [72]. To examine the dependence on model parameters, we show in Fig. 5.9 the production cross section of $W_H^+ W_H^-$ pair

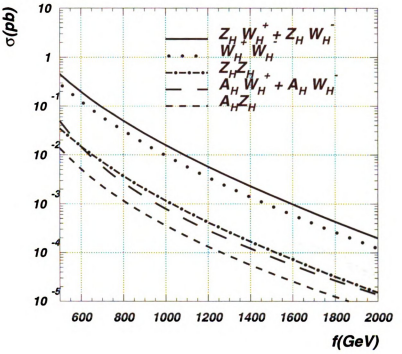

Figure 5.8: T-odd gauge boson pair productions at the LHC.

at the LHC as a function of f for various choices of κ values. We note that the curve for $\kappa \to \infty$ corresponds to the calculation without including the T-odd heavy quark contribution which overestimates $W_H^+ W_H^-$ production rate by a significant factor. In the later section, we shall come back to discuss its detection strategies at the LHC.

5.2.5 T-odd Triplet Higgs Bosons Production

In the LHT model, the direct production mechanism of the normal (T-even) Higgs boson is similar to the SM Higgs boson production though with somewhat suppressed couplings, as shown in Sec. 4.3. In high energy collision, the T-odd triplet Higgs bosons can be produced in $qq \to \phi\phi$ processes at the tree level via gauge interactions of ϕ, where ϕ denotes any of the T-odd heavy triplet Higgs bosons. Their direct

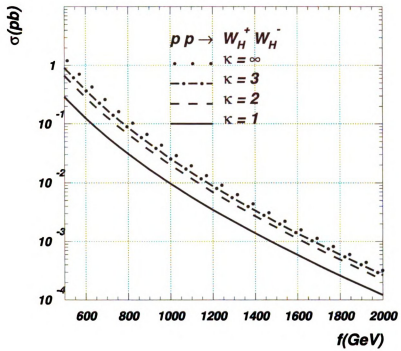

Figure 5.9: Heavy T-odd gauge boson pair, $pp \to W_H^+ W_H^-$, production rates at the LHC.

production rates are small, as one can see in Fig. 5.10, because at tree level they are produced via s-channel processes with highly virtual gauge boson propagators. Though t-channel diagrams also take place, they are strongly suppressed because they involve heavy T-odd quarks and the $qq_-\phi$ coupling is suppressed at least by v/f.

Nevertheless, the T-even Higgs bosons can be copiously produced from the decay of T-odd heavy quarks, as to be discussed below. For that, we shall first examine the decay branching ratios of the T-odd heavy quarks and gauge bosons predicted in this model.

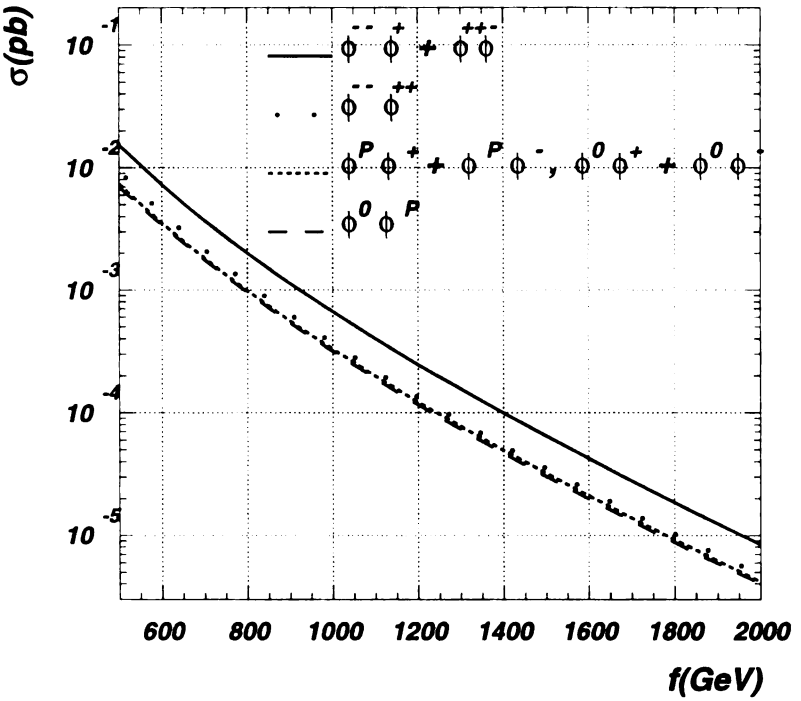

Figure 5.10: T-odd triplet Higgs bosons productions at the LHC.

5.3 Decay Branching Ratios of New Particles

In order to study the phenomenology of the T-odd heavy particles predicted in the LHT model, we need to know about their decay branching ratios. In addition to the SM parameters, the dominant two-body decay modes of the first and second generation T-odd quarks only depend on two more parameters: f and κ, i.e. f determines the mass of the T-odd heavy gauge bosons and both f and κ determines the mass of T-odd heavy quark. If κ is of the order of 1, then because of the smallness of gauge coupling strength, the T-odd gauge bosons are typically lighter than the T-odd quarks. When the lightest T-odd particle (LTP) is A_H so that it could be a good candidate for dark matters, the heavy T-odd quarks mainly decay into a SM light quark, which will generate a QCD jet, plus a T-odd heavy gauge boson $W_H^{\pm}$, Z_H or

Particle	Decay mode	Branching ratio (%)	Particle	Decay mode	Branching ratio (%)
u_-	$W_H^+ d$	61	d_-	$W_H^- u$	62
	$Z_H u$	30		$Z_H d$	31
	$A_H u$	8.6		$A_H d$	6.3
b_-	$W_H^- t$	60	t_-	$W_H^+ b$	62
	$Z_H b$	32		$Z_H t$	29
	$A_H b$	6.6		$A_H t$	8.2
T_-	$A_H t$	100	T_+	$W^+ b$	46
				$Z t$	22
				$H t$	20
W_H^+	$A_H W^+$	100		$A_H T_-$	12
ϕ^+	$A_H W^+$	100	Z_H	$A_H H$	100
ϕ^p	$A_H H$	100	ϕ^0	$A_H Z$	100

Table 5.1: Decay branching ratios of heavy particles in Littlest Higgs Model with T-parity. Values in this table are calculated with parameters $\kappa_q = \kappa_\ell = 1$, $f = 1$ TeV, $m_h = 120$ GeV and $m_t = 175$ GeV. We notice that for this set of model parameter values, the T-odd triplet Higgs ϕ^{++} doesn't have two-body decay modes at tree level.

A_H.

As shown in Table 5.1, the decay branching ratio (BR) into $W_H^\pm + jet$ is about twice of BR($Z_H + jet$) and one order of magnitude larger than BR($A_H + jet$) for $f = 1$ TeV and $\kappa = 1$. This feature also holds for the T-odd heavy top (t_-) and bottom (b_-) quarks which are originated from the T-odd $SU(2)$ doublet quark fields and gain their masses from κ terms. The T-odd heavy $SU(2)$ singlet top quark

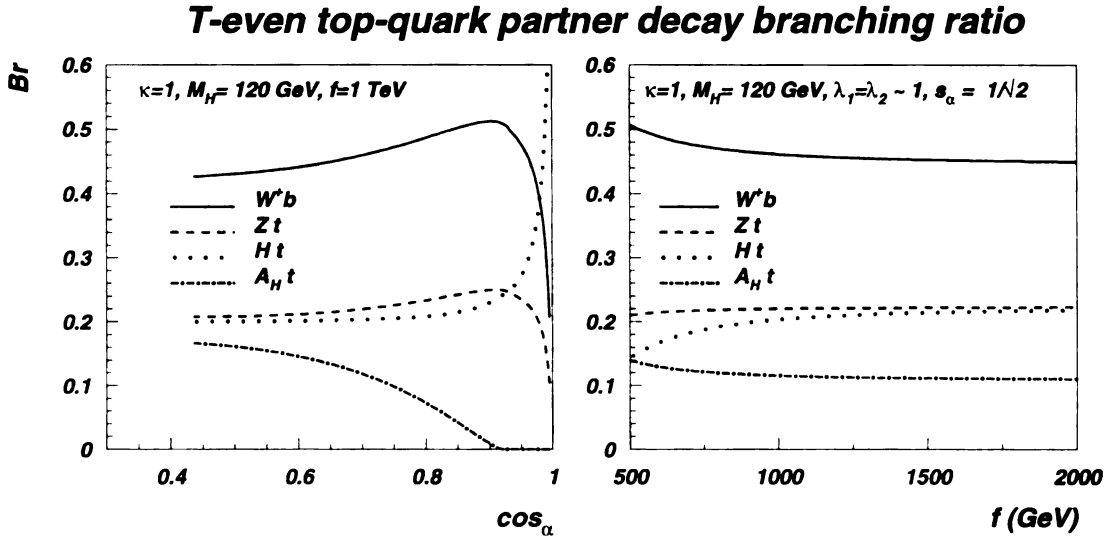

Figure 5.11: Decay branching ratios of the T-even heavy T_+ quark.

(T_-), originated from the top quark Yukawa interaction Lagrangian, decays almost 100 % into the tA_H. The T-even heavy $SU(2)$ singlet top quark (T_+) has a more complicated decay pattern and can decay into W^+b, Ht, Zt and A_Ht_- modes with nontrivial dependence on the model parameters such as f, λ_1 and λ_2 (or, equivalently, the masses of heavy T-odd gauge bosons, T_+ and T_-). In Fig. 5.11, we present the decay branching ratios for the above decay channels of T_+ as a function of $\cos\alpha$ (left frame) for $f = 1\,\text{TeV}$, and as a function of f for $\sin\alpha = 1/\sqrt{2}$ (right frame)

One can see that at $c_\alpha \simeq 1$, $\text{BR}(T_+ \to Ht)$ becomes dominant since for small s_α, HT_+t coupling is proportional to c_α while the couplings of T_+ in the other decay channels are suppressed by s_α. Note that for our analysis, the coefficient of the $W^+\bar{t}b$ coupling $V_{tb}^{eff} \equiv V_{tb}c_\beta$ varies as c_β ($c_\beta \equiv \cos\beta$, where β is the mixing angle between the left-handed top quark and the T-even T_+ quark, see Sec. 2.3). Here V_{tb} is taken to be 1. On the other hand, the BR of T-odd heavy quarks are quite insensitive to the LHT model parameters as long as the mass of the T-odd heavy quark is larger than A_H. For example, the values of BRs shown in Table 5.1 also hold (within a

few percents) for $f = 0.5 - 1$ TeV range. Hereafter, we will take $f = 1$ TeV as the reference point.

The striking feature of the T-odd heavy gauge boson decay pattern is that $W_H^\pm$ almost exclusively decay into a $W_H^\pm A_H$ pair, while Z_H decays into a $Z\,H$ pair, for κ being of the order 1 and the mass of the (T-even) Higgs boson is about 120 GeV. This is because the masses of $W_H^\pm$ and Z_H are about the same and are smaller than the T-odd heavy quark masses (unless κ is much less than 1). In such cases, the normal (T-even) Higgs boson can be copiously produced from the decay of T-odd heavy gauge boson Z_H which can be produced either associatively with T-odd heavy quarks or another heavy T-odd gauge bosons, as discussed above.

For the chosen model parameters, with $\kappa = 1$ and $\lambda_1 = \lambda_2$ (or $s_\alpha = 1/\sqrt{2}$) and $M_H = 120$ GeV, there is no tree-level two-body decay mode for the T-odd doubly charged triplet Higgs boson, $\phi^{\pm\pm}$, while $\phi^\pm$ decays into $W^\pm\,A_H$ mode, and ϕ^0 and ϕ^p decay into $Z\,A_H$ and $H\,A_H$ modes, respectively. However, for $M_H \geq 130$ GeV, the $W_H^\pm W^\pm$ mode could be opened for $\phi^{\pm\pm}$ Higgs boson.

5.4 Collider Signatures at the LHC

In this section, we shall discuss various experimental signatures of signal processes at the LHC for the same values of model parameters as given in the previous section. For simplicity, we shall concentrate on the pure leptonic decay modes of gauge bosons in the final decay chain of T-odd heavy quarks and gauge bosons.

5.4.1 The First and Second Generation T-odd Quark Pair

According to the multiplicity and charge of the leptons produced from the first and second generation T-odd heavy quark chain decays, we can classify the T-odd heavy

quark pair event signature as signal events with like-sign di-leptons, opposite-sign di-leptons, and single charged lepton with large missing transverse momentum.

(1) *like-sign di-lepton ($\ell^\pm\ell^\pm + \not{E}_T$+jets) signature (LSL)*: As shown in Fig. 5.3, the valence quark initiated $pp \to q_-q_-$ processes via the exchange of heavy electroweak gauge bosons could give rise to a large production rate of signal events with a pair of like-sign charged leptons in the final state to yield a distinct experimental signature. For example,

$$u_-u_- \to W_H^+ d W_H^+ d \to W^+W^+ A_H A_H dd \text{ and}$$
$$u_-\bar{d}_- \to W_H^+ d W_H^+ \bar{u} \to W^+W^+ A_H A_H d\bar{u},$$

chains lead to the $\ell^+\ell^+ + \not{E}_T +$ jets signature, while

$$d_-d_- \to W_H^- u W_H^- u \to W^-W^- A_H A_H uu \text{ and}$$
$$d_-\bar{u}_- \to W_H^- u W_H^- \bar{d} \to W^-W^- A_H A_H u\bar{d},$$

processes produce $\ell^-\ell^- + \not{E}_T +$ jets final state, with $W^\pm \to \ell^\pm + \nu_\ell$, and note that both the lightest T-odd particles A_H and neutrinos contribute to the missing energy signatures. The overall decay branching ratios for the above processes can be easily calculated from Table 5.1 which yields $Br[q_-q_- \to LSL] = 0.62^2 \times (2/9)^2 \simeq 0.019$. Depending on the values of f, the LSL signal event rate for positively charged leptons is about at 23 fb level for a lower value of $f = 500$ GeV and about 0.6 fb for $f = 1$ TeV, as the solid line shown in Fig. 5.12. LSL signal event rate for negatively charged leptons is 5 fb and 0.1 fb for $f = 500$ GeV and 1 TeV, respectively, as shown by the dotted line in Fig. 5.12.

With the high luminosity option of the LHC, around $300\,\text{fb}^{-1}$, there will be a large number of signal events with like-sign di-leptons, with large transverse momentum (p_T), and large missing transverse momentum ($\not{E}_T$) in the $\ell^-\ell^- + \not{E}_T + jets$ or $\ell^+\ell^+ +$

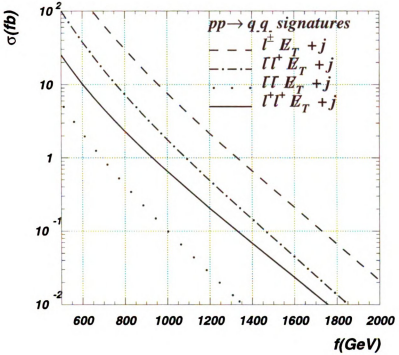

Figure 5.12: Event signal rates for like-sign di-lepton ($\ell^{\pm}\ell^{\pm}$), opposite-sign di-lepton ($\ell^{\pm}\ell^{\mp}$) and single charged lepton ($\ell^{\pm}$) from the first and second generation heavy T-odd quark pair production at the LHC.

jets+ $\not{E}_T$ signature. The prominent feature of this signal signature is that it is free of large $t\bar{t}$ background. This is similar to the case for studying the longitudinal weak boson scattering processes in the TeV region, with emphasis on the so called Gold-platted purely leptonic decay mode of weak bosons. As shown in Ref. [157,158], after imposing the kinematic cuts on the charged leptons, the SM background rate, which is dominated by the intrinsic electroweak $qqW^{\pm}W^{\pm}$ production and the $Wt\bar{t}$ associate production, is already down to the level of a few tenth fb. It is expected that one can further discriminate the signal event from the SM background event by requiring a large scalar sum of the transverse momenta, contributed by the two high p_T charged leptons, jets and $\not{E}_T$, which is known as the H_T parameter in the search for top

quark at the Tevatron [159,160]. Furthermore, one can use the kinematic constraints, similar to those used in the $t\bar{t}$ analysis carried out at the Tevatron, to purify the data sample with T-odd heavy quarks. Finally, one can construct the transverse mass of the final state system, in analogy to the one introduced in Ref. [157,158] for studying the longitudinal weak boson scattering, to further discriminate the SM background from the signal events. Therefore, the LSL signature of the T-odd quark pair events is expected to provide a clear verification or disproof of the Littlest Higgs model with T-parity unless the signal production rate is largely suppressed for very large f and therefore very heavy T-odd quarks.

(2) *Opposite-sign lepton ($\ell^{\pm}\ell^{\mp}+$ $\not{E}_T$ + jets) signatures (OSL)*: As shown in Fig. 5.12, the production of a T-odd heavy quark pair with opposite electric charges has a higher rate than the like-sign heavy quark pairs. For example,

$$u_-\bar{u}_- \to W_H^+ d W_H^- \bar{d} \to W^+W^- A_H A_H \bar{d}d,$$
$$u_-d_- \to W_H^+ d W_H^- u \to W^+W^- A_H A_H du,$$
$$d_-\bar{d}_- \to W_H^- u W_H^+ \bar{u} \to W^-W^+ A_H A_H u\bar{u} \text{ and}$$
$$d_-\bar{u}_- \to W_H^- u W_H^+ \bar{d} \to W^-W^- A_H A_H u\bar{d}$$

processes all give rise to the $\ell^+\ell^-+ \not{E}_T +$jets signature. When the mass of the T-odd heavy quark increases, the electroweak production rate becomes more important than the QCD production rate. One of the reasons is that the former process is dominated by the t-channel exchange of a relative light A_H boson, and the latter process is induced by the s-channel exchange of a virtual gluon. Another reason is that the former process can be initiated by two valence quarks (via t-channel process) while the latter process must involve a sea-quark parton whose density function becomes smaller in the large x-region for producing a heavier T-odd heavy quark pair.

The overall decay branching ratio for the above reactions is equal to Br[$q_-q_- \to$

LSL]. Hence, the OSL signal event rate is larger than the LSL signal event rate as indicated by the dot-dashed line in Fig. 5.12. However, the OSL signal suffers from a much larger SM background rate induced by the $t\bar{t}$ production. Nevertheless, the same strategies discussed above to suppress the SM background rate in the LSL analysis also applies to the OSL case because the signal events are all generated from a system with a much larger mass (i.e., the invariant mass of the heavy T-odd quark pair) as compared to the SM background processes. To be certain, a detailed Monte Carlo analysis is needed.

(3) *Single charged lepton ($\ell^{\pm}+\not{E}_T+$ jets) signature (1L)*: One may also consider the signal event signature with only one charged lepton in its final state, with one of $W^{\pm}$ decaying leptonically and another hadronically. The overall decay branching for the above reactions is equal to $Br[q_-q_- \to 1L] = Br[q_-q_- \to W_HW_Hqq \to 1L] + Br[q_-q_- \to W_HA_Hqq \to 1L] = 0.62^2 \times 2/9 \times 2/3 \times 2 + 0.62 \times 0.086 \times 2/9 \times 2 \simeq 0.14 \simeq 6 \times Br[q_-q_- \to LSL]$. The production rate is also higher, as presented by the dashed line in Fig. 5.12, for all the above T-odd heavy quark pair production channels are combined. On the other hand, the expected background will also be orders of magnitude higher. Hence, it is more challenging to detect the signal events in the single charged lepton mode.

5.4.2 The Third Generation Particles

In order to cancel the quadratic divergence induced by the top quark loop for Higgs boson mass correction at the one-loop order, we need to introduce additional heavy quarks (heavy partners of top quark) into the LHT model. In general, there are T_+ and T_- originated from the top quark Yukawa sector, cf. Eq. (2.20), and t_-, originated from the κ term interaction with b_- as its isospin partner, cf. Eq. (2.18).

(1) *$T_-\bar{T}_-$ production with $T_-\bar{T}_- \to A_HA_Ht\bar{t}$*: The $T_-\bar{T}_-$ production rate at the

LHC is quite large, which is about 30 fb for $f = 1$ TeV. The experimental signature of this signal event can be either OSL or 1L. Its production rate only depends on T_- mass and the decay branching ratio of $T_- \to tA_H$ is about 100 %. Therefore, it is important to test this production mode at the LHC, for the signal rate can be predicted with great confidence. We present OSL rates for $T_-\bar{T}_-$ production in Fig. 5.13 as the solid line. There have been a few studies in the literature discussing how to detect this channel at the LHC [64, 72, 80, 143], though more detailed Monte Carlo analysis is needed to confirm how well this channel can be detected. It was also pointed out that it could be very challenging to distinguish this production channel with the top-squark (stop) pair productions predicted by the Minimal Supersymmetric Standard Model (MSSM) with the subsequent decay of stop into top quark and the lightest supersymmetric particle (neutralino) [64,143]. Distinguishing the LHT model from the MSSM generally requires studying of all detectable experimental signatures induced by various production mechanisms predicted by the models. However, since the spin of the heavy particles (1/2 for T_- in the LHT model and scalar for stop in the MSSM) are different, the correlations of the final state particles may provide some useful discrimination tools.

(2) *$t_-\bar{t}_-$ and $b_-\bar{b}_-$ production*: For a particular choice of $\kappa = 1$, which makes t_- and b_- heavier then T_-, the $t_-\bar{t}_-$ production rate is at least one order of magnitude (depending on the value of f) lower than the $T_-\bar{T}_-$ rate. In case of $t_-\bar{t}_-$ production, there will be two b-jets associatively produced with a pair of OSL or 1L in its event signature. Likewise, the $b_-\bar{b}_-$ process gives rise to a $t\bar{t}$ pair in addition to the OSL or 1L signature. The rate for OSL+$t\bar{t}$ signature is presented in Fig. 5.13 by the dashed line. The rate for OSL+$b\bar{b}$ from $t_-\bar{t}_-$ production is very similar and is not shown. Depending on κ, $t_-\bar{t}_-$ production rate could be higher or lower than the $T_-\bar{T}_-$ production rate, making it, respectively, harder or easier to observe.

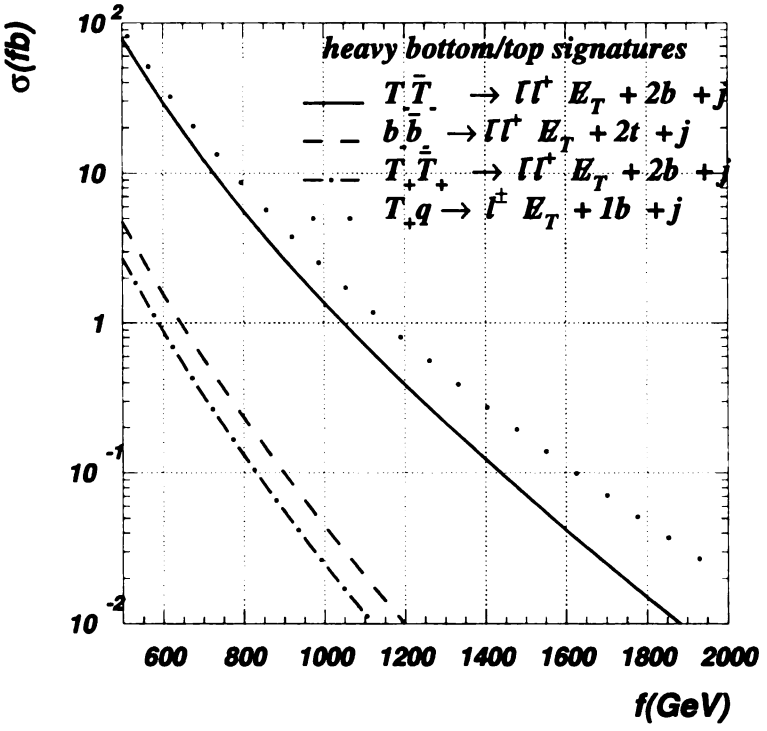

Figure 5.13: Rate for opposite-sign di-lepton and single charged lepton signatures from the third generation heavy quark pair production at the LHC.

(3) $T_+\bar{T}_+$ *production*: Since T_+ is heavier than T_-, the $pp \rightarrow T_+\bar{T}_+$ production rate (similar to the $t_-\bar{t}_-$ or $b_-\bar{b}_-$ production rate) is at least one order of magnitude lower than the $T_-\bar{T}_-$ production rate (depending on the value of f). The highest rates are for $T_+\bar{T}_+ \rightarrow W^+W^-b\bar{b}$ signature which should be checked against the SM $t\bar{t}$ background. The rate for OSL+$b\bar{b}$ signature is presented in Fig. 5.13 by the dot-dashed line. Again, the techniques discussed about for using the large invariant mass of the heavy system in the signal event to distinguish it from the SM background event could be useful for detecting the signal event in this channel.

(4) *Single* T_+ *production*: The rate of single-T_+ production associated with a light quark via t-channel electroweak interaction is actually higher than the rate of

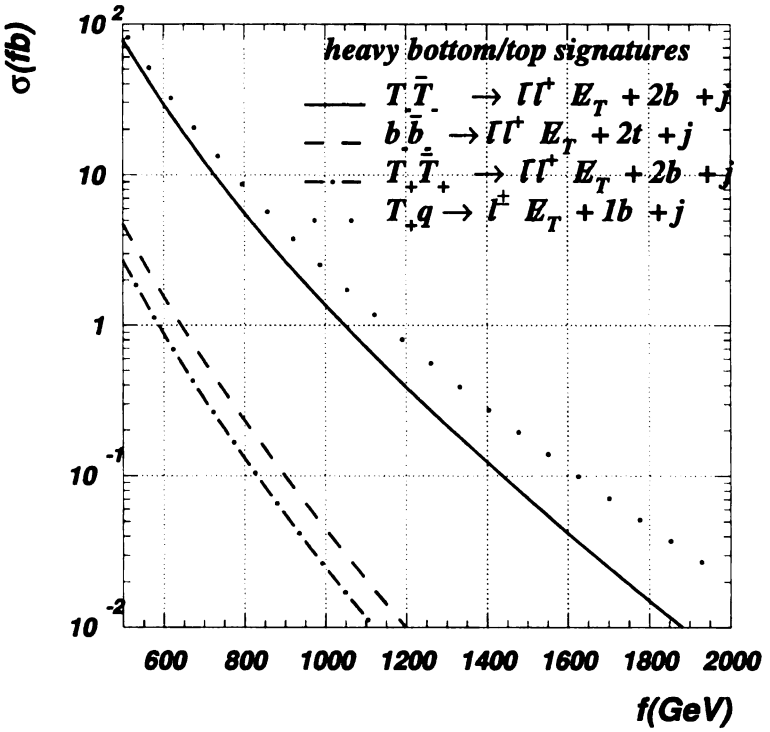

Figure 5.13: Rate for opposite-sign di-lepton and single charged lepton signatures from the third generation heavy quark pair production at the LHC.

(3) $T_+\bar{T}_+$ *production*: Since T_+ is heavier than T_-, the $pp \rightarrow T_+\bar{T}_+$ production rate (similar to the $t_-\bar{t}_-$ or $b_-\bar{b}_-$ production rate) is at least one order of magnitude lower than the $T_-\bar{T}_-$ production rate (depending on the value of f). The highest rates are for $T_+\bar{T}_+ \rightarrow W^+W^-b\bar{b}$ signature which should be checked against the SM $t\bar{t}$ background. The rate for OSL+$b\bar{b}$ signature is presented in Fig. 5.13 by the dot-dashed line. Again, the techniques discussed about for using the large invariant mass of the heavy system in the signal event to distinguish it from the SM background event could be useful for detecting the signal event in this channel.

(4) *Single* T_+ *production*: The rate of single-T_+ production associated with a light quark via t-channel electroweak interaction is actually higher than the rate of

$T_+\bar{T}_+$ pair production via strong interaction, as clearly shown in Fig. 5.13. The dominant experimental signature of the signal event is the same as the SM single-top event though it is expected with a much larger missing transverse momentum. In Fig. 5.13 the dotted line presents the rate of 1L signature originated from the single T_+ production in association with the light quark. Furthermore, the transverse mass of the signal event will be larger than that of the SM single-top event. In analogy to the SM single-top event, the single-T_+ signature is also characterized by a forward-jet which populates in the large rapidity region and can be used to suppress $t\bar{t}$ and $Wb\bar{b}$ backgrounds [150]. Again, a Monte Carlo study is needed to draw any definite conclusion about its detection at the LHC.

5.4.3 q_-V_H Associated Production

As discussed in Sec. 4.3, the Higgs boson production rate via gluon-gluon fusion process is always smaller than that predicted by the SM. However, because in most part of the model parameter space, a heavy T-odd Z_H decays almost entirely into a ZH pair, it provides a new production channel for the SM-like Higgs boson. The experimental signature of the q_-V_H pair production can be classified as follows.

(1) *q_-W_H production*: This signal process gives rise to OSL and 1L signatures with one less jet as compared to the T-odd heavy quark pair production, but without the LSL signature. The OSL signature rate for this process is presented as the solid line in Fig. 5.14.

(2) *q_-Z_H production*: The interesting decay chain of this signal process is $q_-Z_H \to q'W_HZ_H \to q'W^+A_HA_HH$ in which a high p_T Higgs boson is associatively produced with a W-boson. Its event rate is large, at about 12 fb level for $f = 1$ TeV and $\kappa = 1$. With a large $\not{E}_T$ in the event, it could be detectable, though a detailed Monte Carlo study is needed. The respective rate for $q'W^+A_HA_HH$ signature is presented in

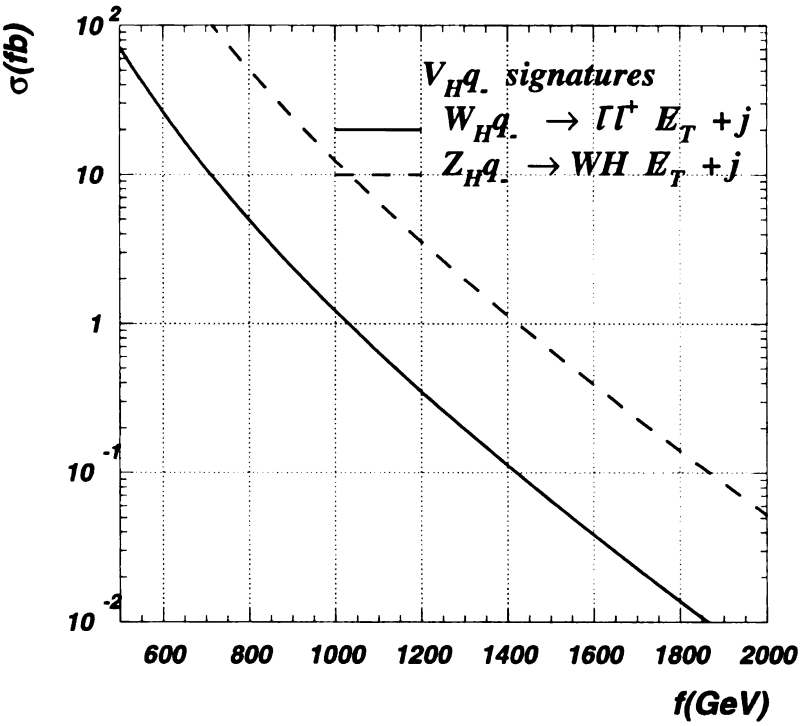

Figure 5.14: Rates for opposite-sign lepton and the Higgs associated production signatures from T-odd boson and quark associated production, $V_H q_-$, at the LHC.

Fig. 5.14 by the dashed line.

(3) $q_- A_H$ *production*: The decay chain $q_- A_H \to W_H q' A_H \to W A_H q' A_H$ provides the $W^{\pm} + \not{E}_T$ signature which is, however, not a promising channel to look for the signal, because the SM backgrounds, such as the $WZ(\to \nu\bar{\nu})$ production, is much larger than the signal event.

5.4.4 The T-odd Gauge Boson Pair Production

The experimental signatures of $V_H V_H$ events are similar to that of $q_- V_H$ events, but with one less high-p_T jet. Therefore, it requires a larger production cross section to detect such a signal event.

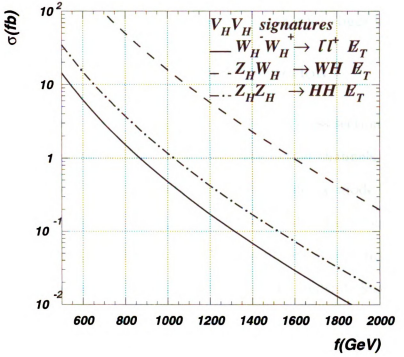

Figure 5.15: Rates for OSL, WH and HH signatures for various $V_H V_H$ production at the LHC.

(1) $Z_H W_H$ *production*: The event rate of $Z_H W_H \to A_H H W A_H$ is about the same as that for q_V_H production, but with almost 100 % decay branching ratio. The rate as a function of f is presented in Fig. 5.15 by the dashed line. Its experimental signature is the WH associated production with large $\not{E}_T$.

(2) $W_H^+ W_H^-$ *production*: The event rate of $W_H^+ W_H^- \to W^+ A_H W^- A_H$ is about 5 times smaller than that for q_V_H production. The solid line of Fig. 5.15 presents this OSL signature rate. Hence, it may be more challenging to detect such a signal event in the pure leptonic channel.

(3) $Z_H Z_H$ *production*: The event signature of $Z_H Z_H \to A_H H A_H H$ is the production of a pair of Higgs bosons with large $\not{E}_T$ in the event. Its production rate is

about one order of magnitude smaller than the $Z_H W_H$ production rate, as indicated by the dot-dashed line in Fig. 5.15. On the other hand, in spite of its small production rate, this process offers an interesting production channel for Higgs boson pairs.

5.4.5 Heavy T-odd Higgs Boson Production

The highest heavy T-odd Higgs production rate, with its cross section around 1 fb for $f \simeq 1$ TeV, comes from the $\phi^{++}\phi^{-}$ or $\phi^{--}\phi^{+}$ production channels. For the model parameters under study, there is no allowed two-body decay mode for ϕ^{++} boson, due to mass constraints. Nevertheless, 3-body decay modes of ϕ^{++} can take place at tree level, and it is also possible to have 2-body radiative decay modes dominating the decay branching ratios of ϕ^{++}. Hence, there will be multiple jets and leptons in such kind of signal events. However, the signal event rates are too small.

5.5 Searching for the $W_H^+ W_H^-$ Production at the LHC

In previous section, we show the productions of all the new particles predicted in the LHT model and categorize their interesting signatures at the LHC. We also estimate the signal event rates for given parameters. In this section, we will present a detailed Monte Carlo study on how to search for the signatures and examine the discovery potential of the T-odd gauge boson, W_H, at the LHC, including background study from the SM. The motivation of choosing W_H is because that, the mass of the W_H depends only on the symmetry breaking scale f. If we could measure its mass at the LHC, i.e. f is determined, it will provide a very useful information to test the LHT model.

The matrix elements of both signal and background processes are calculated by using MadGragh [161,162], while the decay widths of the new particles are calculated

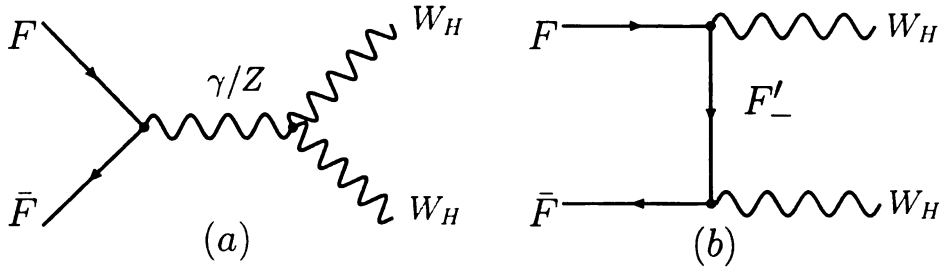

Figure 5.16: The tree-level diagrams for a W_H pair production at colliders.

in CalcHEP [146] with the LHT model files given by Ref. [125] , and we adopt CTEQ 6.1L parton distribution function [131] for our numerical studies.

5.5.1 Production

The tree-level diagrams for a W_H pair production are shown in Fig. 5.16, where F and F' denote quarks, and the subscript "$-$" means the T-odd particle. The W_H boson pair can be produced either via the s-channel process with a photon or a Z-boson exchanged or via the t-channel process with a T-odd fermion exchanged. Since the t-channel diagram involves the heavy T-odd fermion, therefore, its contribution depends on both m_{W_H} and m_{F_-}. Here, we choose the model parameters (f, κ_q) instead of the physical masses of the new particles as the theoretical inputs.

In Fig. 5.17(a) and Fig. 5.17(b) we show the total cross section of the W_H pair production as a function of κ_q and f, respectively. The T-odd quark in the t-channel diagram affects the total cross section significantly: (i) for $500\,\text{GeV} < f < 1000\,\text{GeV}$, there exists a κ_q^{min} (~ 0.6) which minimizes the total cross section; (ii) for a fixed κ_q, the cross section decreases rapidly with increasing f. In order to understand why the minimum of the total cross section occurs, we separate the total cross section into three pieces,

$$\sigma_{tot} = \sigma_s + \sigma_t + \sigma_{\text{int}}, \tag{5.5}$$

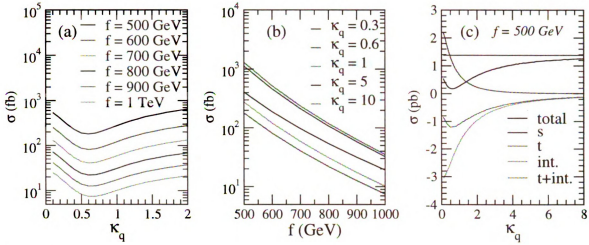

Figure 5.17: Production rates of the $pp \to W_H^+ W_H^-$ process at the LHC for various values of parameters f and κ_q.

where σ_s, σ_t and σ_{int} denote the contributions of the s-channel diagram, t-channel diagram and the interference between the s- and t-channel diagrams, respectively. For illustration, we choose $f = 500\,\text{GeV}$ and plot each individual contribution in Fig. 5.17(c). The s-channel diagram involves the gauge bosons only, therefore, its contribution depends on f but not on κ_q, cf. the flat blue curve. On the contrary, the t-channel contribution decreases with increasing κ_q, because the mass of the T-odd quark in the t-channel propagator grows with increasing κ_q, cf. the red curve. Although the s-channel and t-channel contributions are both constructive, their interference is destructive. The total cross section reaches the minimum when $\kappa_q \sim \kappa_q^{min}$, where the s- and t-channel contributions are comparable. When $\kappa_q > \kappa_q^{min}$, the total cross section is dominated by the s-channel contribution, therefore it drops rapidly with increasing f since the s-channel contribution suffers from the $1/\hat{s}$ suppression, where $\hat{s}$ is the invariant mass of the W_H boson pair. When $\kappa_q \gg \kappa_q^{min}$, the total cross section approaches to the s-channel contribution and both the t-channel contribution and the interference effect are negligible.

5.5.2 Decay of W_H boson

The W_H boson will decay into a T-odd particle and a T-even SM particle. Its decay pattern is mainly determined by the masses of new T-odd particles. In the LHT model,

$$\begin{aligned} m_{A_H} &\simeq \frac{g'f}{\sqrt{5}} \simeq 0.156f, \\ m_{W_H} &\simeq gf \simeq 0.653f, \\ m_{\ell_-} &\simeq \sqrt{2}\kappa_\ell f \simeq 1.414\kappa_\ell f, \\ m_{q_-} &\simeq \sqrt{2}\kappa_q f \simeq 1.414\kappa_q\, f. \end{aligned} \tag{5.6}$$

It is clear that the A_H boson is always lighter than the W_H boson. But the T-odd quark (lepton) can be heavier or lighter than the W_H boson, depending on the parameter κ_q (κ_ℓ). Let us denote F_- as the T-odd fermion whose mass m_{F_-} is $\sqrt{2}\kappa f$. When $\kappa < 0.11$, $m_{F_-} < m_{A_H} < m_{W_H}$, therefore the T-odd lepton or T-odd quark will be the lightest T-odd particle and plays the role as a dark matter candidate. As pointed out in Ref. [163], the dark matter candidates should be charge neutral and colorless objects. Hence, we focus our attention to the case of $\kappa_\ell\,(\kappa_q) > 0.11$ our study, i.e. demanding A_H to be the lightest T-odd particle. When both κ_q and κ_ℓ are larger than 0.462, i.e. $m_{A_H} < m_{W_H} < m_{F_-}$, the W_H boson only decays via the $W_H \to W + A_H$ channel. When $0.11 < \kappa < 0.462$, i.e. $m_{A_H} < m_{F_-} < m_{W_H}$, then W_H boson can decay into either WA_H or F_-F' (F' being a usual SM fermion).

In Fig. 5.18(a) we summarize the decay pattern of W_H in the plane of κ_q and κ_ℓ, where the following decay modes are considered:

$$W_H \to WA_H \to \ell\bar{\ell}'\,(q\bar{q}')\,A_H,$$

$$W_H \to \ell_-\nu_\ell \to \ell A_H \nu_\ell,$$

$$W_H \to \nu_{\ell_-}\ell \to \nu_\ell A_H \ell,$$

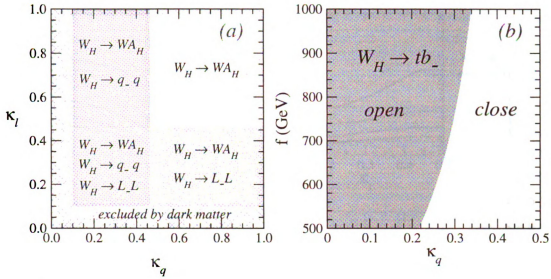

Figure 5.18: (a) Pictorial illustration of the decay pattern of the W_H in the plane of κ_q and κ_ℓ; (b) The allowed region (blue) of κ_q for the $W_H \to tb\_$ mode being opened.

$$W_H \to q\_q' \to qA_H q'.$$

Here, $\ell(\nu,\ q)$ denotes the charged leptons (neutrinos, quarks). We also include the subsequent decay of the second T-odd fermions whose decay branching ratio is 100 % for $0.11 < \kappa < 0.462$. In the above decay modes, the $W_H \to tb\_ \to tbA_H$ mode is special because of the large top quark mass (m_t). In order to open the decay mode $W_H \to tb\_$, the mass constraint $m_{W_H} > m_t + m_{b\_}$ has to be satisfied and the allowed region of κ_q and f is shown in Fig. 5.18(b). As shown in Eq. (5.6), the mass relation between the W_H, A_H and $F\_$ is fixed by κ and does not depend on f. Thus, the decay branching ratios of the $W_H \to WA_H$ and $W_H \to F\_F'$ modes do not depend on f if the $tb\_$ mode is not opened. Once the $tb\_$ mode is opened, the decay branching ratios of other modes will be slightly reduced.

In Fig. 5.19, we show the decay branching ratios of the W_H boson as a function of κ_ℓ and κ_q, respectively. Explicit numbers of the decay branching ratios for the selected benchmark points are listed in Table 5.2.

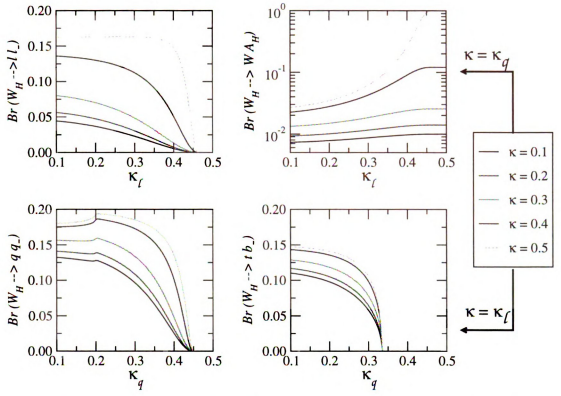

Figure 5.19: Decay branching ratios of the W_H boson for $f = 500$ GeV.

5.5.3 Phenomenology at the LHC

The production rate of a $W_H^+ W_H^-$ pair at the LHC is sizable, but the detection for its signatures at the hadron collider was expected to be challenging in the literature [72, 125]. However, we will demonstrate that the LHC not only has a great potential to discover the collider signature of the $W_H^+ W_H^-$ pair production, but also has the capability to explore enormous parameter space of f and κ.

At the LHC, we demand the two W_H bosons both decay leptonically in order to avoid the huge QCD backgrounds. We further require the two charged leptons in the final state having different lepton flavors. Hence, the collider signature of the signal events is $e^+\mu^- \not{E}_T$ (or $e^-\mu^+ \not{E}_T$), where the missing energy ($\not{E}_T$) is originated from two lightest T-odd particles A_H and two neutrinos. For simplicity, we will present the study of $e^+\mu^- \not{E}_T$ signature throughout this section, but it is very straightforward to

(κ_ℓ, κ_q)	(0.3, 0.3)			(0.5, 0.3)			(0.3, 0.5)			(0.5, 0.5)
f (GeV)	500	700	1000	500	700	1000	500	700	1000	500
ℓ_ν	4.45	4.61	4.33	0	0	0	15.0	15.9	16.3	0
ν_ℓ	4.84	4.81	4.41	0	0	0	16.3	16.5	16.6	0
U_D	14.5	14.4	13.2	20.1	20.1	17.9	0	0	0	0
D_U	13.4	13.8	13.0	18.5	19.3	17.6	0	0	0	0
t_b	14.5	14.4	13.2	20.1	20.1	17.9	0	0	0	0
$tb\_$	0	0	7.79	0	0	10.6	0	0	0	0
$W A_H$	1.84	0.8	0.33	2.55	1.12	0.45	6.19	2.76	1.25	100

Table 5.2: Decay branching ratios (%) of the W_H boson for a few benchmark points, where $\ell = e, \mu, \tau$, $\nu = \nu_e, \nu_\mu, \nu_\tau$, $U = u, c$ and $D = d, s$. Note that all the SM fermions (except the top quark) are treated as massless.

include the contribution of $e^-\mu^+ \not{E}_T$ mode as those two decay modes are identical *.

When W_H is the second lightest T-odd particle, i.e. κ_q and κ_ℓ are both larger than 0.462, the signal events only come from the following process

$$pp \to W_H^+ W_H^- \to A_H W^+(\to e^+\nu_e) A_H W^-(\to \mu^-\bar{\nu}_\mu). \tag{5.7}$$

However, when the T-odd leptons are lighter than W_H, i.e. $\kappa_\ell < 0.462$, the signal will mainly come from the process

$$pp \to W_H^+ W_H^- \to \ell_1\_\ell_2\ell_3\_\ell_4 \to e^+\mu^-\nu_e\bar{\nu}_\mu A_H A_H, \tag{5.8}$$

where $\ell_i = e$, μ, ν_e or ν_μ. The total cross sections of these two processes are shown in Fig. 5.20 where the left plot is for the process in Eq. (5.7) with $\kappa_\ell = 0.5$

*The mass difference between e and μ can be safely ignored in our study since we are dealing with new particles whose masses are at the order of TeV.

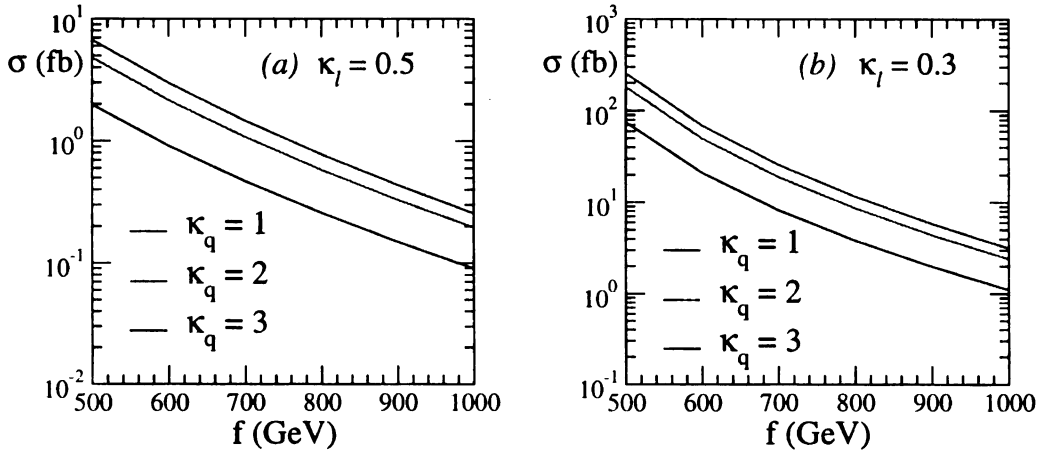

Figure 5.20: The total cross section of $pp \to W_H^+ W_H^- \to e^+\mu^- + \not{E}_T$ at the LHC for different parameter space: Left plot: $\kappa_\ell > 0.462$; Right plot: $\kappa_\ell < 0.462$.

while the right plot is for the process in Eq. (5.8) with $\kappa_\ell = 0.3$. If W_H is the second lightest T-odd particle, the signal will only come from Eq. (5.7) since the W_H can only decay to WA_H; otherwise, the process in Eq. (5.8) dominates. The total rate of the signal events depends on the masses of ℓ_-, q_- and W_H, and as shown in Fig. 5.20, the total cross section is sizable when f is small and κ_q is large. This is because that the mass of T-odd gauge boson is light and the destructive effect from t-channel and s-channel interference term is small.

The main intrinsic backgrounds come from the W^+W^- and the ZW^+W^- continuum productions with the subsequent decays $W^+ \to \ell^+\nu_\ell$, $W^- \to \ell^-\bar{\nu}_\ell$ and $Z \to \nu\nu$[†] . There also exist other reducible backgrounds from the top quark pair production and the Wt associated production which can be highly suppressed by vetoing the additional b-jet from the top quark decay with large transverse momentum or in the central rapidity region. The vetoing efficiency is so large, about 99.9 % for the $t\bar{t}$ background and 99.6 % for the Wt background, that we only need to consider the intrinsic

[†]Generally speaking, we also need to consider the background from Higgs boson decay into a W boson pair, which is $gg \to H \to W^+W^-$. The total rate depends on the mass of Higgs boson. For instance, the total cross section is $\sim$ 95 fb when the Higgs boson is 120 GeV, and $\sim$ 230 fb when Higgs boson is 170 GeV. However, it can be completely suppressed by imposing the kinematics cuts discussed later.

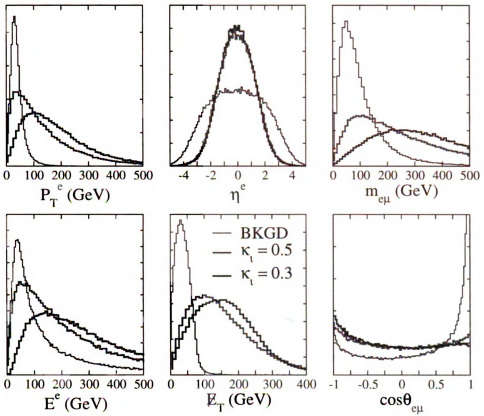

Figure 5.21: Transverse momentum of e^+/μ^- ($p_T^{e/\mu}$), rapidity of e^+/μ^- ($\eta^{e/\mu}$), invariant mass of e^+ and μ^- ($m_{e\mu}$), energy of e^+/μ^- ($E^{e/\mu}$), missing transverse momentum ($\not{E}_T$), cosine of the opening angle between e^+ and μ^-($\cos\theta_{e\mu}$) distributions for $\kappa_q = 1$ and $f = 700\,\text{GeV}$. All curves are normalized by their total cross sections.

backgrounds in this study. The total cross section of the W^+W^- pair production background is about 0.865 pb while the other intrinsic background from W^+W^-Z is negligible (~ 0.08 fb). These cross sections already include the decay branching ratios of $W \to \ell\nu$ and $Z \to \nu\nu$. Below, we just consider the W^+W^- pair production as the background at the LHC.

Kinematics of the signal events is distinctively different from that of background events. As to be shown later, these differences can be used to significantly suppress the background and enhance the ratio of signal to background (S/B). For illustration, we show normalized distributions of various kinematics observables of the signal and

background events in Fig. 5.21: transverse momentum ($p_T^{e/\mu}$), rapidity ($\eta^{e/\mu}$), energy ($E^{e/\mu}$) of charged leptons, invariant mass of two charged leptons ($m_{e\mu}$), missing transverse momentum ($\not{E}_T$) and cosine of the opening angle between two charged leptons ($\cos\theta_{e\mu}$). The curves labeled by $\kappa_\ell = 0.5$ and $\kappa_\ell = 0.3$ correspond to the signals described in Eq. (5.7) and Eq. (5.8), respectively. A few interesting points are summarized below:

- Compared to the background, the typical feature of the signal events is that the final state particles are more energetic, cf. Fig. 5.21(a), (c), (d), (e).

- As the decay products of heavy W_H bosons, the two charged leptons mainly appear in the central region, cf. Fig. 5.21(b), because W_H is hardly boosted.

- We also note that, unlike the background, two charged leptons of the signal do not exhibit strong correlations, see the nearly flat behavior in the $\cos\theta_{e\mu}$ distribution. It can be understand as follows. Since m_{W_H} is much larger than m_W and m_{A_H}, W and A_H will be predominately in the longitudinal polarization state, i.e. behaving as scalars. Thus, the spin correlation between e^+ and μ^- is lost, which results in a flat distribution. On the contrary, the two charged leptons in the SM background are highly correlated.

- The signal distributions change a lot when varying the value of κ_ℓ. In particular, for a Small κ_ℓ, i.e. $\kappa_\ell = 0.3$, the peak positions of the $p_T^{e/\mu}$, $m_{e\mu}$, $E_e^{e/\mu}$ and $\not{E}_T$ distributions are shifted to the large value region when compared to those of large κ_ℓ, i.e. $\kappa_\ell = 0.5$. This is due to the fact that for a small κ_ℓ, the charged leptons (e^+ and μ^-) or the neutrinos (ν_e and $\bar{\nu}_\mu$) are directly generated from the W_H boson decay, e.g. $W_H^+ \to e^+\nu_{e\_}$ or $W_H^+ \to \nu_e e_-^+$, and therefore are more energetic.

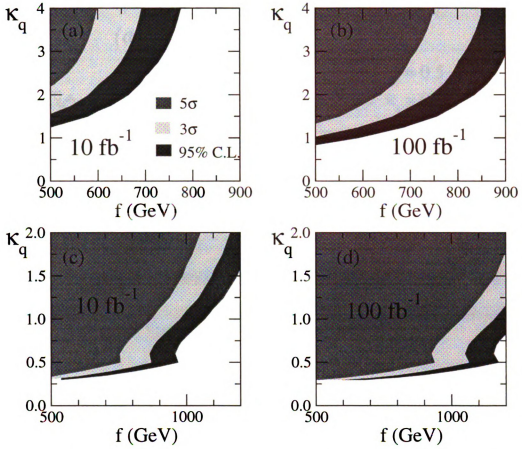

Figure 5.22: Statistical significance contour of signature of $pp \to W_H^+ W_H^- \to \ell^+\ell'^-\nu_\ell\bar{\nu}_{\ell'}A_H A_H$ in the plane of κ_q and f at the LHC. The upper two plots are for $\kappa_\ell = 0.5$ while the lower two are for $\kappa_\ell = 0.3$.

In order to mimic the detector, we require $p_T^{e/\mu}$ and $\eta^{e/\mu}$ to satisfy the following basic cuts:

$$p_T^e > 20.0\,\text{GeV}\,,\; p_T^\mu > 20.0\,\text{GeV}\,,\; |\eta^e| < 2.0\,,\; |\eta^\mu| < 2.0$$

Furthermore, taking advantage of the differences between the kinematics of the signal and background events, we impose the following *optimal cuts* to extract the signal out of the SM background,

$$\not{E}_T > 175\,\text{GeV}\,,\; \cos\theta_{e\mu} < 0.6 \tag{5.9}$$

After imposing the optimal cuts, the main background from the W^+W^- pair produc-

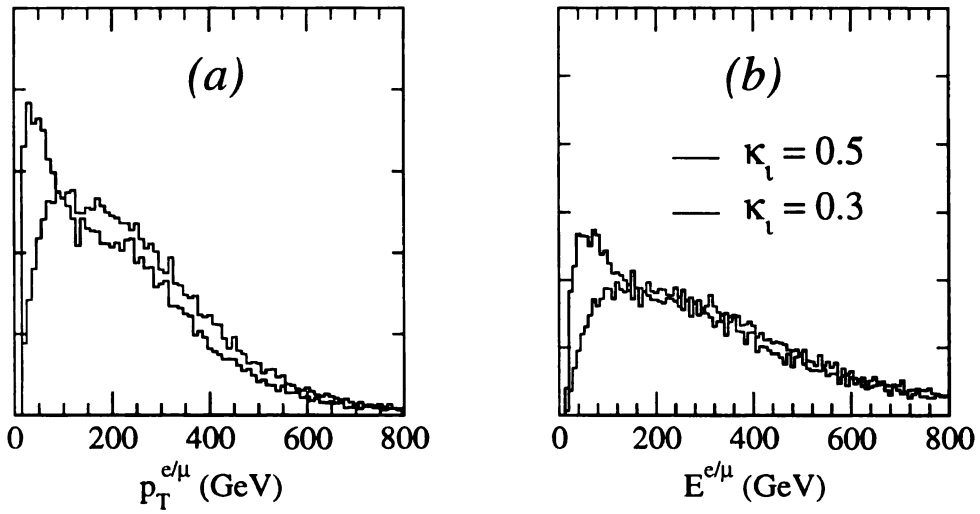

Figure 5.23: Normalized distributions of $p_T^{e/\mu}$ and $E^{e/\mu}$ for $f = 700\,\text{GeV}$ and $\kappa_q = 1$ for $pp \to W_H^+ W_H^- \to e^+\mu^-\nu_e\bar{\nu}_\mu A_H A_H$ process after imposing the kinematics cuts given in Eq. (5.9) at the LHC.

tion can be suppressed by more than 99% and gives rise to 19 background events for $\mathcal{L} = 10\,\text{fb}^{-1}$ while 192 events for $\mathcal{L} = 100\,\text{fb}^{-1}$, where $\mathcal{L}$ denotes the integrated luminosity. These background rates include both $e^+\mu^-$ and $e^-\mu^+$ modes. In Fig. 5.22 we present the 5σ, 3σ statistical significance and 95% confidence level (C.L.) for $\kappa_\ell = 0.5$ (top raw) and $\kappa_\ell = 0.3$ (bottom raw). For $\kappa_\ell = 0.5$, the W_H boson is the second lightest T-odd particle and the signal events come from Eq. (5.7) only. When f is 500 GeV, the signal can reach more than 3σ statistical significance for $\kappa_q \gtrsim 1.5$ with $\mathcal{L} = 10\,\text{fb}^{-1}$ and $\kappa_q \gtrsim 1$ with $\mathcal{L} = 100\,\text{fb}^{-1}$, respectively. Furthermore, the f can be probed up to about 770 GeV with $\mathcal{L} = 10\,\text{fb}^{-1}$ and 950 GeV with $\mathcal{L} = 100\,\text{fb}^{-1}$, respectively, at the 95% C.L.. On the other hand, for $\kappa_\ell = 0.3$, the T-odd leptons are lighter than W_H and the signal events predominantly come from Eq. (5.8) due to the large decay branching ratios. In this case, one can probe more parameter space of the LHT model, cf. Fig. 5.22 (c) and (d). For example, assuming $\kappa_q = 1$, one can probe f up to 900 GeV with $\mathcal{L} = 10,\text{fb}^{-1}$ and 1050GeV with $\mathcal{L} = 100\,\text{fb}^{-1}$, respectively, at the 5σ level.

As shown above, it is very promising to use the $e\mu+ \not{E}_T$ signature to detect the $W_H W_H$ pair production at the LHC. But such a signature can originate from two processes, either Eq. (5.7) or Eq. (5.8), depending on the value of κ_ℓ. Therefore, one immediate task after observing such a signature is to determine from which process it comes. It turns out that this question can be easily answered by the $p_T^{e/\mu}$ and $E^{e/\mu}$ distributions, cf. Fig. 5.23 where we have imposed the optimal cuts. In case of $\kappa_\ell = 0.3$, the charged lepton is directly emitted from the T-odd gauge boson decay, therefore its transverse momentum is typically larger than the one of the charged lepton emitted form the W-boson decay, i.e. $\kappa_\ell = 0.5$. Same argument also works for the energy distributions. Hence, one can fit the observed $p_T^{e/\mu}$ and $E^{e/\mu}$ distributions to the LHT model predictions to measure κ_ℓ, though κ_q, which merely change the normalization of both distributions, remains unknown.

5.6 Searching for a $W_H^+ W_H^-$ Pair Production at Linear Collider

Compared to the LHC, the Linear Collider (LC) does not have a sufficient energy to produce very heavy W_H bosons. For example, a TeV LC can only probe the W_H boson mass up to 500 GeV, which corresponds to $f \simeq 750$ GeV. However, the LC provides a much cleaner experimental environment (no QCD backgrounds) which is perfect for precision measurements. As mentioned before, because of suffering from the extremely huge QCD backgrounds, one has to use the leptonic decay mode for the W_H boson search at the LHC. One can observe a deviation from the SM prediction, but one cannot determine the mass or spin of the W_H boson due to the four missing particles (two lightest T-odd particles A_H and two neutrinos) in the final state. In this section we preform a comprehensive study of the W_H pair production at the LC and address on the following questions:

- Can one determine the masses of W_H and A_H?
- Can we reconstruct the kinematics of the missing particle A_H?
- Can we measure the spin of W_H?

As to be shown later, all these questions can be answered at the LC with the help of the known center-of-mass (c.m.) energy.

5.6.1 Production

The tree level diagrams of producing a $W_H^+W_H^-$ pair at the LC are shown in Fig. 5.16, with F being electron e^- and F_- being T-odd neutrino ν_{e-}. We present the total cross section of the W_H pair production as a function of κ_ℓ and f in Fig. 5.24(a) and (b), respectively. In analogue to the W_H pair production at the LHC, there also exists a κ_ℓ^{min} due to the destructive interference effect, but now κ_ℓ^{min} is very sensitive to f. As shown in Fig. 5.24 (a), κ_ℓ^{min} shifts from about 0.5 to 1.0 when f increases from 500 GeV to 750 GeV. We also note that when κ_ℓ is small (e.g. $\kappa_\ell = 0.3$), the total cross section drops much slower than the total cross section of large κ_ℓ, see Fig. 5.24 (b).

Following the LHC study, we split the total cross section into the s-channel, t-channel and the interference contributions. In Fig. 5.25 we explicitly plot the total cross section (black curve), the s-channel contribution (blue curve), the t-channel contribution (red curve) and the interference contribution (INT) (green curve). Fig. 5.25 (a) and (b) show the total cross section as a function of κ_ℓ for $f = 500\,\text{GeV}$ and 750 GeV, respectively. We have learned from the LHC study that the minimal cross section for a fixed f occurs when $\sigma(s) \simeq \sigma(t)$. When f increases from 500 GeV to 750 GeV, the s-channel contribution drops rapidly since it suffers from the $1/\hat{s}$ suppression, but on the other hand, the t-channel contribution does not. Of course,

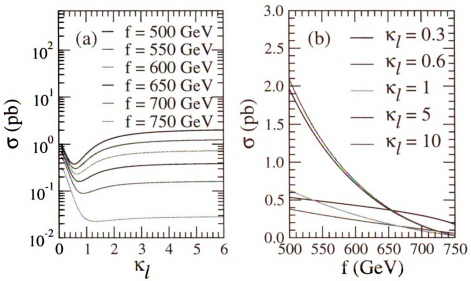

Figure 5.24: Total cross sections of a $W_H^+ W_H^-$ pair production at Linear Collider for various f and κ_ℓ.

increasing f value will increase the mass of W_H boson and reduce the t-channel contribution, but the suppression in the t-channel contribution is much less than that in the s-channel contribution. Therefore, the position for $\sigma(s) \simeq \sigma(t)$ is shifted to larger κ_ℓ region. The reason why the cross section of $\kappa_\ell = 0.3$ drops slowly in the large f region can also be understood from the competition between the s- and t-channel contributions. In Fig. 5.25 (c) we show the total cross section as a function of f for $\kappa_\ell = 0.3$. For such a small κ_ℓ, the T-odd neutrino's mass is small ($m_{\nu_-} \simeq 0.42f$). Then the t-channel contribution dominates over the s-channel contribution. In the large f region, i.e. $600\,\text{GeV} < f < 750\,\text{GeV}$, the s-channel contribution as well as the interference effect both decrease to zero, and the total cross section approaches to the t-channel contribution which does not drop rapidly with increasing f.

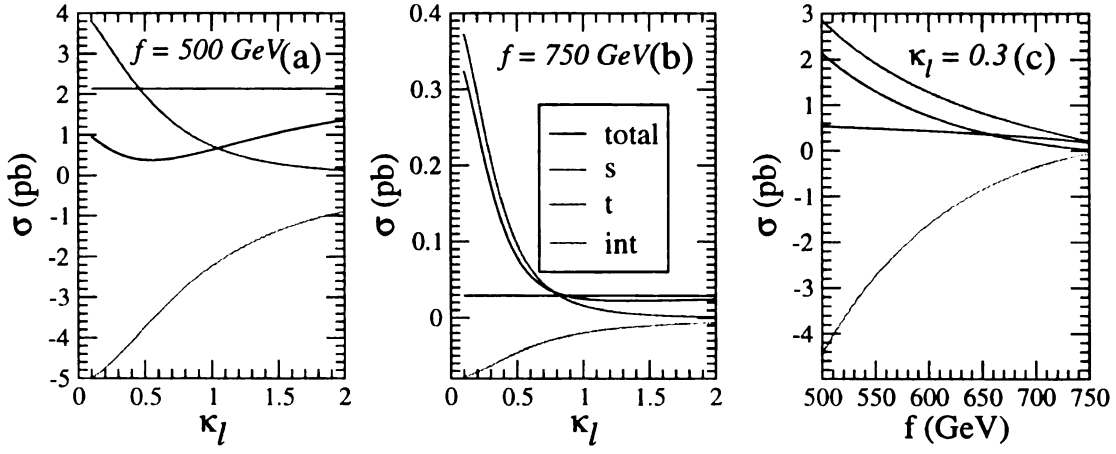

Figure 5.25: The distributions of s-, t-channel diagrams and interference term in the $W_H^+W_H^-$ production at the LC.

5.6.2 Collider Phenomenology at the LC

At the LC, we are able to search the W_H boson using its hadronic decay mode $W_H \to A_H W \to A_H jj$. Below, we consider the following signal process

$$e^+e^- \to W_H^+W_H^- \to W^+(\to jj)W^-(\to jj)A_H A_H, \tag{5.10}$$

which gives rise to a collider signature of four isolated jets associated with large missing energy originated from the two undetectable A_H bosons in the final state. The main intrinsic background is from the process $e^+e^- \to W^+W^-Z \to jjjj\nu\bar{\nu}$ whose cross section is about 5.6 fb. In Fig. 5.26, we show the cross section of the signal process given in Eq. (5.10) at the LC. The total cross section relies on how large the decay branching ratio of the $W_H \to WA_H$ mode is: (1) when both κ_ℓ and κ_ℓ are large, $Br(W_H \to WA_H) = 1$ which leads to a large cross section, see the black (solid) curve; (2) when either κ_q or κ_ℓ is small, $Br(W_H \to WA_H)$ is highly suppressed, so the total cross section becomes small, see the blue (dashed), the red (dotted) and the green (dot-dashed) curves. In this work we focus our attention on the first case, i.e. large κ_q and κ_ℓ, in which W_H is the second lightest T-odd particle. Since the cross section of the signal process is much higher than the WWZ background, it

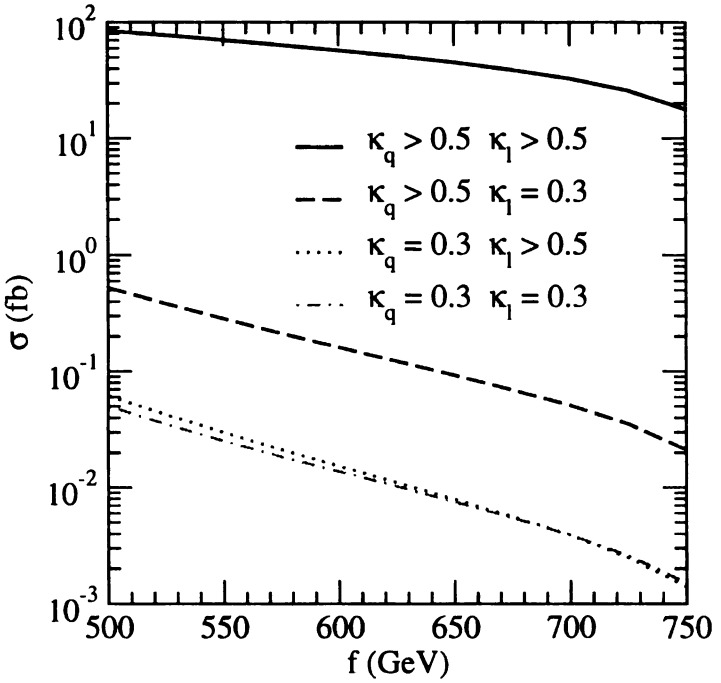

Figure 5.26: Total cross section for $e^+e^- \to W_H^+ W_H^- \to A_H A_H jjjj$ at the LC.

is not difficult to disentangle the signal from the background. Therefore, only the basic kinematics cuts, but no further hard cuts, are applied to select the event in the following study. For comparison, we also present the background distributions.

5.6.2.1 Mass measurement of W_H

In order to simulate the detector acceptance, we require the transverse momentum (p_T^j) and rapidity (η^j) of all the final state jets to satisfy the following basic cuts

$$p_T^j > 15\,\mathrm{GeV}, \qquad \left|\eta^j\right| < 3\,.$$

We also demand that the four jets are resolvable as separated objects, i.e. requiring the separation in $\Delta R \equiv \sqrt{(\delta\eta)^2 + (\delta\phi)^2}$ between any two jets to be larger than 0.4, where $\delta\eta$ and $\delta\phi$ denote the separation in the rapidity and azimuthal angles, respectively. In order to reconstruct the two W bosons, one need to isolate the four jets coming from the W boson decay. Unfortunately, one cannot tell the jets apart experimentally because the information of quark's charge and flavor is lost during the

hadronization of the light quarks. In order to measure m_{W_H}, one needs to reconstruct the two W bosons, i.e. finding out which two jets come from which W boson. In this study we use the W boson mass as a constraint to reconstruct two W bosons:

- In order to identify the jets, we order the four jets by their transverse momentum,

$$p_T^{j_1} \geq p_T^{j_2} \geq p_T^{j_3} \geq p_T^{j_4}.$$

- We loop over all combinations of the four jets, i.e. (j_1j_2, j_3j_4), (j_1j_3, j_2j_4) and (j_1j_4, j_2j_3), and calculate the invariant masses of the reconstructed W bosons. We then calculate the deviations from the true W boson mass (m_W) for each combination,

$$\Delta = \sqrt{(m_1(jj) - m_W)^2 + (m_2(jj) - m_W)^2},$$

and select the combination giving rise to the minimal deviations to reconstruct the W bosons. Although the efficiency of the W boson reconstruction procedure is very high ($\sim 99.1\%$), we cannot distinguish the two reconstructed W bosons because the charge information is lost. But as to be shown below, we do not need the information of the W boson charge to determine the mass and spin of W_H. Just for bookmark we denote the W boson consisting the highest p_T jet as W_1 while the other W boson as W_2.

In Fig. 5.27, we present the energy distributions of the reconstructed W bosons (E_W) where the energy of W_1 (E_{W_1}) peaks in the large energy region while the energy of W_2 (E_{W_2}) in the small energy region. The asymmetry between W_1 and W_2 is due to our requirement that the W_1 boson includes the leading-p_T jet. Since the A_H bosons are massive, the E_W distributions exhibit sharp drops in both small and large

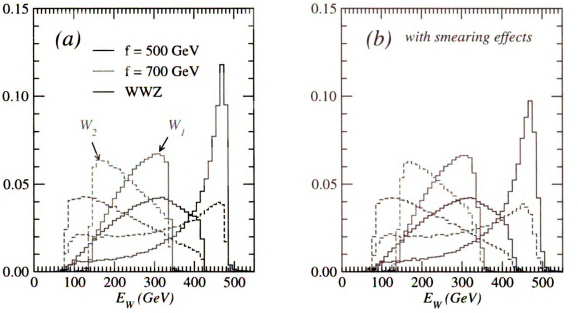

Figure 5.27: Normalized energy distributions of the reconstructed W bosons for $\kappa_q = 1$ at the LC.

energy regions, which can be used to measure the masses of W_H and A_H [164]. The ending points of the energy distribution of the W boson are given by

$$E_{\pm} = \gamma \left(E_W^{\star} \pm \beta p_W^{\star} \right), \tag{5.11}$$

where $\beta = \sqrt{1 - 4m_{W_H}^2/s}$, $\gamma = 1/\sqrt{1-\beta^2}$ and $E_W^{\star}$ ($p_W^{\star}$) is the energy (momentum) magnitude of the W boson in the rest frame of W_H,

$$E_W^{\star} = \frac{m_{W_H}^2 - m_{A_H}^2 + m_W^2}{2m_{W_H}}, \tag{5.12}$$

$$p_W^{\star} = \frac{\sqrt{\left[m_{W_H}^2 - \left(m_{A_H} + m_W\right)^2\right]\left[m_{W_H}^2 - \left(m_{A_H} - m_W\right)^2\right]}}{2m_{W_H}}. \tag{5.13}$$

From $E_{\pm}$ we can derive m_{W_H} and m_{A_H} as follows:

$$m_{W_H} = \sqrt{\frac{s}{2}} \frac{\sqrt{E_+ E_-}}{E_+ + E_-} \sqrt{1 + \frac{m_W^2}{E_+ E_-} + \sqrt{\left(1 - \frac{m_W^2}{E_+^2}\right)\left(1 - \frac{m_W^2}{E_-^2}\right)}}, \tag{5.14}$$

$$m_{A_H} = m_{W_H}\sqrt{1 - \frac{2\,(E_+ + E_-)}{\sqrt{s}} + \frac{m_W^2}{m_{W_H}^2}}. \tag{5.15}$$

In this study, we choose two sample points: (1) $m_{W_H} = 320\,\text{GeV}$ and $m_{A_H} = 66\,\text{GeV}$ for $f = 500\,\text{GeV}$; (2) $m_{W_H} = 450\,\text{GeV}$ and $m_{A_H} = 101\,\text{GeV}$ for $f = 700\,\text{GeV}$. Hence, for the former sample point, $E_+ = 426\,\text{GeV}$ and $E_- = 85\,\text{GeV}$, while for the latter sample point, $E_+ = 345\,\text{GeV}$ and $E_- = 146\,\text{GeV}$. The small tails of the lower and higher ending points are due to the width effects of W_H boson and W-boson. After reading out the ending points from the E_W distribution, one can determine m_{W_H} and m_{A_H} from Eqs. (5.14) and (5.15). The accuracy of this method highly depends on how well one can reconstruct the W boson momentum and how well one can determine the ending points. Furthermore, the collider detection is not perfect. In order to mimic the finite detection efficiency of the detector, we smear the momenta of all the final state jets by a Gaussian distribution with

$$\frac{\Delta E}{E} = \frac{50\%}{\sqrt{E}}, \tag{5.16}$$

where E is the energy of the observed parton and the resolution of the energy measurement is assumed to be $50\%\sqrt{E}$. The E_W distributions after energy smearing are shown in Fig. 5.27 (b). We note that the shapes of the distributions of both signal and background are changed slightly, but the positions of the ending points remain almost the same, which lead to 4% and 8% error in the mass measurements of W_H and A_H for $f = 700$ GeV, respectively.

5.6.2.2 Spin correlations

Although one can derive the W_H mass by using E_+ and E_- from the E_W distributions, one still needs to verify that such a signal indeed comes from the LHT model and not from other new physics models. For example, the minimal supersymmetric

extension of the standard model (MSSM) with R-parity can also have exactly the same collider signature ($4j + \not{E}_T$) from the process

$$e^+e^- \to \widetilde{W}^+\widetilde{W}^- \to \tilde{\gamma}\tilde{\gamma}W^+(\to jj)W^-(\to jj),$$

where the photino ($\tilde{\gamma}$) is the lightest SUSY particle which plays as the dark matter candidate. Examining the kinematics distributions is not sufficient to discriminate the LHT model from the MSSM. Below we will show that the spin correlation between the W boson and its mother particle is a good tool to tell these two models apart.

Taking advantage of the known c.m. energy of the LC, one can reconstruct the kinematics of the two missing A_H bosons and in turn study the spin correlation effects for model discrimination. Details of the event reconstruction are shown in the Appendix. Below, we only present our results of the phenomenological study. After event reconstruction, we denote A_{H1} as the reconstructed A_H boson associated with W_1 while A_{H2} as the one with W_2. The inequality $\mathbb{C}^2 > 0$ (cf. Eq. (C.16)), has to be satisfied in order to reconstruct the momentum of A_H's. Since $\mathbb{C}^2$ depends on m_{W_H} and m_{A_H}, inputting the correct masses of W_H and A_H will significantly enhance the efficiency of the event reconstruction. Furthermore, it is easy to show that the dependence of $\mathbb{C}^2$ upon m_{W_H} is much stronger than the one upon m_{A_H}. Hence, if one inputs the correct m_{W_H}, then one may reach the maximal reconstruction efficiency. The reconstruction efficiencies are summarized in Table 5.3 where we consider both cases with and without detector smearing effects. The detector effects reduce the efficiency of the signal reconstruction about 10% but increase the efficiency of the background reconstruction by a factor $2 \sim 3$.

Using the known kinematics of the A_H bosons, we can reconstruct the momentum of the W_H bosons. We then can plot the $\cos\theta^*$ distribution of the W boson in Fig. 5.28 where θ^* is the angle between W boson and W_H boson in the rest frame of W_H boson.

f (GeV)	input (GeV)		no smearing		with smearing	
	m_{W_H}	m_{A_H}	signal	BKGD	signal	BKGD
500	317	66	87%	0.5%	80%	1.4%
600	384	84	90%	0.3%	82%	0.7%
700	450	101	89%	0.1%	79%	0.3%

Table 5.3: Efficiencies of the A_H reconstruction after requiring $\mathbb{C}^2 > 0$.

The left figure shows the true $\cos\theta^*$ distribution where we assume all the particles in the final state, including the A_H bosons, are perfectly tagged. The right figure shows the $\cos\theta^*$ distributions after the W boson reconstruction. The distributions can be understood as follows. In the LHT model, the decay products of the W_H boson, W and A_H, are highly boosted because W_H is much heavier than A_H and W. Then the A_H and W bosons would be predominately in the longitudinal polarization states. Therefore, the decay of $W_H \to A_H W$ could be treated as a vector boson decaying into two scalars. Due to the angular momentum conservation, the spacial function of A_H and W_H would be dominated by p-wave ($\sim \sin^2\theta^*$), as shown in Fig. 5.28 (a). Duo to the W boson reconstruction, cf. Fig. 5.27, W_1, the W boson containing the leading jet, prefers to move parallel with the W_H and thus peaks in the forward direction while W_2 peaks in the backward direction.

How could we use this angular correlation to distinguish different models? Let us consider the signature of $W^+W^- + \not{E}_T$ which is generated by two heavy vector bosons in the LHT model. That signature could also be induced by many other new physics models:

- It can come from the decays of a heavy scalar (Φ) pair, e.g. $e^+e^- \to \Phi\Phi \to$

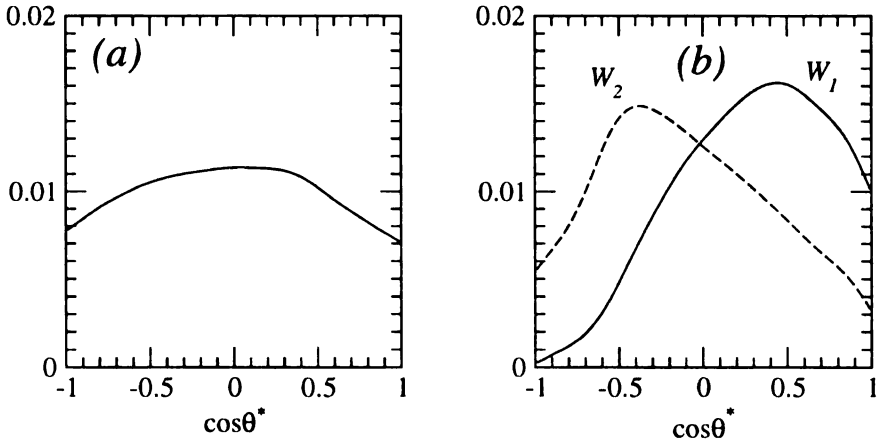

Figure 5.28: Normalized distribution of $\cos\theta^*$, where θ^* is the angle between the W boson and its mother particle W_H in the rest frame of W_H for $f = 500$ GeV: (a) true distribution; (b) after the W boson reconstruction.

$W^+W^- + VV$, and the missing particle (V) must be a vector boson. Due to the scalar decay, the $\cos\theta^*$ distribution should be flat, cf. the red dotted curve in Fig. 5.29(a).

- It can also come from the decays of a heavy fermion ($\mathcal{F}$) pair, e.g. $e^+e^- \to \mathcal{F}\mathcal{F} \to W^+W^- + \chi\chi$, and the missing particle (χ) must also be a fermion. It is well know that the $\cos\theta^*$ distribution should be in the form of $1 - \cos\theta^*$, $1 + \cos\theta^*$, or the combination of them. Here we plot the first two distributions in Fig. 5.29(a), cf. the blue dashed and green dashed curves.‡

The distinctive difference in the true $\cos\theta^*$ distributions will be affected by the W boson reconstruction, but the predictions from different models are still distinguishable, cf. Fig. 5.29(b) and (c).

‡

– We note that the $\cos\theta^*$ distribution is flat if the heavy fermion is produced unpolarized. It then is impossible to tell Φ and $\mathcal{F}$ apart from the $\cos\theta^*$ distribution. However, the distribution of the W_H pair production in the LHT model is still distinguishable from those of Φ and $\mathcal{F}$.

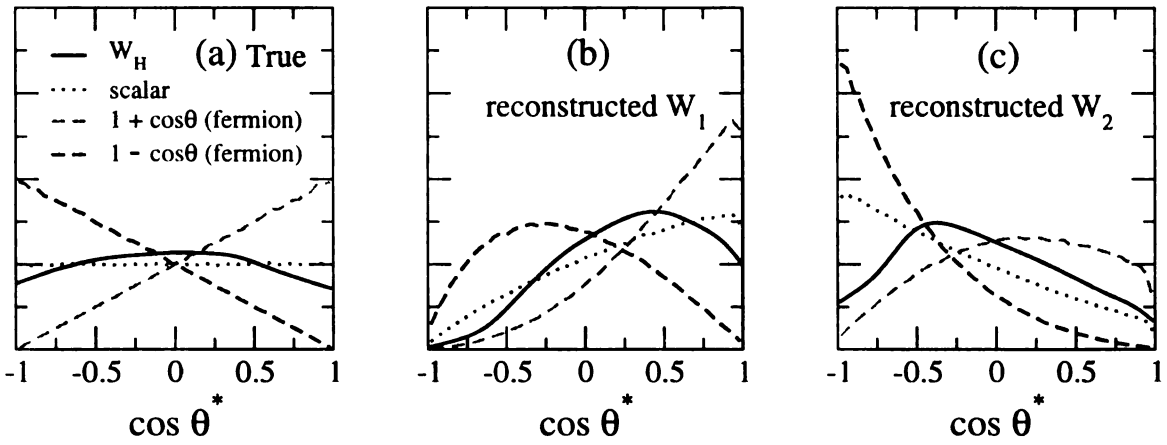

Figure 5.29: Normalized $\cos\theta^*$ distributions for different spin particles: (a) the true distribution while (b) and (c) are the distributions after W boson reconstruction.

Chapter 6

Summary

The Littlest Higgs model with T-parity (LHT) [37,54,57,72,74] is an attractive Little Higgs model which provides not only a solution to the Little hierarchy problem but also a possible dark matter candidate. The detailed model structure and the effective Lagrangian of the LHT model could be seen in Chapter 2. Because of the T-parity, T-odd gauge bosons do not mix with the Standarf Model gauge bosons, the mass scale (f) of new particles predicted in this model can be as low as 500 GeV [76], as shown in Fig. 3.2. From the partial wave analysis of the scattering processes of ($t\bar{t}$, $T_+\bar{T}_+$, $b\bar{b}$, W^+W^-, Zh) system, the model parameter λ_1 has to be bounded in the region of $0.71 \sim 2.5$, as shown in Fig. 3.3. In order to implement T-parity in the fermion sector of the model, the heavy T-odd $SU(2)$-doublet fermions, which are T-parity partners of the SM fermion doublets, have to be introduced. The mass of the T-odd fermion will be bounded from four-fermion operators. If the parameter κ is universal for all of the T-odd fermions, the mass of the T-odd fermion should be lighter than 4.8 TeV as $f = 1$ TeV. However, if T-odd leptons have different values of κ from that in the quark sector, the constraints are quite loose, as shown in Fig. 3.5. The importance of the T-odd fermions in the $u\bar{u} \to W_H^+W_H^-$ scattering precess has also been stressed through partial wave analysis in Sec. 5.1.

The LHT model modifies the coupling of the top quark to W- boson and bottom quark, known as the Wtb coupling, due to the mixing between the top quark and the T-even T_+ quark. Therefore, the single-top quark production at the LHC will different form the predictions in the SM. The deviations of the single-top quark production cross section from the SM will strongly imply the allowed region of f, cf. Fig. 4.1. Moreover, the T-odd particles have significant effects to the Higgs boson and top quark physics at the LHC through the quantum corrections. We study the production and decay of the Higgs boson in the LHT model. The production cross section via gluon-gluon fusion, which is the main process producing the Higgs boson at the LHC, could be highly suppressed, while the vector boson fusion process is about the same as the SM predictions. The branching ratio of the di-photon mode, on the other hand, is enhanced by as large as 35%. As a result, the discovery modes of the Higgs boson produced via vector boson fusion processes will become more important in the LHT model than in the SM. The various channels of searching for the Higgs boson at the LHC are summarized in Table 4.2. The heavy new particles in the LHT model can also modify the $gt\bar{t}$ coupling via quantum corrections, and affect the production cross section of $t\bar{t}$. Since the LHC is a true top factory, producing hundreds of millions of top quarks every year, it becomes possible to accurately measure the total cross section of the top quark pair production, which provides a good probe of searching for new physics. In Sec. 4.2, we study the anomalous $gt\bar{t}$ couplings induced by the one-loop electroweak (EW) corrections in the LHT model by using the Goldstone-boson equivalence theory, and study its effects in the $t\bar{t}$ pair production through quark-antiquark annihilation process at the LHC. We found that the negative EW corrections in the SM are partially canceled by the positive EW corrections from the new heavy particle loops in the LHT model. The net one-loop electroweak correction is close to zero in the range of $500\,\text{GeV} \lesssim m_{t\bar{t}} \lesssim 2000\,\text{GeV}$. For a larger value of $m_{t\bar{t}}$,

the new heavy particle loop correction dominates, and the leading EW corrections in the LHT model could increase the cross section by about 20%. However, such a deviation might hardly be recognized as the cross section drops rapidly with increasing $m_{t\bar{t}}$.

Because the mass of the new particles in the LHT model could be lighter than TeV, they can be copiously produced at high energy colliders. In Chapter 5, we study the collider phenomenology of the LHT model with emphasis on the contributions of the T-odd fermion to the production of the heavy T-parity partners (either bosons or fermions) at the LHC and Linear Collider (LC). We show in Sec. 5.2 the production cross sections of all of the new particles, including the first and second generation heavy T-odd quarks (q_-, $q = u, d, c, s$), the third generation heavy T-odd (t_-, b_- and T_-) and T-even (T_+) quarks, T-odd fermion vector boson associated production, the heavy T-odd gauge boson pairs and also heavy T-odd Higgs bosons productions for completeness. After discussing the typical decay branching ratios in Sec. 5.3, we study the probable experimental signatures predicted by this model at the LHC. We conclude that the like-sign di-lepton signature of the 1st and 2nd generation heavy T-odd quark pair production is the most useful channel to discover these new have quarks at the LHC. Also, because the heavy T-odd gauge boson Z_H almost always decays into a pair of a Higgs boson H and a T-odd photon A_H, the production processes with Z_H in the final state provides a new production mechanism for single-Higgs or Higgs-pair production.

In order to search for signatures of new physics at colliders, we need to consider the background from the SM which could generate the same collider signatures and whose event rate is usually much larger than the signal from the new physics. In the LHT model, the T-odd heavy gauge boson W_H pair production is of particular importance because the mass of W_H only depends on the symmetry breaking scale

f. One thus can unambiguously determine f by measuring m_{W_H}. In Sec. 5.5 and Sec. 5.6, we present detailed Monte Carlo studies about the collider phenomenology of a W_H pair production at the LHC and the LC, respectively. In order to avoid huge QCD background at the LHC, the purely leptonic decay modes are considered. Depending on the mass order of W_H and the T-odd fermions, the discovery potential at the LHC could reach a 5σ statistical significance level even for f about 1 TeV with an integrated luminosity of $100\,\text{fb}^{-1}$, by using $e\mu + \not{E}_T$ signatures, as shown in Fig. 5.22. However, the mass of W_H is very challenging to be reconstructed at the LHC due to four missing particles in the final state.

At LC, owing to the clean background at the LC, we are able to search the W_H boson using its hadronic decay mode which leads to a 4 jets associated with large $\not{E}_T$ signature. Due to the known center-of-mass energy at the LC, the masses of W_H and A_H can be determined from the ending points of the energy distributions of the two reconstructed W bosons. For example, one can measure the mass of W_H (A_H) within an error of 4% (8%) for $f = 700$ GeV, even after including the detector smearing effects. Following the study of the W^+W^- pair production at the LEP [165], we present an algorithm of reconstructing the kinematics of two undetectable A_H bosons. It enables us to study the spin correlation between the W boson and its mother particle (W_H) which is a powerful tool to distinguish other new physics models from the LHT model, as shown in Fig. 5.29.

Appendix A

Feynman Rules

The CalcHEP LHT model files, which include the complete Feynman rules, are available at the website http://hep.pa.msu.edu/LHT/ . In this appendix, I will list part of the Feynman rules which are used very frequently for the phenomenology study. And also note that some Feynman rules of LHT model are presented in the literature [72, 125, 126], and the Feynman rules shown here are based on Ref. [166], which has been checked to agree with the results in the arXiv version (v3) of Ref [72] with the substitutions: $T_+ \to -t'_+$ and $T_- \to -t'_-$. In Tables A.1, A.2 and A.3, we have defined the following coefficients. $s_H = \sin\theta_H$ describes the sine of the mixing angle between heavy neutral gauge bosons, cf. Eq. (2.15) and $c_H = \cos\theta_H$. Also, $s_\beta = \sin\beta$ ($s_\alpha = \sin\alpha$) is the sine of the mixing angle between left-handed (right-handed) top quark and T-even T_+ quark, cf. Eq. (2.23) (Eq. (2.24)). In addition, $P_L = \frac{1-\gamma_5}{2}$ and $P_R = \frac{1+\gamma_5}{2}$ are the left-handed and right-handed projection operators, respectively. We note that in those tables we have suppressed the CKM matrix element dependence. For example, from Table A.3, we can read out the coupling of $W^+_\mu \bar{t} b$ to be $V_{tb}(i\frac{g}{\sqrt{2}} c_\beta \gamma_\mu P_L)$, after restoring the CKM matrix element V_{tb} derived from the interaction Lagrangian. In the above expression, the product of $V_{tb} c_\beta$, which is defined as V^{eff}_{tb}, should be identified with the CKM matrix element determined from the low energy processes (or from measuring the SM single-top direct production rate at the

Interaction	Feynman rule	Interaction	Feynman rule
$W^+_{H\mu}\bar{u}d_-$	$i\frac{g}{\sqrt{2}}\gamma_\mu P_L$	$W^-_{H\mu}\bar{d}u_-$	$i\frac{g}{\sqrt{2}}\gamma_\mu P_L$
$Z_{H\mu}\bar{u}u_-$	$i(\frac{gc_H}{2} - -\frac{g's_H}{10})\gamma_\mu P_L$	$Z_{H\mu}\bar{d}d_-$	$i(-\frac{gc_H}{2} - \frac{g's_H}{10})\gamma_\mu P_L$
$A_{H\mu}\bar{u}u_-$	$i(-\frac{gs_H}{2} - \frac{g'c_H}{10})\gamma_\mu P_L$	$A_{H\mu}\bar{d}d_-$	$i(\frac{gs_H}{2} - \frac{g'c_H}{10})\gamma_\mu P_L$

Table A.1: Feynman rules for the first and second generation T-odd fermion interactions with heavy T-odd gauge bosons and the SM fermions.

Interaction	Feynman rule	Interaction	Feynman rule
$W^+_{H\mu}\bar{t}b_-$	$i\frac{gc_\beta}{\sqrt{2}}\gamma_\mu P_L$	$W^-_{H\mu}\bar{b}t_-$	$i\frac{g}{\sqrt{2}}\gamma_\mu P_L$
$W^+_{H\mu}\bar{T}_+b_-$	$i\frac{gs_\beta}{\sqrt{2}}\gamma_\mu P_L$		
$Z_{H\mu}\bar{t}t_-$	$i(\frac{gc_H}{2} - \frac{g's_H}{10})c_L\gamma_\mu P_L$	$Z_{H\mu}\bar{b}b_-$	$i(-\frac{gc_H}{2} - \frac{g's_H}{10})\gamma_\mu P_L$
$Z_{H\mu}\bar{T}_+t_-$	$i(\frac{gc_H}{2} - \frac{g's_H}{10})s_L\gamma_\mu P_L$	$Z_{H\mu}\bar{t}T_-$	$-i\frac{2}{5}g's_H\gamma_\mu(s_\beta P_L + s_\alpha P_R)$
$Z_{H\mu}\bar{T}_+T_-$	$i\frac{2}{5}g's_H\gamma_\mu(c_\beta P_L + c_\alpha P_R)$		
$A_{H\mu}\bar{t}t_-$	$i(-\frac{gs_H}{2} - \frac{g'c_H}{10})c_\beta\gamma_\mu P_L$	$A_{H\mu}\bar{b}b_-$	$i(\frac{gs_H}{2} - \frac{g'c_H}{10})\gamma_\mu P_L$
$A_{H\mu}\bar{T}_+t_-$	$i(-\frac{gs_H}{2} - \frac{g'c_H}{10})s_\beta\gamma_\mu P_L$	$A_{H\mu}\bar{t}T_-$	$-i\frac{2}{5}g'c_H\gamma_\mu(s_\beta P_L + s_\alpha P_R)$
$A_{H\mu}\bar{T}_+T_-$	$i\frac{2}{5}g'c_H\gamma_\mu(c_\beta P_L + c_\alpha P_R)$		

Table A.2: Feynman rules for the third generation T-odd fermions interactions with T-odd heavy gauge bosons and the top quark, bottom quark and T-even T_+ quark.

Tevatron or the LHC [148–156]. Thus, from Table A.3, we read out the coupling of $W^+\bar{T}_+b$ to be $V_{tb}(i\frac{g}{\sqrt{2}}s_\beta\gamma_\mu P_L)$, after restoring the CKM matrix element dependence, which can be rewritten as $V^{eff}_{tb}(i\frac{g}{\sqrt{2}}\frac{s_\beta}{c_\beta}\gamma_\mu P_L)$. The coefficient of $W^+\bar{T}_+b$ coupling $V^{eff}_{tb}\frac{s_\beta}{c_\beta}$ is approximately equal to $V^{eff}_{tb}s_\beta$ up to v^2/f^2 corrections, for $s_\beta \propto v/f$, cf. Eq. (2.23).

Interaction	Feynman rule	Interaction	Feynman rule
$W^+_\mu\bar{t}b$	$i\frac{g}{\sqrt{2}}c_\beta\gamma_\mu P_L$	$W^+\bar{T}_+b$	$i\frac{g}{\sqrt{2}}s_\beta\gamma_\mu P_L$
$Z_\mu\bar{t}t$	$i\frac{g}{c_W}\gamma_\mu\left\{(\frac{1}{2}c^2_\beta - \frac{2}{3}s^2_W)P_L - \frac{2}{3}s^2_W P_R\right\}$	$Z_\mu\bar{t}T_+$	$i\frac{g}{c_W}\frac{s_\beta c_\beta}{2}\gamma_\mu P_L$
$Z_\mu\bar{T}_+T_+$	$i\frac{g}{c_W}\gamma_\mu\left\{(\frac{1}{2}s^2_\beta - \frac{2}{3}s^2_W)P_L - \frac{2}{3}s^2_W P_R\right\}$		

Table A.3: Feynman rules for the SM guage interaction with the top sector.

Appendix B

Scalar Functions

The one-loop integrals could be decomposed in terms of Passarino-Veltman [121] functions which are defined in $n = 4 - 2\epsilon$ dimensions. Definitions of one-point (A), two-point (B) and three-point (C) functions are:

$$\mu^{2\epsilon} \int \frac{d^n k}{(2\pi)^n} \frac{1}{k^2 - m^2} = \frac{i}{16\pi^2} A_0(m),$$

$$\mu^{2\epsilon} \int \frac{d^n k}{(2\pi)^n} \frac{1,\, k_\mu,\, k_\mu k_\nu}{(k^2 - m_1^2)\left[(k+l)^2 - m_2^2\right]} = \frac{i}{16\pi^2} B_0,\, B_\mu,\, B_{\mu\nu}(l,\, m_1,\, m_2),$$

$$\mu^{2\epsilon} \int \frac{d^n k}{(2\pi)^n} \frac{k^2,\, k^2 l_\mu}{(k^2 - m_1^2)\left[(k+l)^2 - m_2^2\right]} = \frac{i}{16\pi^2} \tilde{B}_0,\, \tilde{B}_\mu(l,\, m_1,\, m_2),$$

$$\mu^{2\epsilon} \int \frac{d^n k}{(2\pi)^n} \frac{1,\, k_\mu,\, k_\mu k_\nu}{(k^2 - m_1^2)\left[(k+l)^2 - m_2^2\right]\left[(k+l+s)^2 - m_3^2\right]}$$

$$= \frac{i}{16\pi^2} C_0,\, C_\mu,\, C_{\mu\nu}(l,\, s,\, m_1,\, m_2,\, m_3).$$

The integration formula of these scalar functions are as

$$A_0(m) = m^2 \left[\Delta - \ln \frac{m^2}{\mu^2} + 1\right],$$

$$B_0(\ell,\, m_1,\, m_2) = \Delta - \int_0^1 dx \ln \frac{x^2 \ell^2 - x(\ell^2 + m_1^2 - m_2^2) + m_1^2}{\mu^2},$$

$$B_1(\ell,\, m_1,\, m_2) = -\frac{\Delta}{2} + \int_0^1 dx x \ln \frac{x^2\ell^2 - x(\ell^2 + m_1^2 - m_2^2) + m_1^2}{\mu^2},$$

$$C_0(\ell,\, s,\, m_1,\, m_2,\, m_3) = \int_0^1 dx \int_0^x dy \frac{1}{ax^2 + by^2 + cxy + dx + ey + f},$$

where

$$\Delta = \frac{1}{\epsilon} - \gamma_E + \ln 4\pi,$$

$$a = -s^2,\ b = -\ell^2,\ c = -2\ell \cdot s,\ d = -m_2^2 + m_3^2 + s^2,$$

$$e = -m_1^2 + m_2^2 + \ell^2 + 2\ell \cdot s,\ f = -m_3^2.$$

The tensor integrals could be further decomposed and written in terms of the external momenta and the metric tensor $g_{\mu\nu}$ with the scalar functions. The explicit decomposition for B_μ, C_μ and $C_{\mu\nu}$ is given below [167].

For two-point finctions,

$$B_\mu(\ell,\, m_1,\, m_2) = \ell_\mu B_1(\ell,\, m_1,\, m_2),$$

$$B_1(\ell,\, m_1,\, m_2) = \frac{1}{2l^2}\left[A_0(m_1) - A_0(m_2) - (\ell^2 + m_1^2 - m_2^2)B_0(\ell,\, m_1,\, m_2)\right],$$

$$B_{\mu\nu}(\ell,\, m_1,\, m_2) = \ell_\mu \ell_\nu B_{21}(\ell,\, m_1,\, m_2) + g_{\mu\nu} B_{22}(\ell,\, m_1,\, m_2),$$

$$B_{21}(\ell,\, m_1,\, m_2) = \frac{1}{3\ell^2}\left[A_0(m_2) - m_1^2 B_0 - 2(\ell^2 + m_1^2 - m_2^2)B_1 - \frac{m_1^2 + m_2^2}{2} + \frac{\ell^2}{6}\right],$$

$$B_{22}(\ell,\, m_1,\, m_2) = \frac{1}{6}\left[A_0(m_2) + 2m_1^2 B_0 + (\ell^2 + m_1^2 - m_2^2)B_1 + m_1^2 + m_2^2 - \frac{\ell^2}{3}\right],$$

$$\tilde{B}_0(\ell,\, m_1,\, m_2) = A_0(m_2) + m_1^2 B_0(\ell,\, m_1,\, m_2),$$

$$\tilde{B}_\mu(\ell,\, m_1,\, m_2) = \ell_\mu \tilde{B}_1(\ell,\, m_1,\, m_2),$$

$$\tilde{B}_1(\ell,\, m_1,\, m_2) = -A_0(m_2) + m_1^2 B_1(\ell,\, m_1,\, m_2).$$

For three-point functions,

$$C_\mu(\ell,\, s,\, m_1,\, m_2,\, m_3) = \ell_\mu C_{11}(\ell,\, s,\, m_1,\, m_2,\, m_3) + s_\mu C_{12}(\ell,\, s,\, m_1,\, m_2,\, m_3),$$

$$C_{\mu\nu}(\ell,\, s,\, m_1,\, m_2,\, m_3) = \ell_\mu \ell_\nu C_{21} + s_\mu s_\nu C_{22} + (\ell_\mu s_\nu + \ell_\nu s_\mu) C_{23} + g_{\mu\nu} C_{24},$$

with

$$C_{11}(\ell,\, s,\, m_1,\, m_2,\, m_3) = \frac{1}{\kappa}\left(s^2 R_1 - \ell \cdot s R_2\right),$$

$$C_{12}(\ell,\, s,\, m_1,\, m_2,\, m_3) = \frac{1}{\kappa}\left(-\ell \cdot s R_1 + \ell^2 R_2\right),$$

$$C_{24}(\ell,\, s,\, m_1,\, m_2,\, m_3) = \frac{1}{4}\left[B_0(s,\, m_2,\, m_3) + r_1 C_{11} + r_2 C_{12} + 2m_1^2 C_0 + 1\right],$$

$$C_{21}(\ell,\, s,\, m_1,\, m_2,\, m_3) = \frac{1}{\kappa}\left(s^2 R_3 - \ell \cdot s R_5\right),$$

$$C_{22}(\ell,\, s,\, m_1,\, m_2,\, m_3) = \frac{1}{\kappa}\left(-\ell \cdot s R_4 + \ell^2 R_6\right),$$

$$C_{23}(\ell,\, s,\, m_1,\, m_2,\, m_3) = \frac{1}{\kappa}\left(-\ell \cdot s R_3 + \ell^2 R_5\right) = \frac{1}{\kappa}\left(s^2 R_4 - \ell \cdot s R_6\right),$$

where

$$\kappa = \ell^2 s^2 - (\ell \cdot s)^2,$$

$$r_1 = \ell^2 + m_1^2 - m_2^2,$$

$$r_2 = (\ell + s)^2 - \ell^2 + m_2^2 - m_3^2,$$

$$R_1 = \frac{1}{2}\left[B_0(\ell + s,\, m_1,\, m_3) - B_0(s,\, m_2,\, m_3) - (\ell^2 + m_1^2 - m_2^2) C_0\right],$$

$$R_2 = \left[B_0(\ell,\, m_1,\, m_2) - B_0(\ell + s,\, m_1,\, m_3) + (-s^2 - 2\ell \cdot s - m_2^2 + m_3^2) C_0\right],$$

$$R_3 = -C_{24} - \frac{1}{2}\left[r_1 C_{11} - B_1(\ell + s,\, m_1,\, m_3) - B_0(s,\, m_2,\, m_3)\right],$$

$$R_4 = -\frac{1}{2}\left[r_1 C_{12} - B_1(\ell + s,\, m_1,\, m_3) + B_1(s,\, m_2,\, m_3)\right],$$

$$R_5 = -\frac{1}{2}\left[r_2 C_{11} - B_1(\ell,\, m_1,\, m_2) + B_1(\ell + s,\, m_1,\, m_3)\right],$$

$$R_6 = -C_{24} - \frac{1}{2}\left[r_2 C_{12} + B_1(\ell + s,\, m_1,\, m_3)\right].$$

Among above functions, some of them contain UV divergence. It is very useful to track these divergenses in the calculations. Here I list the UV divergences of the integrals up to $\mathcal{O}(1/\epsilon)$:

$$
\begin{aligned}
A_0(m) &\Rightarrow \frac{m^2}{\epsilon}, \\
B_0(\ell,\, m_1,\, m_2) &\Rightarrow \frac{1}{\epsilon}, \\
B_1(\ell,\, m_1,\, m_2) &\Rightarrow -\frac{1}{2\epsilon}, \\
B_{21}(\ell,\, m_1,\, m_2) &\Rightarrow \frac{1}{3\epsilon}, \\
B_{22}(\ell,\, m_1,\, m_2) &\Rightarrow -\frac{1}{12\epsilon}(\ell^2 - 3m_1^2 - 3m_2^2), \\
C_{24}(\ell,\, s,\, m_{1,},\, m_2,\, m_3) &\Rightarrow \frac{1}{4\epsilon}.
\end{aligned}
$$

Appendix C

A_H reconstruction at the LC

In this Appendix, we present an algorithm of determining the kinematics of A_H at the LC. This algorithm has been proposed in the study of the W boson at the LEP through the process $e^+e^- \to W^+W^- \to \ell^+\nu_\ell \ell'^-\bar{\nu}_{\ell'}$ [165]. The difficulty is attributed to the existence of two missing particles in the final state. The following kinematics analysis, presented below, shows that the two unobserved momenta of A_H bosons can be determined from the reconstructed W bosons up to a twofold discrete ambiguity, in the limit where the W- and W_H-width are neglected.

Here we consider the process

$$e^+e^- \to AA', \;\; A \to BC, \;\; A' \to B'C' \tag{C.1}$$

where $A(A')$ is the mother particle while $B(B')$ and $C(C')$ are the decay products of the mother particles. Here we require $B(B')$ is observable while $C(C')$ undetectable. Furthermore, we assume

$$m_A = m_{A'}, \quad m_C = m_{C'}. \tag{C.2}$$

One of the advantage of the LC is the known center-of-mass energy of the system. For example, the momentum of the incoming particles are

$$p_{e^+} = (\; E_t, \;\; 0, \;\; 0, \;\; E_t \;), \; p_{e^-} = (\; E_t, \;\; 0, \;\; 0, \;\; -E_t \;), \tag{C.3}$$

where $E_t = \sqrt{s}/2$, where $\sqrt{s}$ is the total energy of the linear collider.

From the momentum conservation, we obtain

$$E_A = E_B + E_C, E_{A'} = E_{B'} + E_{C'}, \tag{C.4}$$

$$\vec{p}_A = \vec{p}_B + \vec{p}_C, \vec{p}_{A'} = \vec{p}_{B'} + \vec{p}_{C'}, \tag{C.5}$$

where $E_i(\vec{p}_i)$ denotes the energy (three momentum) of the particle i, respectively. At the LC,

$$E_A = E_{A'} = E_t, \quad E_C = E_t - E_B, \quad E_{C'} = E_t - E_{B'}. \tag{C.6}$$

From Eq. (C.5) and the on-shell conditions of the final state particles we obtain

$$2\vec{p}_B \cdot \vec{p}_C = E_A^2 - m_A^2 - \left(E_B^2 - m_B^2\right) - \left(E_C^2 - m_C^2\right), \tag{C.7}$$

$$2\vec{p}_{B'} \cdot \vec{p}_{C'} = E_{A'}^2 - m_{A'}^2 - \left(E_{B'}^2 - m_{B'}^2\right) - \left(E_{C'}^2 - m_{C'}^2\right). \tag{C.8}$$

Using the momentum conservation,

$$\vec{p}_B + \vec{p}_{B'} + \vec{p}_C + \vec{p}_{C'} = 0, \tag{C.9}$$

one obtains

$$2\vec{p}_{B'} \cdot \vec{p}_C = \left(E_{C'}^2 - m_{C'}^2\right) - \left(E_{A'}^2 - m_{A'}^2\right) - \left(E_{B'}^2 - m_{B'}^2\right) - 2\vec{p}_B \cdot \vec{p}_B. \tag{C.10}$$

At last, the on-shell condition of particle C gives us

$$|\vec{p}_C|^2 = E_C^2 - m_C^2. \tag{C.11}$$

Hence, one can determine $\vec{p}_C$ from Eqs. (C.7), (C.10), and (C.11). We expand $\vec{p}_C$ in term of $\vec{p}_B$ and $\vec{p}_{B'}$ as following

$$\vec{p}_C = \mathbb{A}\vec{p}_B + \mathbb{B}\vec{p}_{B'} + \mathbb{C}\vec{p}_B \times \vec{p}_{B'}. \tag{C.12}$$

Then one can derive a and b from Eqs. (C.7) and (C.10)

$$\begin{pmatrix} \mathbb{A} \\ \mathbb{B} \end{pmatrix} = \frac{1}{|\vec{p}_B|^2 |\vec{p}_{B'}|^2 - (\vec{p}_B \cdot \vec{p}_{B'})^2} \begin{pmatrix} |\vec{p}_{B'}|^2 & -\vec{p}_B \cdot \vec{p}_{B'} \\ -\vec{p}_B \cdot \vec{p}_{B'} & |\vec{p}_B|^2 \end{pmatrix} \begin{pmatrix} M \\ N \end{pmatrix}, \quad \text{(C.13)}$$

where

$$M \equiv \frac{1}{2}\left[E_A^2 - m_A^2 - \left(E_B^2 - m_B^2\right) - \left(E_C^2 - m_C^2\right)\right], \quad \text{(C.14)}$$

$$N \equiv \frac{1}{2}\left[\left(E_{C'}^2 - m_{C'}^2\right) - \left(E_{A'}^2 - m_{A'}^2\right) - \left(E_{B'}^2 - m_{B'}^2\right) - 2\vec{p}_B \cdot \vec{p}_B\right]. \quad \text{(C.15)}$$

The remaining variable $\mathbb{C}$ is determined using Eq. (C.11):

$$\mathbb{C}^2 = \frac{1}{|\vec{p}_B \times \vec{p}_{B'}|^2}\left[E_C^2 - m_C^2 - \mathbb{A}^2 |\vec{p}_B|^2 - \mathbb{B}^2 |\vec{p}_{B'}|^2 - 2\mathbb{A}\mathbb{B}\vec{p}_B \cdot \vec{p}_{B'}\right]. \quad \text{(C.16)}$$

The sign of $\mathbb{C}$ cannot be determined. This explicitly exhibits a twofold discrete ambiguity. The inequality $\mathbb{C}^2 > 0$ is expected to be violated only by finite W- and W_H-width effects. Needless to say, using wrong m_C and m_A will lead to a negative $\mathbb{C}^2$ which can serve to measure m_A and m_C as mentioned earlier. In the exceptional case where the momenta of particle B and B' are parallel, one obtains a one-parameter family of solution for which the azimuthal angle of $\vec{p}_C$ with respect to $\vec{p}_B$ is left undetermined.

Bibliography

[1] F. Halzen, A. D. Martin. *Quarks and Leptons: An Introductory Course in Modern Particle Physics.* John Wiley and Sons, Inc., 1984.

[2] Ta-Pei Cheng, Ling-Fong Li. *Gauge Theory of Elementary Particle Physics.* Oxford University Press, 1984.

[3] Gordon Kane. *Modern Elementary Particle Physics.* Addison-Wesley, 1987.

[4] see: http://lepewwg.web.cern.ch/LEPEWWG/.

[5] R. Davis. A review of the homestake solar neutrino experiment. *Prog. Part. Nucl. Phys.*, 32:13–32, 1994.

[6] B. T. Cleveland, i in. Measurement of the solar electron neutrino flux with the homestake chlorine detector. *Astrophys. J.*, 496:505–526, 1998.

[7] J. N. Abdurashitov, i in. Measurement of the solar neutrino capture rate with gallium metal. *Phys. Rev.*, C60:055801, 1999.

[8] W. Hampel, i in. Gallex solar neutrino observations: Results for gallex iv. *Phys. Lett.*, B447:127–133, 1999.

[9] M. Altmann, i in. Gno solar neutrino observations: Results for gno i. *Phys. Lett.*, B490:16–26, 2000.

[10] S. Fukuda, i in. Determination of solar neutrino oscillation parameters using 1496 days of super-kamiokande-i data. *Phys. Lett.*, B539:179–187, 2002.

[11] C. M. Cattadori. Update of solar neutrino interaction rate measurements from gno at lngs. *Nucl. Phys. Proc. Suppl.*, 110:311–314, 2002.

[12] Q. R. Ahmad, i in. Direct evidence for neutrino flavor transformation from neutral-current interactions in the sudbury neutrino observatory. *Phys. Rev. Lett.*, 89:011301, 2002.

[13] Q. R. Ahmad, i in. Measurement of day and night neutrino energy spectra at sno and constraints on neutrino mixing parameters. *Phys. Rev. Lett.*, 89:011302, 2002.

[14] S. N. Ahmed, i in. Measurement of the total active b-8 solar neutrino flux at the sudbury neutrino observatory with enhanced neutral current sensitivity. *Phys. Rev. Lett.*, 92:181301, 2004.

[15] Y. Fukuda, i in. Evidence for oscillation of atmospheric neutrinos. *Phys. Rev. Lett.*, 81:1562–1567, 1998.

[16] A. Surdo. Atmospheric neutrino oscillations in the macro experiment. *Nucl. Phys. Proc. Suppl.*, 110:342–345, 2002.

[17] G. Giacomelli, A. Margiotta. New macro results on atmospheric neutrino oscillations. *Phys. Atom. Nucl.*, 67:1139–1146, 2004.

[18] Mayly C. Sanchez, i in. Observation of atmospheric neutrino oscillations in soudan 2. *Phys. Rev.*, D68:113004, 2003.

[19] K. Eguchi, i in. First results from kamland: Evidence for reactor anti- neutrino disappearance. *Phys. Rev. Lett.*, 90:021802, 2003.

[20] T. Araki, i in. Measurement of neutrino oscillation with kamland: Evidence of spectral distortion. *Phys. Rev. Lett.*, 94:081801, 2005.

[21] M. H. Ahn, i in. Indications of neutrino oscillation in a 250-km long- baseline experiment. *Phys. Rev. Lett.*, 90:041801, 2003.

[22] J. C. Kapteyn. *Astrophys. J.*, 55:302, 1922.

[23] F. Zwicky. *Helv. Phys. Acta.*, 6:110, 1933.

[24] D. N. Spergel, i in. Wilkinson microwave anisotropy probe (wmap) three year results: Implications for cosmology. *Astrophys. J. Suppl.*, 170:377, 2007.

[25] Steven Weinberg. Phenomenological lagrangians. *Physica*, A96:327, 1979.

[26] Riccardo Barbieri, Alessandro Strumia. What is the limit on the higgs mass? *Phys. Lett.*, B462:144–149, 1999.

[27] G. D'Ambrosio, G. F. Giudice, G. Isidori, A. Strumia. Minimal flavour violation: An effective field theory approach. *Nucl. Phys.*, B645:155–187, 2002.

[28] A combination of preliminary electroweak measurements and constraints on the standard model. 2004.

[29] W. M. Yao, i in. Review of particle physics. *J. Phys.*, G33:1–1232, 2006.

[30] P. Fayet, S. Ferrara. Supersymmetry. *Phys. Rept.*, 32:249–334, 1977.

[31] J. Wess and J. Bagger, Supersymmetry and Supergravity, (Princeton University Press, 1983).

[32] M. F. Sohnius. Introducing supersymmetry. *Phys. Rept.*, 128:39–204, 1985.

[33] P. West, Introduction to Supersymmetry and Supergravity, (World Scientific, 1986).

[34] Hans Peter Nilles. Supersymmetry, supergravity and particle physics. *Phys. Rept.*, 110:1, 1984.

[35] Howard E. Haber, Gordon L. Kane. The search for supersymmetry: Probing physics beyond the standard model. *Phys. Rept.*, 117:75–263, 1985.

[36] Markus A. Luty. 2004 tasi lectures on supersymmetry breaking. 2005.

[37] N. Arkani-Hamed, A. G. Cohen, E. Katz, A. E. Nelson. The littlest higgs. *JHEP*, 07:034, 2002.

[38] Tao Han, Heather E. Logan, Bob McElrath, Lian-Tao Wang. Phenomenology of the little higgs model. *Phys. Rev.*, D67:095004, 2003.

[39] Nima Arkani-Hamed, Andrew G. Cohen, Howard Georgi. Electroweak symmetry breaking from dimensional deconstruction. *Phys. Lett.*, B513:232–240, 2001.

[40] Martin Schmaltz, David Tucker-Smith. Little higgs review. *Ann. Rev. Nucl. Part. Sci.*, 55:229–270, 2005.

[41] Howard Georgi, A. Pais. Calculability and naturalness in gauge theories. *Phys. Rev.*, D10:539, 1974.

[42] Howard Georgi, A. Pais. Vacuum symmetry and the pseudogoldstone phenomenon. *Phys. Rev.*, D12:508, 1975.

[43] David B. Kaplan, Howard Georgi. Su(2) x u(1) breaking by vacuum misalignment. *Phys. Lett.*, B136:183, 1984.

[44] David B. Kaplan, Howard Georgi, Savas Dimopoulos. Composite higgs scalars. *Phys. Lett.*, B136:187, 1984.

[45] Howard Georgi, David B. Kaplan. Composite higgs and custodial su(2). *Phys. Lett.*, B145:216, 1984.

[46] Howard Georgi, David B. Kaplan, Peter Galison. Calculation of the composite higgs mass. *Phys. Lett.*, B143:152, 1984.

[47] Michael J. Dugan, Howard Georgi, David B. Kaplan. Anatomy of a composite higgs model. *Nucl. Phys.*, B254:299, 1985.

[48] N. Arkani-Hamed, i in. The minimal moose for a little higgs. *JHEP*, 08:021, 2002.

[49] Ian Low, Witold Skiba, David Smith. Little higgses from an antisymmetric condensate. *Phys. Rev.*, D66:072001, 2002.

[50] David E. Kaplan, Martin Schmaltz. The little higgs from a simple group. *JHEP*, 10:039, 2003.

[51] Spencer Chang. A 'littlest higgs' model with custodial su(2) symmetry. *JHEP*, 12:057, 2003.

[52] Witold Skiba, John Terning. A simple model of two little higgses. *Phys. Rev.*, D68:075001, 2003.

[53] Roberto Contino, Yasunori Nomura, Alex Pomarol. Higgs as a holographic pseudo-goldstone boson. *Nucl. Phys.*, B671:148–174, 2003.

[54] Hsin-Chia Cheng, Ian Low. Tev symmetry and the little hierarchy problem. *JHEP*, 09:051, 2003.

[55] Emanuel Katz, Jae-yong Lee, Ann E. Nelson, Devin G. E. Walker. A composite little higgs model. *JHEP*, 10:088, 2005.

[56] Spencer Chang, Jay G. Wacker. Little higgs and custodial su(2). *Phys. Rev.*, D69:035002, 2004.

[57] Hsin-Chia Cheng, Ian Low. Little hierarchy, little higgses, and a little symmetry. *JHEP*, 08:061, 2004.

[58] David E. Kaplan, Martin Schmaltz, Witold Skiba. Little higgses and turtles. *Phys. Rev.*, D70:075009, 2004.

[59] Ian Low. T parity and the littlest higgs. *JHEP*, 10:067, 2004.

[60] Martin Schmaltz. The simplest little higgs. *JHEP*, 08:056, 2004.

[61] Jesse Thaler, Itay Yavin. The littlest higgs in anti-de sitter space. *JHEP*, 08:022, 2005.

[62] Kaustubh Agashe, Roberto Contino, Alex Pomarol. The minimal composite higgs model. *Nucl. Phys.*, B719:165–187, 2005.

[63] Tuhin Roy, Martin Schmaltz. Naturally heavy superpartners and a little higgs. *JHEP*, 01:149, 2006.

[64] Hsin-Chia Cheng, Ian Low, Lian-Tao Wang. Top partners in little higgs theories with t-parity. *Phys. Rev.*, D74:055001, 2006.

[65] Adam Martin. Dark matter in the simplest little higgs model. 0200.

[66] Csaba Csaki, Jay Hubisz, Graham D. Kribs, Patrick Meade, John Terning. Big corrections from a little higgs. *Phys. Rev.*, D67:115002, 2003.

[67] JoAnne L. Hewett, Frank J. Petriello, Thomas G. Rizzo. Constraining the littlest higgs. ((u)). *JHEP*, 10:062, 2003.

[68] Csaba Csaki, Jay Hubisz, Graham D. Kribs, Patrick Meade, John Terning. Variations of little higgs models and their electroweak constraints. *Phys. Rev.*, D68:035009, 2003.

[69] Mu-Chun Chen, Sally Dawson. One-loop radiative corrections to the rho parameter in the littlest higgs model. *Phys. Rev.*, D70:015003, 2004.

[70] W. Kilian, J. Reuter. The low-energy structure of little higgs models. *Phys. Rev.*, D70:015004, 2004.

[71] Zhenyu Han, Witold Skiba. Effective theory analysis of precision electroweak data. *Phys. Rev.*, D71:075009, 2005.

[72] Jay Hubisz, Patrick Meade. Phenomenology of the littlest higgs with t-parity. *Phys. Rev.*, D71:035016, 2005.

[73] Jay Hubisz, Seung J. Lee, Gil Paz. The flavor of a little higgs with t-parity. *JHEP*, 06:041, 2006.

[74] Chuan-Ren Chen, Kazuhiro Tobe, C. P. Yuan. Higgs boson production and decay in little higgs models with t-parity. *Phys. Lett.*, B640:263–271, 2006.

[75] J. Hubisz, unpublished work.

[76] Jay Hubisz, Patrick Meade, Andrew Noble, Maxim Perelstein. Electroweak precision constraints on the littlest higgs model with t parity. *JHEP*, 01:135, 2006.

[77] Michael Edward Peskin, Tatsu Takeuchi. Estimation of oblique electroweak corrections. *Phys. Rev.*, D46:381–409, 1992.

[78] S. Eidelman, i in. Review of particle physics. *Phys. Lett.*, B592:1, 2004.

[79] C. P. Burgess, Stephen Godfrey, Heinz Konig, David London, Ivan Maksymyk. Model independent global constraints on new physics. *Phys. Rev.*, D49:6115–6147, 1994.

[80] Qing-Hong Cao, Chong Sheng Li, C. P. Yuan. Impact of single-top measurement to littlest higgs model with t-parity. 2006.

[81] TEVWWG. A combination of cdf and d0 results on the mass of the top quark. 2007.

[82] A. Stange, S. Willenbrock. Yukawa correction to top quark production at the tevatron. *Phys. Rev.*, D48:2054–2061, 1993.

[83] Hong-Yi Zhou, Chong-Sheng Li, Yu-Ping Kuang. Yukawa corrections to top quark production at the lhc in two-higgs-doublet models. *Phys. Rev.*, D55:4412–4420, 1997.

[84] W. Hollik, W. M. Mosle, D. Wackeroth. Top pair production at hadron colliders in non-minimal standard models. *Nucl. Phys.*, B516:29–54, 1998.

[85] Chung Kao, Doreen Wackeroth. Parity violating asymmetries in top pair production at hadron colliders. *Phys. Rev.*, D61:055009, 2000.

[86] Chung Kao. Parity violation in top quark pair production at the fermilab tevatron collider. *Phys. Lett.*, B348:155–162, 1995.

[87] Chong-Sheng Li, Bing-Quan Hu, Jin-Min Yang, Chen-Guo Hu. Supersymmetric qcd corrections to top quark production in p anti-p collisions. *Phys. Rev.*, D52:5014–5017, 1995.

[88] Jin Min Yang, Chong Sheng Li. Top squark mixing effects in the supersymmetric electroweak corrections to top quark production at the tevatron. *Phys. Rev.*, D54:4380–4384, 1996.

[89] Jaewan Kim, Jorge L. Lopez, Dimitri V. Nanopoulos, R. Rangarajan. Enhanced supersymmetric corrections to top-quark production at the tevatron. *Phys. Rev.*, D54:4364–4373, 1996.

[90] Chong-Sheng Li, Hong-Yi Zhou, Yun-Lun Zhu, Jin-Min Yang. Strong supersymmetric quantum effects on top quark production at the fermilab tevatron. *Phys. Lett.*, B379:135–140, 1996.

[91] S. Alam, K. Hagiwara, S. Matsumoto, K. Hagiwara, S. Matsumoto. One loop supersymmetric qcd radiative corrections to the top quark production in p anti-p collisions. (revised version). *Phys. Rev.*, D55:1307–1315, 1997.

[92] Zack Sullivan. Supersymmetric qcd correction to top-quark production at the tevatron. *Phys. Rev.*, D56:451–457, 1997.

[93] Chong-Sheng Li, Robert J. Oakes, Jin Min Yang, C. P. Yuan. Supersymmetric electroweak parity nonconservation in top quark pair production at the fermilab tevatron. *Phys. Lett.*, B398:298–304, 1997.

[94] Hong-Yi Zhou, Chong-Sheng Li. Supersymmetric qcd corrections to top quark pair production at cern lhc. *Phys. Rev.*, D55:4421–4429, 1997.

[95] W. Hollik, W. M. Mosle, C. Kao, D. Wackeroth. Mssm radiative corrections to the top pair production processes at hadron colliders. 1997.

[96] Hong-Yi Zhou, Chong-Sheng Li. Supersymmetric electroweak corrections to top quark production at lhc. *Commun. Theor. Phys.*, 30:465–470, 1998.

[97] Stefan Berge, Wolfgang Hollik, Wolf M. Mosle, Doreen Wackeroth. Susy qcd one-loop effects in (un)polarized top-pair production at hadron colliders. *Phys. Rev.*, D76:034016, 2007.

[98] D. A. Ross, M. Wiebusch. Mssm effects in top-antitop production at the lhc. *JHEP*, 11:041, 2007.

[99] For a review, see J. Gunion, H. Haber, G. Kane and S. Dawson, The Higgs Hunter's Guide.

[100] W. Beenakker, i in. Electroweak one loop contributions to top pair production in hadron colliders. *Nucl. Phys.*, B411:343–380, 1994.

[101] C. Kao, G. A. Ladinsky, C. P. Yuan. Leading weak corrections to the production of heavy top quarks at hadron colliders. *Int. J. Mod. Phys.*, A12:1341–1372, 1997.

[102] J. H. Kuhn, A. Scharf, P. Uwer. Electroweak corrections to top-quark pair production in quark-antiquark annihilation. *Eur. Phys. J.*, C45:139–150, 2006.

[103] S. Moretti, M. R. Nolten, D. A. Ross. Weak corrections to gluon-induced top-antitop hadro- production. *Phys. Lett.*, B639:513–519, 2006.

[104] J. H. Kuhn, A. Scharf, P. Uwer. Electroweak effects in top-quark pair production at hadron colliders. *Eur. Phys. J.*, C51:37–53, 2007.

[105] John M. Cornwall, David N. Levin, George Tiktopoulos. Derivation of gauge invariance from high-energy unitarity bounds on the s matrix. *Phys. Rev.*, D10:1145, 1974.

[106] C. E. Vayonakis. Born helicity amplitudes and cross-sections in nonabelian gauge theories. *Nuovo Cim. Lett.*, 17:383, 1976.

[107] Benjamin W. Lee, C. Quigg, H. B. Thacker. Weak interactions at very high-energies: The role of the higgs boson mass. *Phys. Rev.*, D16:1519, 1977.

[108] Michael S. Chanowitz, Mary K. Gaillard. The tev physics of strongly interacting w's and z's. *Nucl. Phys.*, B261:379, 1985.

[109] G. J. Gounaris, R. Kogerler, H. Neufeld. Relationship between longitudinally polarized vector bosons and their unphysical scalar partners. *Phys. Rev.*, D34:3257, 1986.

[110] York-Peng Yao, C. P. Yuan. Modification of the equivalence theorem due to loop corrections. *Phys. Rev.*, D38:2237, 1988.

[111] Jonathan Bagger, Carl Schmidt. Equivalence theorem redux. *Phys. Rev.*, D41:264, 1990.

[112] Helene G. J. Veltman. The equivalence theorem. *Phys. Rev.*, D41:2294, 1990.

[113] Hong-Jian He, Yu-Ping Kuang, Xiao-yuan Li. On the precise formulation of equivalence theorem. *Phys. Rev. Lett.*, 69:2619–2622, 1992.

[114] Hong-Jian He, Yu-Ping Kuang, Xiao-yuan Li. Further investigation on the precise formulation of the equivalence theorem. *Phys. Rev.*, D49:4842–4872, 1994.

[115] Hong-Jian He, Yu-Ping Kuang, Xiao-yuan Li. Proof of the equivalence theorem in the chiral lagrangian formalism. *Phys. Lett.*, B329:278–284, 1994.

[116] A. Dobado, J. R. Pelaez. On the equivalence theorem in the chiral perturbation theory description of the symmetry breaking sector of the standard model. *Nucl. Phys.*, B425:110–136, 1994.

[117] Antonio Dobado, Jose Ramon Pelaez. The equivalence theorem for chiral lagrangians. *Phys. Lett.*, B329:469–478, 1994.

[118] Hong-Jian He, Yu-Ping Kuang, C. P. Yuan. Equivalence theorem and probing the electroweak symmetry breaking sector. *Phys. Rev.*, D51:6463–6473, 1995.

[119] Riccardo Barbieri, Matteo Beccaria, Paolo Ciafaloni, Giuseppe Curci, Andrea Vicere. Radiative correction effects of a very heavy top. *Phys. Lett.*, B288:95–98, 1992.

[120] Riccardo Barbieri, Matteo Beccaria, Paolo Ciafaloni, Giuseppe Curci, Andrea Vicere. Two loop heavy top effects in the standard model. *Nucl. Phys.*, B409:105–127, 1993.

[121] G. Passarino, M. J. G. Veltman. One loop corrections for e+ e- annihilation into mu+ mu- in the weinberg model. *Nucl. Phys.*, B160:151, 1979.

[122] T. Hahn, M. Perez-Victoria. Automatized one-loop calculations in four and d dimensions. *Comput. Phys. Commun.*, 118:153–165, 1999.

[123] G. J. van Oldenborgh, J. A. M. Vermaseren. New algorithms for one loop integrals. *Z. Phys.*, C46:425–438, 1990.

[124] G. J. van Oldenborgh. Ff: A package to evaluate one loop feynman diagrams. *Comput. Phys. Commun.*, 66:1–15, 1991.

[125] Alexander Belyaev, Chuan-Ren Chen, Kazuhiro Tobe, C. P. Yuan. Phenomenology of littlest higgs model with t-parity: Including effects of t-odd fermions. *Phys. Rev.*, D74:115020, 2006.

[126] Monika Blanke, i in. Rare and cp-violating k and b decays in the littlest higgs model with t-parity. *JHEP*, 01:066, 2007.

[127] Joanne L. Hewett, Thomas G. Rizzo. Using b $\rightarrow$ s gamma to probe top quark couplings. *Phys. Rev.*, D49:319–322, 1994.

[128] R. Martinez, J-Alexis Rodriguez. Using the radiative decay b $\rightarrow$ s gamma to bound the chromomagnetic dipole moment of the top quark. *Phys. Rev.*, D55:3212–3214, 1997.

[129] R. Martinez, J. Alexis Rodriguez. The anomalous chromomagnetic dipole moment of the top quark in different frameworks and using the b -> s gamma process. *Phys. Rev.*, D65:057301, 2002.

[130] R. Martinez, M. A. Perez, N. Poveda. Chromomagnetic dipole moment of the top quark revisited. *Eur. Phys. J.*, C53:221–230, 2008.

[131] J. Pumplin, i in. New generation of parton distributions with uncertainties from global qcd analysis. *JHEP*, 07:012, 2002.

[132] J. Gunion, H. Haber, G. Kane and S. Dawson, The Higgs Hunter's Guide.

[133] Tao Han, Heather E. Logan, Bob McElrath, Lian-Tao Wang. Loop induced decays of the little higgs: H -> g g, gamma gamma. *Phys. Lett.*, B563:191–202, 2003.

[134] A. Djouadi, J. Kalinowski, M. Spira. Hdecay: A program for higgs boson decays in the standard model and its supersymmetric extension. *Comput. Phys. Commun.*, 108:56–74, 1998.

[135] Aneesh Manohar, Howard Georgi. Chiral quarks and the nonrelativistic quark model. *Nucl. Phys.*, B234:189, 1984.

[136] D. Zeppenfeld, R. Kinnunen, A. Nikitenko, E. Richter-Was. Measuring higgs boson couplings at the lhc. *Phys. Rev.*, D62:013009, 2000.

[137] A. Djouadi, i in. The higgs working group: Summary report. 2000.

[138] Dieter Zeppenfeld. Higgs couplings at the lhc. 2002.

[139] Alexander Belyaev, Laura Reina. p p -> t anti-t h, h -> tau+ tau-: Toward a model independent determination of the higgs boson couplings at the lhc. *JHEP*, 08:041, 2002.

[140] M. Duhrssen, i in. Extracting higgs boson couplings from lhc data. *Phys. Rev.*, D70:113009, 2004.

[141] A. Freitas, D. Wyler. Phenomenology of mirror fermions in the littlest higgs model with t-parity. *JHEP*, 11:061, 2006.

[142] S. Rai Choudhury, A. S. Cornell, Naveen Gaur, Ashok Goyal. Little higgs model effects at gamma gamma collider. *Phys. Rev.*, D73:115002, 2006.

[143] Shigeki Matsumoto, Mihoko M. Nojiri, Daisuke Nomura. Hunting for the top partner in the littlest higgs model with t-parity at the lhc. *Phys. Rev.*, D75:055006, 2007.

[144] Marcela Carena, Jay Hubisz, Maxim Perelstein, Patrice Verdier. Collider signature of t-quarks. *Phys. Rev.*, D75:091701, 2007.

[145] Qing-Hong Cao, Chuan-Ren Chen. Signatures of extra gauge bosons in the littlest higgs model with t-parity at future colliders. *Phys. Rev.*, D76:075007, 2007.

[146] A. Pukhov. Calchep 3.2: Mssm, structure functions, event generation, batchs, and generation of matrix elements for other packages. 2004.

[147] A. Semenov. Lanhep: A package for automatic generation of feynman rules from the lagrangian. *Comput. Phys. Commun.*, 115:124–139, 1998.

[148] Sally Dawson. The effective w approximation. *Nucl. Phys.*, B249:42–60, 1985.

[149] Scott S. D. Willenbrock, Duane A. Dicus. Production of heavy quarks from w gluon fusion. *Phys. Rev.*, D34:155, 1986.

[150] C. P. Yuan. A new method to detect a heavy top quark at the tevatron. *Phys. Rev.*, D41:42, 1990.

[151] R. Keith Ellis, Stephen J. Parke. Top quark production by w gluon fusion. *Phys. Rev.*, D46:3785–3788, 1992.

[152] Douglas O. Carlson, C. P. Yuan. Studying the top quark via the w - gluon fusion process. *Phys. Lett.*, B306:386–390, 1993.

[153] G. Bordes, B. van Eijk. Calculating qcd corrections to single top production in hadronic interactions. *Nucl. Phys.*, B435:23–58, 1995.

[154] A. P. Heinson, A. S. Belyaev, E. E. Boos. Single top quarks at the fermilab tevatron. *Phys. Rev.*, D56:3114–3128, 1997.

[155] T. Stelzer, Z. Sullivan, S. Willenbrock. Single-top-quark production via w-gluon fusion at next-to- leading order. *Phys. Rev.*, D56:5919–5927, 1997.

[156] Qing-Hong Cao, Reinhard Schwienhorst, Jorge A. Benitez, Raymond Brock, C. P. Yuan. Next-to-leading order corrections to single top quark production and decay at the tevatron. ii: t-channel process. *Phys. Rev.*, D72:094027, 2005.

[157] J. Bagger, i in. The strongly interacting w w system: Gold plated modes. *Phys. Rev.*, D49:1246–1264, 1994.

[158] J. Bagger, i in. Lhc analysis of the strongly interacting w w system: Gold plated modes. *Phys. Rev.*, D52:3878–3889, 1995.

[159] F. Abe, i in. Observation of top quark production in $\bar{p}p$ collisions. *Phys. Rev. Lett.*, 74:2626–2631, 1995.

[160] S. Abachi, i in. Observation of the top quark. *Phys. Rev. Lett.*, 74:2632–2637, 1995.

[161] T. Stelzer, W. F. Long. Automatic generation of tree level helicity amplitudes. *Comput. Phys. Commun.*, 81:357–371, 1994.

[162] Fabio Maltoni, Tim Stelzer. Madevent: Automatic event generation with madgraph. *JHEP*, 02:027, 2003.

[163] Joel R. Primack, David Seckel, Bernard Sadoulet. Detection of cosmic dark matter. *Ann. Rev. Nucl. Part. Sci.*, 38:751–807, 1988.

[164] Kyoungchul Kong, Seong Chan Park. Phenomenology of top partners at future colliders. 2007.

[165] K. Hagiwara, R. D. Peccei, D. Zeppenfeld, K. Hikasa. Probing the weak boson sector in e+ e- → w+ w-. *Nucl. Phys.*, B282:253, 1987.

[166] Andreas Birkedal, Andrew Noble, Maxim Perelstein, Andrew Spray. Little higgs dark matter. *Phys. Rev.*, D74:035002, 2006.

[167] Ansgar Denner. Techniques for calculation of electroweak radiative corrections at the one loop level and results for w physics at lep-200. *Fortschr. Phys.*, 41:307–420, 1993.